FABRICATION AND OPTIMIZATION OF FLEXIBLE DYE SENSITIZED SOLAR CELLS

Xue Zhaosheng

NATIONAL UNIVERSITY OF SINGAPORE

2013

FABRICATION AND OPTIMIZATION OF FLEXIBLE DYE SENSITIZED SOLAR CELLS

Xue Zhaosheng

(*B.Appl.Sc.(Hons), NUS)*

A THESIS SUBMITTED

FOR THE DEGREE OF DOCTOR OF PHILOSOPHY

NUS GRADUATE SCHOOL FOR INTEGRATIVE SCIENCES AND ENGINEERING

NATIONAL UNIVERSITY OF SINGAPORE

2013

Declaration

I hereby declare that the thesis is my original work and it has been written by me in its entirety. I have duly acknowledged all the sources of information which have been used in the thesis.

This thesis has also not been submitted for any degree in any university previously.

Xue Zhaosheng

Xue Zhaosheng

3 Dec 2013

ACKNOWLEDGEMENT

This thesis, though describes my work, would not be possible without the efforts of many others.

My supervisor, associate professor Liu Bin has been truly helpful in my pursuit of this dissertation. She has painstakingly nurtured me as a researcher over the past 4 years. The time and energy she invested in my works is of paramount importance, without which my projects would have been impossible.

My senior teammates Dr Yin Xiong, Dr Liu Xizhe, Dr Zhang Wei and Wang Long have taught me countless skills and techniques especially in the early days of my post graduate education. Special thanks must to given to Dr Yin Xiong who has taught me the basics of DSSC fabrication which I know almost nothing of at the beginning. Countless discussions with Wang Long, academic and otherwise, have made my post graduate life much more interesting and fulfilling. Liu Wei, though a newcomer to the team, has helped me in many tasks and will no doubt become a valuable member of the team in future.

The members of the biosensor team: Dr Cai Liping, Dr Liu Jie, Dr Li Kai, Dr Yuan Youyong, Dr Gao Meng, Geng Junlong, Liang Jing, Feng Guangxue and Zhang Ruoyu have treated me as more an equal although they are many notches more capable. Our work did not overlap significantly but all members of the team have aided me in countless ways over my 4 years of PhD study.

Lab technologists in NUS have played various roles (from purchasing consumables to maintenance of the laboratories and even the operation of common facilities) during my pursuit of PhD. The list is not exhaustive and it includes Jamie, Mr Boey, Chai Keng, Zhi Cheng, Evan, Sandy, Wee Siong, etc who have provided assistance to me.

I am also thankful for my friends in and out of NUS, beer *kakis* included, and family members who have always been supportive of my post graduate education.

I would like to specially give thanks to my life partner, Joyce, for her unwavering love and support of my pursuit of a postgraduate degree.

Last but not least, without the financial sponsorship from NUS Graduate School for Integrative Sciences and Engineering, none of these would have been possible.

TABLE OF CONTENTS

SUMMARY

Current fossil energy sources are polluting and will eventually run out, leading to an energy crisis. Solar energy is clean, safe and abundant and a switch to solar power is a gateway to solving the coming energy crisis. The current dominant photovoltaic technology, the silicon photovoltaic, is too expensive and faces material constrains for large scale applications. In this regard, dye sensitized solar cells (DSSCs) represent a low cost alternative technology for solar to electric conversion. Overcoming issues such as rigidity, electrolyte leakage will be critical for the large scale application of DSSC technology. This thesis focuses on development of new fabrication techniques to solve existing challenges. Moreover, the flexible DSSC devices are optimized for high efficiency in the following works.

This thesis is organized into 6 chapters. Chapter 1 provides a background to photovoltaic technologies and introduces DSSC as a strong alternative. The progress of DSSC research and issues faced by the DSSC community are also highlighted in a literature review. Chapters 2 to 5 report the major findings of my research work. The conclusions and future outlook of these works will be discussed in chapter 6. A list of publications is provided at the end of the thesis.

In chapter 2, the size of TiO_2 nanoparticles is optimized for high efficiency plastic DSSCs. A series of TiO_2 nanoparticles with different sizes are synthesized by simple hydrothermal method. The nanoparticles were characterized and all of them are found to be of anatase phase. They are deposited as the photoanode by electrophoretic deposition (EPD). The effect of nanoparticle size on device efficiency was systematically investigated. It was found that increasing nanoparticle size increases the charge collection efficiency of the devices but decreases dye loading. A moderate size of 19 nm TiO_2 give the best efficiency due to a combination of good dye loading

and desirable charge collection. Under optimized conditions, plastic DSSCs fabricated at low temperature gave an efficiency of 6% under standard 100 $mWcm^{-2}$ AM 1.5G illumination.

In Chapter 3, the challenge of narrow light absorption in DSSCs is addressed. In order to improve the J_{sc} of DSSCs, extending the light absorption range of the devices is necessary. Co-sensitization of the DSSC with different sensitizers will enhance light response but unfavorable interactions between sensitizer molecules in close proximity present challenges. A new fabrication technique that enables the layer by layer co-sensitization is introduced. The technique is also compatible with plastic substrates. A proof of concept is shown using D131 and SQ2 sensitizers, which has minimal spectra overlap. Devices fabricated using the layered technique is found to have higher dye loading and photovoltaic performance than the devices using the traditional cocktail method. Electrochemical impedance spectroscopy (EIS) shows that cocktail devices have significantly lower recombination resistance compared to the layered devices. This leads to the cocktail devices having lower V_{oc} and J_{sc} than layered devices. For plastic devices tested under standard 100 $mWcm^{-2}$ AM 1.5G illumination, the layered method gave an efficiency of 4.1%, significantly higher than 3.3% for devices sensitized using the traditional cocktail method.

Chapter 4 presents the fabrication of flexible solid-state DSSCs on titanium substrates. The key challenge in flexible solid-state DSSCs is the fabrication of a dense TiO_2 blocking layer at low temperature. The use of a high temperature resistant metallic foil as substrate circumvents this issue and allows the fabrication of high quality TiO_2 layers. However, since metal substrates are not transparent, the key challenge is to fabricate a semi-transparent cathode. In addition, it is difficult to fabricate pinhole-free TiO_2 dense film on the rough titanium surface and the adhesion of the TiO_2 mesoporous layer on the titanium substrate is weak. The rough surface of titanium

was smoothened until a mirror finish to reduce unevenness. In addition, the substrates are sintered in air to grow a native layer of TiO_2 which aids in reducing pinholes in the blocking layer and increasing adhesion of the subsequent layers to the substrate. After optimization of various parts of the device, an efficiency of 1.20 % was obtained under standard 100 $mWcm^{-2}$ AM 1.5G illumination for the first ever reported flexible solid-state DSSC device on titanium substrate. The cause for the relatively low efficiency is due to light loss from the backside illumination of the devices.

Chapter 5 addresses the challenge of low efficiency of solid-state devices fabricated on titanium substrates. Backside illuminated devices show poor performance due to significant light loss and hence, poor device performance. For high performance flexible DSSCs, front side illumination is preferred. Atomic Layer Deposition (ALD) is used for the deposition of thin pin-hole free amorphous TiO_2 blocking layer which is shown to exhibit good rectifying behavior. The active mesoporous TiO_2 layer is deposited by EPD. The entire fabrication process does not exceed 150 ^oC, hence is suitable for some plastic substrates. Solid-state flexible devices are fabricated on plastic substrates and under optimized conditions, efficiencies of up to 1.9 % can be achieved, a relative improvement of 58 % over the device on metal substrates (1.2 %) under standard 100 $mWcm^{-2}$ AM 1.5G illumination. This work represents the first report of a flexible solid-state DSSC on plastic substrates.

A LIST OF TABLES

A LIST OF FIGURES

Chapter 1 Literature review and introduction

1.1 Energy Use and Future Energy Challenges

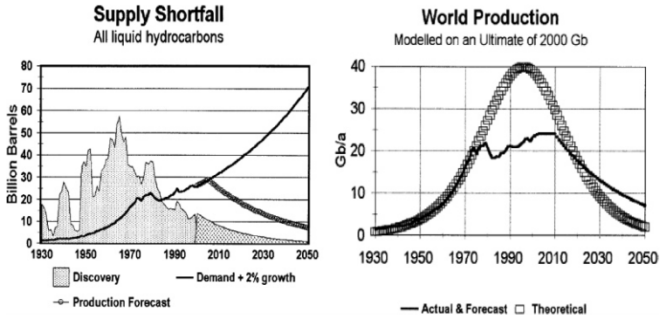

Figure 1.1 Left: Discovery trend. Right: World production of oil, which by definition needs to mirror oil discovery. [1]

Energy requirement for human use is expected to grow at an average of 2% per year for the next 25 years.[1] This increase in demand, coupled with decreasing reserves of various fossil fuel as well as the various environmental problems associated with it, requires a clean renewable source of energy. Issues arising from the use of fossil fuels as a main source of energy have been highlighted in the mainstream media as well as in scientific fields in the recent decades. Such issues include:

1. Limited supply that is expected to grow tighter as shown in Figure 1.1
2. A significant amount of crude oil is in politically unstable regions
3. Climate change caused by extensive production of greenhouse gases.

In addition, massive environmental pollution due to major oil spills [2, 3]has led to public outcry and concern with the current extraction and transportation of oil supplies.

In view of these challenges in the foreseeable future, other non fossil fuel alternative energy sources have been identified. These include solar, wind, tidal, nuclear, biomass and geothermal energies. In the area of alternative energy, solar energy remains the most promising due to the

large abundance of solar energy flux reaching the earth from the sun daily. The amount of solar flux that reaches the Earth's surface daily is so huge (3×10^{24} J year^{-1}) that it is estimated that by merely covering 0.1% of the Earth's surface with cells of 10% efficiency will provide enough energy for annual global consumption.[4, 5] Compared to other forms of alternative energy, this natural abundance of renewable, clean and free solar flux makes solar energy an ideal energy source for large scale applications. However, the large scale application of current photovoltaic technologies has been hampered by high cost, high energy payback times and material limitations. Considerable on-going research efforts have been put into overcoming these challenges. The historical advancement and current progress of photovoltaics will be discussed briefly in the following section.

1.2 A Brief History of Photovoltaic

A photovoltaic cell is a device that can convert solar radiation into electricity. The history of photovoltaic cells goes far back to 1839 when French physicist A. E. Becquerel demonstrated the so called "photovoltaic effect"[4, 6] by illuminating Pt electrodes coated with AgCl or AgBr inserted into an acidic solution, as shown in Figure 1.2. The photovoltaic effect is loosely defined as the emergence of a potential difference between two electrodes attached to a solid or liquid electrolyte upon irradiation. Since that pioneer work of Becquerel, various technologies that convert radiation into electricity have emerged.

In 1876, Adams and Day noted anomalies when Pt contacts were inserted into a selenium bar as shown in Figure 1.3.[6] This led to the development that showed that it is possible to start a current flow in selenium merely by irradiation. Following this development, Fritts fabricated the world's first large area (30 cm^2) photovoltaic device in 1883 using selenium films and gold

electrodes.[7] However, the low efficiency (~1%) and high cost of Fritts' devices did not lead to the widespread use of photovoltaics.

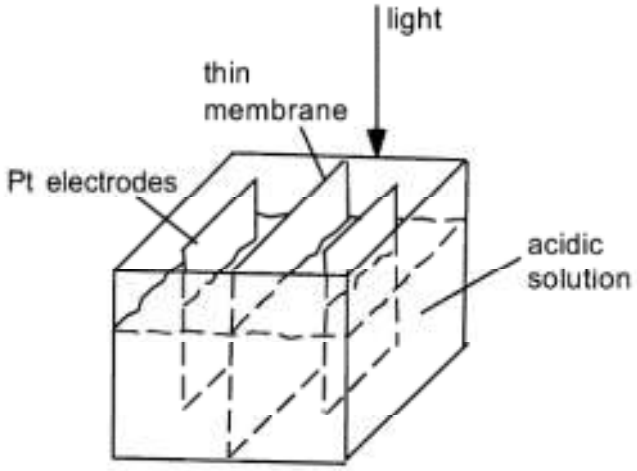

Figure 1.2 Diagram of apparatus described by Becquerel[6]

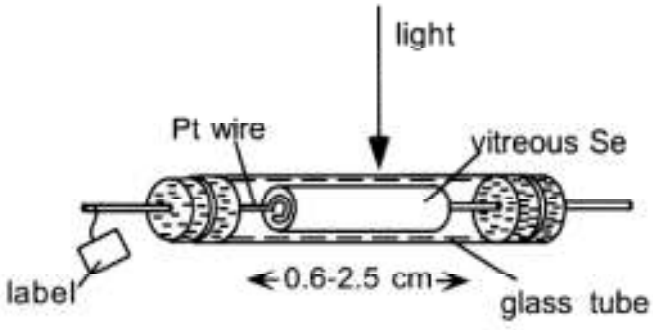

Figure 1.3 Sample geometry used by Adams and Day for the photovoltaic effect[6]

The first modern silicon solar cell was conceived in 1954[8] by Chapin et al at Bell Laboratories. It was discovered that a potential difference was produced by the *pn* diodes under light. Further work produced a functional silicon *pn* junction photovoltaic device with ~6% efficiency which was rapidly improved to ~10%. For many years, these cells are mainly used in space vehicles as a power supply. [9] By the early 1960s, models and fundamental theories like Shockley–Queisser limit were established and the impacts of band gap, temperature, electrical resistance,

etc on *pn* junction device efficiency were investigated and published.[10-14] These discoveries lead to a better understanding of the limits of photovolatics and how to improve them. By mid 1970s, design has evolved to that in Figure 1.4 and has not changed significantly since. Si photovoltaic technologies benefited greatly from the semiconductor industry that has developed high quality Si single crystal purification technologies for transistors and integrated circuits. [9] As such, this contributed to Si based photovoltaic rapid progress and leadership in the photovoltaic industry.

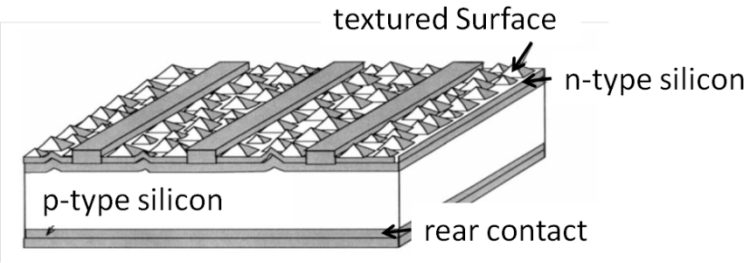

Figure 1.4 Modern design of silicon *pn* junction [6]

1.3 Photovoltaic technologies today

Most commercial solar cells that are used today, up to 80%, are either based on mono crystalline Si or poly crystalline Si.[15, 16] The rest are mainly dominated by thin film technologies such as CdTe and copper indium gallium selenide (CIGS) solar cells.[16] All of these technologies face severe material constrains for large scale development [17] and in the case of CdTe, the well known toxicity of cadmium is a particular concern. Although Si is in principle abundant, high energy inputs, high cost of purification for solar cell grade Si wafers and the use of Ag as a back electrode limit their large scale usage. Studies have shown that materials constrain is a severe limitation for the terawatt scale application of current photovoltaic technologies.[18, 19] In particular, natural availability and economical supply of Te, In, Ga , Ru, Ag used in current photovoltaic technologies will be severely strained if these technologies are ramped up to the

terawatt scale. The best case scenarios for these technologies are shown in Table 1.1. As can be seen, these technologies face severe material constrains for terawatt scale energy production.

Solar cell technology	Module Efficiency (%)	Limiting material	Reserve base (metric ton)	Maximum wattage	Averaged output (GW)	% of 2100 energy demand
CdTe	10.6	Tellurium (Te)	48 000	816 GW_p	120-160	0.4
CIGS	11.5	Indium (In)	16 000	650 GW_p	100-130	0.3
DSSC	7	Ruthenium (Ru)	5 000	890 GW_p	135-180	0.4
Crystalline-Si	15	Silver (Ag)	400 000	5.7 TW_p	860-1150	2.5

Table 1.1 The estimated, best-scenario peak wattage for various solar cell technologies [18]

While the harnessing of solar power is now technologically feasible, issues pertaining to cost and material availability continue to persist. Solar cells need to be made cost competitive in order for consumers to use them over conventional power sources. Currently, the solar cell industry requires large injection of government funds in order to function[1] and this phenomenon implies that the current solar cell technology is still too expensive for mass consumption. As such, alternatives with high material abundance, low cost and reasonable efficiency have to be sought after. There are several alternatives in the scientific literature: Quantum Dot solar cells[20, 21], Organic Photovoltaic[22, 23], Dye Sensitized Solar Cell [24] (DSSC) and chalcopyrite solar

[1] Renewable Energy - Market and Policy Trends in IEA Countries, International Energy Agency, 2004, http://www.iea.org/Textbase/publications/free_new_DESC.asp?PUBS_ID¼1263

cells[25, 26]. In this regard, DSSCs enjoy some great advantages which will be discussed in the below sections.

1.4 Dye sensitized solar cells

The inception of a device that utilizes a dye as a light harvesting material dates back as far as the 1960s[27] when it was discovered that excited dyes have the ability to inject electrons into a semiconductor. It was in principle, a concept that can be materialized but no active device with a good efficiency was produced. A functional device with acceptable efficiency was only published as recently as 1991 by O'Regan and Grätzel. [24] These cells, now known as DSSCs or Grätzel cells, are now a research area that has gained a lot of interest due to the advantage of having low cost, easy fabrication steps, widely available materials as well as an impressive efficiency exceeding 12%.[28]

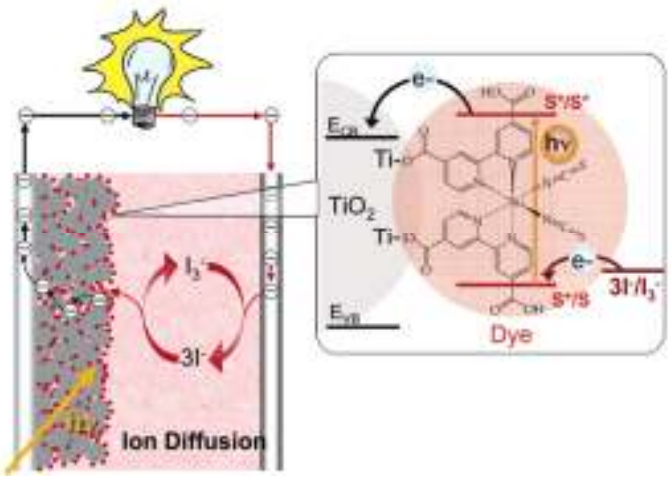

Figure 1.5 Components of a typical DSSC – the working electrode, dye, redox couple and counter electrode[29]

Figure 1.5 shows the typical make up of a conventional DSSC. There are 4 basic components in the DSSC:

i Working electrode – A transparent conducting electrode (Fluorine doped tin oxide, FTO) that is coated with a nanocrystalline, mesoporous high band gap semiconductor, usually TiO_2.

ii Dye sensitizer – a light harvesting material that is adsorbed on the nanocrystalline semiconductor. Ru complexes are traditionally used but organic or other metallic complexes are well known alternatives

iii Redox couple, traditionally I_3^-/I^- for dye regeneration and reduction of electron recombination

iv Counter electrode, typically Pt, for completion of circuit and catalyst for electrolyte regeneration

1.4.1 Mechanism of Action of DSSC

The working principle of DSSC is essentially a process analogous to photosynthesis. It is analogous in the sense that chlorophyll in green plants, similar to dyes in DSSCs, absorbs photons and produce photo electrons but does not participate in charge transport. The DSSC generates a photocurrent *via* a series of steps:

i. Upon absorption of light, the dye molecule D becomes excited and injects an electron into the semiconductor (typically TiO_2), thereby itself oxidized to D^+. Equation (1) and (2) represent these processes.

$$D + h\nu \longrightarrow D^* \qquad (1)$$

$$D^* \longrightarrow D^+ + e^-(TiO_2) \qquad (2)$$

ii The oxidized dye molecule will be reduced by the redox couple (typically I^-/I_3^-). At the same time, the injected electron hops through the semiconductor network and eventually passes through the external circuit. “red’ and “ox” represents the reduced and

oxidized form of the redox couple (I^- and I_3^-) respectively. Equation (3) and (4) show these processes.

$D^+ + red(I^-) \longrightarrow D + ox(I_3^-)$ (3)

iii The photoelectron eventually reaches the counter electrode and regenerate the redox couple.

$e^- + ox(I_3^-) \longrightarrow red(I^-)$ (4)

However, throughout this idealized cycle, loss processes can take place and not all injected electrons eventually reach the counter electrode *via* the external circuit. When the photoelectron is injected into the semiconductor network, there is a non-zero probability that it will recombine with D^+, the oxidized dye species, (equation 5) or the redox couple (equation 6). These processes compete with photocurrent generation and hence should be minimized.

$e^-(TiO_2) + D^+ \longrightarrow D$ (5)

$e\text{-}(TiO_2) + ox(I_3^-) \longrightarrow red(I^-)$ (6)

These cycles are ideally regenerative in nature and no permanent chemical change occurs.

1.3.2 Evaluation of DSSCs

Several parameters are used to evaluate the performance of DSSCs

i Open Circuit Voltage (V_{oc})

This parameter refers to the measure cell voltage under open circuit conditions when no current is flowing. In principle, this is the highest voltage measurable in a solar cell and in the context of DSSC, it is the difference in the Fermi energy of the semiconducting material and redox potential of the redox couple.

ii Short Circuit Current (I_{sc})

Short circuit current refers to the current measured when the "shorted" with zero applied potential difference. It is in principle the highest current that a cell can produce under ideal conditions. As this parameter is dependent on the active area of the solar cell, it is more often expressed in terms of short circuit current density (J_{sc}) which is the short circuit current divided by the active area of the cell that is exposed to light. J_{sc} is affected by the absorption spectrum of the sensitizer as well as charge collection efficiency.

iii Fill Factor (FF)

Fill factor is calculated by taking the ratio of the measured power output ($P_m = J_m \times V_m$) to the theoretical maximum efficiency of the cell ($J_{sc} \times V_{oc}$) which is in practice unobtainable.

$$FF = \frac{J_m \times V_m}{J_{sc} \times V_{oc}}$$

FF is always <1. This represents the energy loss to internal resistance of the cell.

iv. Light to Power Conversion Efficiency (η)

The efficiency of the cell is defined as the ratio of the measured output power (Pm) to the power of the incoming solar radiation (P_{in}).

$$\eta = \frac{P_m}{P_{in}} = FF \times \frac{J_{sc} \times V_{oc}}{P_{in}}$$

Under standard conditions, the Pin is defined as 100 mW/cm^2. As seen from equation, the efficiency of a DSSC is dependent on the FF, J_{sc} and V_{oc}. As such, these 3 parameters need to be fully optimized in order to improve the efficiency. A typical J-V curve is shown in Figure 1.6.

1.3.3 Experimental Techniques for DSSC evaluation

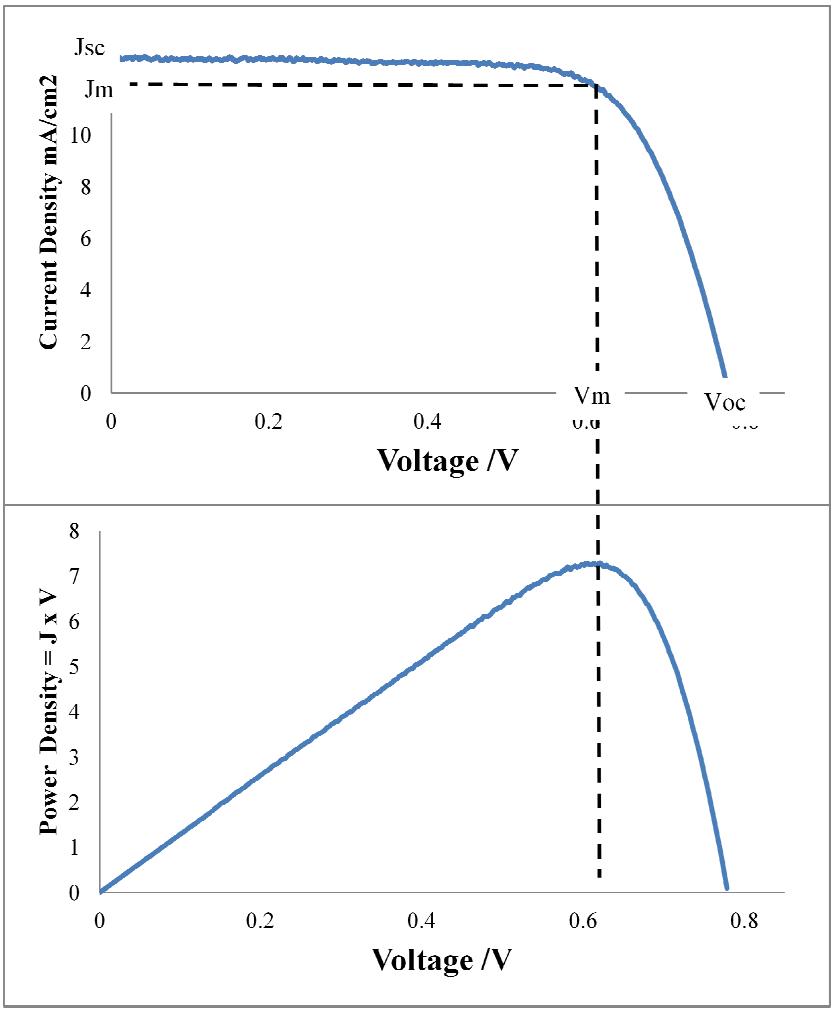

Figure 1.6 Typical J-V curve for a solar cell

a. V_{oc}, J_{sc}, FF and η Determination

The 4 basic parameters V_{oc}, J_{sc}, FF and η can be determined by varying the potential difference across the solar cell and measuring the resultant current

b. Incident-photon-to-electron conversion efficiency (IPCE)

In order to understand how the DSSC responds to different wavelength of light, the IPCE, otherwise known as quantum efficiency, can be measured. The IPCE value represents the current

density produced in the external circuit under monochromatic illumination of the cell divided by the photon flux that hits the cell:

$$\mathrm{IPCE} = 1240 \frac{J_{sc}(\lambda)}{\lambda(\mathrm{nm}) P_{in}(\lambda)}$$

It is a measure of the efficiency of the solar cell in converting monochromatic light into photocurrent. It is dependent on the absorption range of the dye used as well as rate of recombination of the generated photoelectrons. The integration of the IPCE spectrum gives the J_{sc} of the device. The IPCE is often used to measure the effectiveness of the sensitizer in converting monochromatic photons into current.

c. Other measurements

Other methods include the transient photocurrent/photovoltage measurements, intensity-modulated photocurrent/photovoltage spectroscopy (IMPS/IMVS). From the response of the devices, the electron transport time and electron lifetime in the device can be calculated. From the electron transport time and lifetime, the charge collection efficiency of the device can be determined.

Electrochemical impedance spectroscopy (EIS) is a steady-state technique that measures the current response to the application of an ac voltage as a function of the frequency. This allows the analysis and understanding of various interfaces within the DSSC device. An important advantage of EIS over other techniques is the possibility of using tiny ac voltage amplitudes exerting a very small perturbation on the system. EIS is commonly used with a mathematical model to scrutinize the processes of electron transport and ion diffusion at different interfaces in a DSSC.

1.3.3 Comparison of DSSC with other solar cells

Table 1.2 shows a brief comparison of DSSC with other types of competing solar cells. As shown in Table 1.2, DSSC has a reasonable efficiency that is about half of the crystalline silicon solar cells.

Table 1.2 Comparison of various types of solar cells and their challenges[4, 30] [a]cells with active area of at least 1 cm^2.

Solar Cell Type	Efficiency (%)		Challenges
	Cell[a]	Module	
Crystalline Silicon	25.0	22.9	Increase production yields, reduce cost and energy content
Polycrystalline Silicon	20.4	18.5	Lower manufacturing cost and complexity
Amorphous Silicon	10.1	7	Lower production costs, increase production volume and stability
$CuInSe_2$	19.6	15.7	Replace expensive and scarce indium, replace CdS window layer, scale up production
Dye Sensitized Solar Cell	11.0	9.9	Improve efficiency and long term stability, scale up production
Bipolar AlGaAs/Si			
Photoelectrochemical cells	19 - 20	-	Reduce cost of materials, scale up production
Organic Photovoltaic	10.0	5.5	Improve efficiency and long term stability

As Si technology has matured over the years, it is unlikely for major breakthroughs for efficiency. Conversely, functional DSSCs have only ~2 decades of active research, with room for improvement. Scientifically, there appears to be no fundamental reasons prevent DSSCs achieving efficiencies of 15% and higher.[31] Conversely, crystalline Si cells, assuming a band

gap of 1.12 eV, have a theoretical J_{sc} of 43.8 $mAcm^{-2}$ under standard 1 Sun illumination. Reported record cells have virtually reached that limit with a J_{sc} of 42.7 $mAcm^{-2}$. [16, 32] The best commercial modules currently have efficiencies of up to 22.9% which is close to that of small laboratory cells as shown in Table 1.2. These observations effectively mean massive improvements in the future are unlikely. Unlike single semiconductor photovoltaics, opportunities to improve DSSCs stem from the fact that it is essentially a system with independent parts which are made from different materials. This gives DSSCs additional degrees of freedom for tailoring and optimization which are unavailable for single semiconductor solar cells.[16]

DSSCs are unique in that electron transport, light absorption and hole transport are each handled by different materials and parts of the cell.[4, 33] This is in contrast to the conventional *pn* systems where the semiconductor assumes both the task of light absorption and charge carrier transport. This places extreme purity demands on the semiconductor for efficient charge separation and transport which are not required in DSSCs. Moreover, DSSCs made use of readily available materials such as TiO_2 which does not require special treatment processes that drives up cost. In addition, DSSCs are known to work well in low-light conditions, opening the possibility of indoor and other low light conditions usage. [34, 35] Lastly, with a wide array of sensitizers, DSSCs can be made into different colors, an important but often underrated consumer consideration in future commercialization. Despite these advantages, it is evident that there are issues to be overcome before mass commercialization. Some of these issues will be discussed in the following sections.

1.3 Current Progress in DSSCs

1.3.1 Sensitizer

As mentioned in previous sections, the sensitizer plays essential photon absorbing and electron injection roles in the device. Desirable characteristics of the sensitizer include:

i Strong absorption of photons from the blue end to the near infra red region of the solar spectrum. In particular, improving light harvesting in the 650 nm to 900 nm domain is extremely desirable.[28]

ii Appropriate HOMO and LUMO levels to ensure fast charge transfer to the underlying semiconductor and sufficient overpotential for fast reduction kinetics with the electrolyte.

iii Electron injection should occur much faster than electron relaxation. After injection, the oxidized form of the dye should be reduced rapidly compared to electron recombination.

iv. The dye must attach strongly to the semiconductor's surface and be stable for ~10^8 turnover cycles (equivalent to ~20 years outdoor usage)[36]

According to Grätzel, the weakest point in the device during DSSC's initial development is the dye sensitizer.[37] Thus, it is no surprise that great efforts are put into the design and synthesis of high performance sensitizers. The so-called "standard dye" used in DSSCs is the N719 dye [cis-diisothiocyanato-bis(2,2'-bipyridyl-4,4'-dicarboxylato) ruthenium(II) bis(tetrabutylammonium)]. The first high-performance polypyridyl ruthenium complex was the so-called N3 [cis-di(isothiocyanato)bis(2,2'-bipyridyl-4,4'-dicarboxylato)-ruthenium(II)] reported in 1993 by Nazzeruddin *et al*[38]. The breakthrough of the 11% threshold[39] came with the use of the so called "black dye" [triisothiocyanato-(2,2':6',6"-terpyridyl-4,4',4"-tricarboxylato) ruthenium(II) tris(tetra-butylammonium)][40] in 2006 which as an impressive absorption onset of ~900 nm. The structures of these sensitizers are shown in Figure 1.7

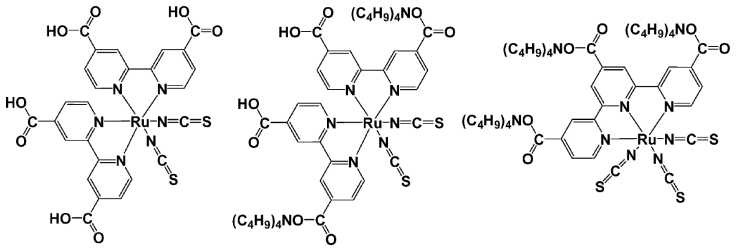

Figure 1.7 Structures (from left to right) of N3, N719 and N749 sensitizers

Traditionally, Ru complexes have produced the most efficient DSSCs and for an extended period of time, they are the only sensitizers that produced efficiency beyond 10% as presented in Figure 1.8. Currently, the best performing Ru sensitizer is the CYC-B11 whose chemical structure and device J-V curve is shown in Figure 1.9.

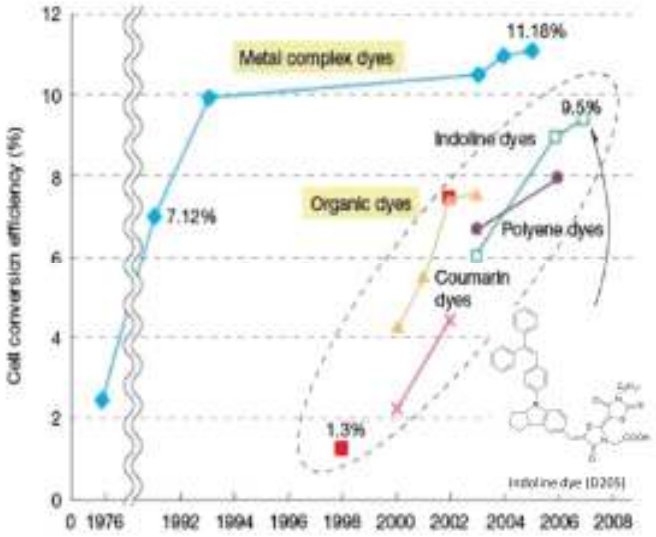

Figure 1.8 Evolution of efficiency under 1 Sun condition for DSSCs based on Ru complexes and organic dyes[41]

Though Ru complexes have produced impressive results, their low molar absorptivities (10,000 to 20,000 $M^{-1}cm^{-1}$)[42, 43] and high cost may eventually limit their large scale usage. More importantly, as seen in Table 1.1, the use of Ru also presents a material limitation for the tetrawatt scale application of DSSCs unless efficiencies are improved tremendously beyond current generation of DSSCs.

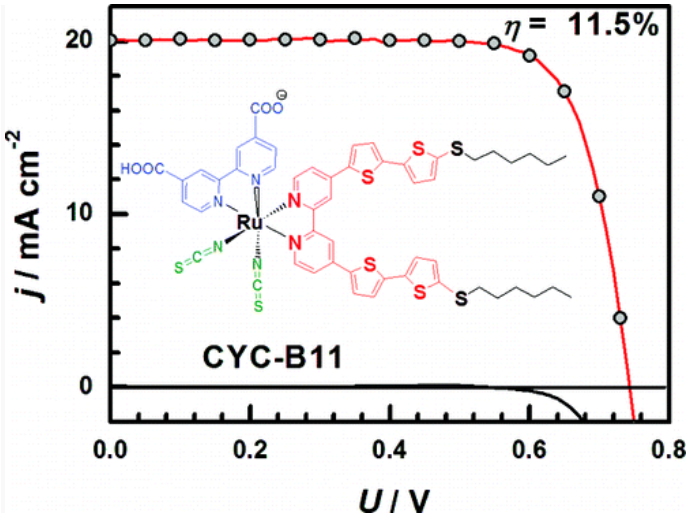

Figure 1.9 Chemical structure of CYC-B11 and J-V curve of the best performing Ru-complex sensitized DSSC using I^-/I_3^- electrolyte[44]

As there is increased concern about the use of Ru based dyes due to the scarcity of Ru, efforts have been ramped up in the research of metal-free organic dyes as replacements[45, 46]. Organic sensitizers which face no practical resource limitation are suitable for use in large scale application of DSSCs. Organic sensitizers also have the advantage of high extinction coefficient (40,000 to 200,000 $M^{-1}cm^{-1}$) [42, 43], low cost and easy structural modification.

Over the years, there is an increase in the fundamental understanding of organic dye design for use in DSSCs.[47] Typical well performing dyes contain both electron rich donor moiety and electron poor acceptor moiety linked by a conjugated π-bridge. The acceptor section is also functionalized with an acidic group for strong binding on the semiconductor's surface. Photoexictation causes a net transfer of electron from the donor to acceptor moiety through the conjugated π-spacer. The acceptor moiety, which is attached to the semiconductor's surface, can then inject electrons readily into the conduction band of the semiconductor. Conversely, the hole left in the donor moiety is well positioned away from the semiconductor surface to accept an electron from the redox couple. [47]

Indoline dyes[48-51] are the most successful class of organic dyes as shown in Figure 1.8. Because of the ease of synthesis and good efficiencies of devices using these sensitizers, work described in this thesis has used indoline dyes as the sensitizer.

1.3.2 Flexible solar cells

The restrictions of rigid solar cells such as heavy weight and limited shapes of traditional substrates were recognized as early as 1967[52] which saw the first reported flexible thin film Si solar cell arrays. In 1990, Kishi and co-workers fabricated the first ever flexible amorphous Si solar cell on a lightweight plastic substrate. [53] Other flexible solar cells were also reported. Several CIGS solar cells on flexible polymer or metallic substrates that produced impressive efficiencies of up to 15.8% were reported. [54-59] Flexible polymer based solar cells were among the most intensively studied as polymeric materials are known to have high flexibility and mechanical toughness as well as good film forming ability.[60] A fully roll-to-roll processed polymer solar module fabricated entirely by solution processing starting from a polyethyleneterephthalate substrate was reported in 2009 by Krebs and co-workers.[61] All processing was performed in ambient conditions air without vacuum and modules comprising eight serially connected cells gave efficiencies as high as 2.1% for the full module with 120 cm^2 active area and up to 2.3% for modules with 4.8 cm^2 active area.

As can be seen, fabrication of flexible solar cells attracts interest in a spectrum of the solar cell community over decades. Within the DSSC community, many notable works on flexible devices were also reported. The specific challenges for the fabrication of flexible DSSCs will be discussed in the following sections.

1.3.3 Review of challenges for flexible DSSCs

In the context of DSSCs, electrolyte and cathode are readily flexible and hence the key challenge lies in the fabrication of flexible photoanodes. In conventional DSSC, the nanocrystalline semiconductor layer is usually applied on the transparent conducting electrode in the form of a paste either by doctor blading or screen printing. This paste usually contains organic polymeric binders that make the paste viscous for easy application. Other additives are also added to aid the formation of the porous network and enhance interparticle adhesion that is essential for efficient DSSCs. These additives have to be removed using a sintering process at 450 to 550 ^{o}C. In addition, the sintering process forms proper necking that improves interparticle connectivity and electron transport.

FTO glass is the most commonly used substrate for DSSCs as it is highly conducting, sintering resistant and transparent, but it is rigid, brittle and heavy. These limitations restrict the application of devices on flat rigid surfaces. For continuous, high throughput and low cost fabrication of solar devices using roll to roll process, a flexible substrate is a prerequisite.[62] Flexible DSSCs have the advantage of having light weight, lower production costs and have outdoor and mobile applications in areas where such flexibility and light weight is desirable. Polymer substrates like polyethylene terephthalate (PET) or polyethylene naphthalate (PEN) are alternatives to conventional rigid glass substrates. Polymeric substrates have high flexibility and toughness but cannot withstand the high temperature sintering as they typically melt/decompose beyond 200 ^{o}C. As such, low temperature fabrication methods have to be improvised. Metal foils such as stainless steel and Ti are desirable as heat resistant flexible conducting substrates but the lack of transparency presents new challenges as light has to shone from the cathode side. A schematic of a flexible DSSC fabricated on Ti substrate is shown in Figure 1.10.

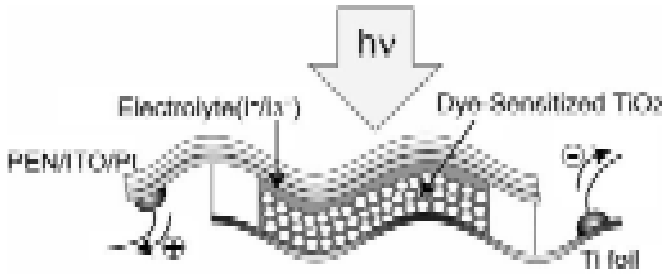

Figure 1.10 Schematic of a flexible DSSC fabricated on titanium foil[63]

The key challenge for glass to plastic conversion is to fabricate mechanically stable films that are free of residual organics and contain good necking without high temperature sintering. An intuitive and straightforward method is to reduce the sintering temperature but the incomplete removal of binders produce films of high resistance and consequentially devices with low efficiency. As a result, several low temperature sintering methods were improvised. Pichot and co-workers first reported in 2000 thin TiO_2 films without organic surfactants that were sintered 100 ^oC although low efficiencies were reported. [64] Low temperature sintering at 100 ^oC while irradiating 28 GHz microwave was first reported to be an effective low temperature fabrication technique by Uchida and co-workers in 2004.[65] Using this method, a high efficiency of 5.51% was reported for rigid device which is comparable to devices fabricated using conventional high temperature sintering. Interestingly, a short irradiation time of 5 min suffices, which is an advantage for high throughput manufacturing.

A novel notion of "chemical sintering" was reported in 2005 by Park and co-workers.[66] Aqueous ammonia was added to an acetic acid containing TiO_2 colloid and it was found that the viscosity of the colloid increases tremendously and the colloid becomes viscous enough to be applied using doctor blading. The phenomenon was attributed to the increase in ammonium acetate salt concentration which causes the flocculation of TiO_2 nanoparticles by acting as

"electrolyte glue". Upon drying of the paste, the acetate ions, which were responsible for the particle linkages can be removed as acetic acid under gentle heating. This "chemically sintered" low temperature TiO_2 film was shown to have high connectivity and low series resistance similar to a sintered sample. This was the first report that acid-base chemistry was used to induce particle connectivity. Following this reports, Weerasinghe and co-workers reported a chemically sintered TiO_2 film using hydrochloric acid as the sole binding agent in 2010. [67] Similarly to Park's initial report, a highly viscous paste was obtained and high mechanical strength of the film was reported. Device efficiencies of up to 5% were recorded.

A new strategy for improving the necking of films prepared at low temperature without polymeric binders was reported by Zhang and co-workers in 2003.[68] The unsintered film lacks the proper necking and interparticle connections but it is overcome by the addition of TiO_2 precursors such as titanium (IV) tetraisopropoxide or titanium tetrachloride in the paste. Under steam treatment at 100 ^{o}C, the precursors form small necking particles within the film which improves mechanical stability and decreases electron transport resistance.[69] An efficiency of 2.3% was reported for all plastic devices. The hydrothermal process in the process was eventually removed from the fabrication process in another report by Zhang and co-workers in 2006.[70] Using an UV-ozone treatment process which removes residual organics, an improved efficiency of 3.27% was reported. Following Zhang's pioneering work in low temperature pastes, many other reports with further optimization and high efficiencies of up to 6.4% surfaced[69, 71, 72] In addition, the method can be easily modified to fabricate good quality ZnO films at low temperature. [73]

Electrophoretic deposition (EPD) is a mature industrial method that has been used in film formation of a wide range of materials. [74-76] In a typical EPD process, particles to be

deposited are suspended in a solvent to form a stable colloid. Two electrodes will be inserted into the colloidal suspension and a potential difference is applied across the electrodes. Charged particles in the suspension will be attracted to the electrodes thereby forming uniform thin films. The film formation and growth on the electrodes is mainly *via* a particle coagulation mechanism. [77]. The process only takes a few minutes and the films formed are highly repeatable.[78] Figure 1.11 shows a typical set up for an EPD process.

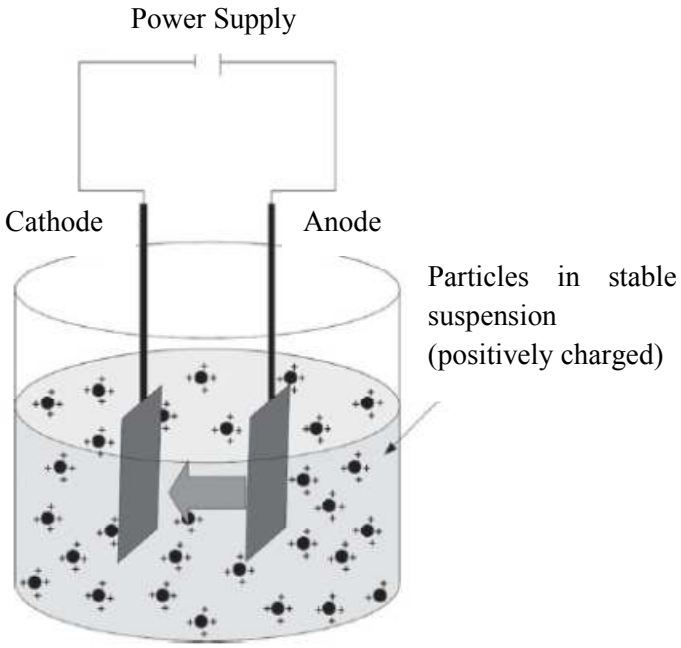

Figure 1.11 A typical EPD set up. In this example, the colloidal is positively charged[77]

Though the colloidal, in principle, can be suspended in water, this is rarely done. As EPD processes uses tens of volts of potential difference, any water present will be electrolyzed, causing gas formation at the electrodes. Films formed under this condition are often grainy, rough and contains pinholes visible to the naked eye.[77, 79] As such, organic liquids are typically preferred. Choosing a solvent for EPD appears to be trivial but there are several considerations in place.[80] Firstly, the particles to be suspended should be physically and chemically stable in the suspension solvent. The solvent of choice should be able to induce

charges on the surface of the particles as the EPD process depends on the movement of charged particles. Thirdly, ionic species should be kept to a minimum as current should be carried across the electrodes *via* suspended particles as far as possible. Lastly, the evaporation rate of the solvent should not be too rapid as rapid evaporation tends to introduce visible cracks in the formed films. In 2004, Miaska and co-workers reported the use of EPD for plastic photoanode fabrication, combined with post chemical necking treatments of TiO_2 layers. [81] An efficiency of more than 3% was achieved and a scheme for roll to roll continuous manufacturing was proposed. Later in 2005, Yum and co-workers[82] did a systematic study of the effects of zeta potential, concentration of particles, applied electric field and the packing density of the resulting film. Subsequently, high efficiencies of up to 6.63% were reported using photoanodes fabricated by EPD.[83, 84] EPD can also be used to fabricate flexible cathodes by the deposition of Pt[85] or carbonaceous materials[86-88] on plastic substrates making it a versatile fabrication technique. Physical compression as a fabrication method for flexible DSSCs was reported by Lindström and co-workers in 2000.[89] After film formation, compression reduces film thickness by physically forcing particles closer to each other. This improves the interparticle connection, that is often poor in unsintered films, and decreases charge transport resistance and back recombination.[90] Physical compression is considered to be a straightforward, low cost, low temperature and effective method for the continuous fabrication of flexible DSSCs[62, 91] Currently, the highest validated efficiency of plastic DSSCs,7.6%[92], is fabricated using compression as one of the steps which shows that compression can produce good results. Physical compression is often used in conjunction with other low temperature film formation methods with good success. Several reports using binder-free pastes[92, 93] and EPD[79, 94-97] in conjunction with compression as a post treatment step has produced plastic DSSCs with good efficiencies. This

shows that physical compression is a fabrication technique that is compatible with several existing film formation techniques.

A different approach in the fabrication of flexible DSSC is to transfer high quality sintered films onto a plastic substrate. The first report of this method that attracted attention was published in 2005 by Dürr and co-workers.[98] The scheme is shown in Figure 1.12. A thin <20 nm gold layer was first deposited on a glass substrate. The mesoporous TiO_2 layer was deposited on the gold layer and sintered conventionally to produce a high quality TiO_2 film. The gold layer was dissolved by a tri-iodide / iodide solution and the free-standing TiO_2 film can be pressed onto another substrate under moderate heating. Various characterization techniques showed that the properties of the sintered film have been retained in after the transfer process. Using a polymer gel electrolyte, efficiencies of up to 5.8% was reported for plastic DSSCs.

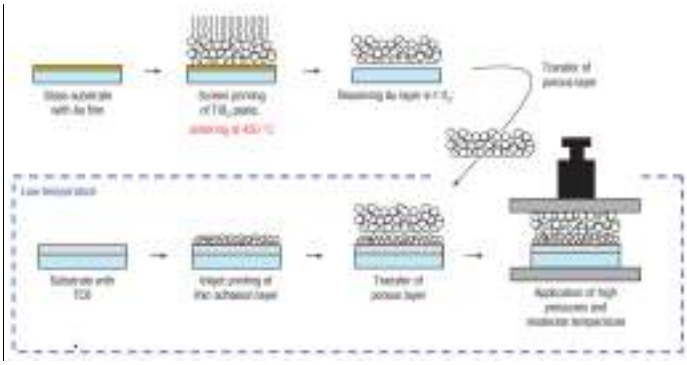

Figure 1.12 Scheme for the lift-off and transfer process[98]

These reports indicate that there is much interest in the DSSC community to fabricate highly efficient flexible devices.

Though these are widely used methods, the results show that the cell efficiency is still very much below the conventional high temperature DSSC. This can be attributed to the higher resistance that the films produced by these stated methods possess. [99] Currently, low temperature fabrication of DSSCs has achieved a validated efficiency of 7.6%.[92], still significantly distance

lower than conventional DSSCs. The development of DSSCs has lowering the cost of solar power as a main motivation and hence optimizing the fabrication of flexible DSSC would be in line with the goal of lowering cost. Flexible DSSCs allow the mass production of DSSCs using a cost efficient roll to roll production method. As such, optimizing flexible DSSCs and increasing their efficiencies are crucial steps towards future commercialization.

1.3.4 Iodine-free solid-state DSSCs

The presence of a liquid electrolyte as well as the corrosive nature of I_2 has raised concerns about the long term stability of the DSSC. As such, massive research efforts have been put into researching alternative device structures that do not use volatile components. These alternatives include using gel-type electrolyte, low volatility ionic liquids and replacing the liquid electrolyte with a solid conductor.[100-102]. The so called solid-state DSSCs refer to devices that have replaced the liquid electrolyte with solid-state p-type hole transporters. The diagram of a typical solid-state DSSC is shown in Figure 1.13.

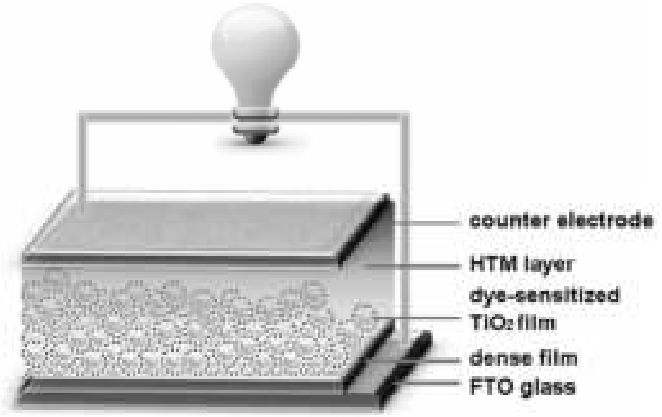

Figure 1.13 Systematic of a typical solid-state DSSC[103]

Hole transporting material (HTM) for solid-state DSSCs need to satisfy several requirements:

i Its HOMO level should be higher than the HOMO level of the sensitizer molecule to drive the hole transfer process from HTM to sensitizer. [104]

ii It should diffuse into the pores of the active TiO_2 layer. Amorphous films are known to have better pore filling as crystallization inhibits the process.[105]

iii It should have good hole mobility for good charge transport

In the first generation of the solid-state DSSCs, common inorganic HTMs such as Cu(I) salts like CuI, CuBr and CuSCN are used in DSSCs in place of the liquid electrolyte but they are found to be either unstable or have low hole mobility, resulting in low efficiencies [102, 106] Recently in 2012, solid state DSSCs using perovskite based inorganic HTMs have been reported with efficiencies exceeding 8.5%, a breakthrough at that time.[107, 108] Compared to inorganic HTMs, organic HTMs have the advantage of plentiful raw materials and easy film formation. 2,20,7,70-tetrakis (N,N-di-p-methoxyphenyl-amine)9,90-spirobifluorene (spiro-OMeTAD) is by far the most commonly used organic HTM because of its amorphous structure, small molecular size and good solubility. [109] Recently, solid state DSSCs with lead iodide perovskite as sensitizer and spiro-OMeTAD as HTM was reported to give an efficiencies up to approximately 15%.[110-112] Other than spiro-OMeTAD, conjugated polymers can also be used as HTMs. Conjugated polymers have the advantage of low fabrication costs, high conductivity and tunable optoelectronic properties.[113] Several conjugated polymers have been used as HTMs in solid-state DSSCs, with mixed success. Polyaniline [114-116] and polypyrrole [117-119] are among the earliest conjugated polymers used in solid-state DSSCs. Efficiencies up to 1.15% were reported after several optimization processes. An outstanding group of the conjugated polymer family is poly(3-alkylthiophene)s, especially poly(3-hexylthiophene) (P3HT). It possesses a hole mobility of up to 0.1 $cm^2V^{-1}s^{-1}$ which is several orders of magnitude higher than spiro-

OMeTAD.[113, 120] Devices using P3HT as HTM gave poor efficiency ($\eta < 1$ %) at first due to the poor efficacy of the sensitizer. [121] However, with optimization of the sensitizer, TiO_2 film and interface treatment, P3HT based hybrid devices give a reasonably high efficiency of up to 3.8%. [122, 123] P3HT can perform simultaneously as a light absorber as well as a HTM due to its strong absorbance. High performance solid-state organic-inroganic heterojunction solar cell of efficiency 5.13% was reported in 2010 by Chang and co-workers. [124] The device was fabricated by depositing Sb_2S_3 and P3HT were onto TiO_2 films. The Sb_2S_3 nanocrystals act principally as the light absorber whereas P3HT supplements the light absorbance and simultaneously acts as the HTM. Recently, devices using lead iodide perovskite as sensitizer and P3HT as HTM, were reported to give reasonable efficiencies of up to 6.7%.[125, 126] These reports show that P3HT can perform as a low cost alternative to spiro-OMeTAD.

Notwithstanding these progress of devices using conjugated polymers as HTM, it is well known that polymeric HTMs have poor penetration and pore filling due to large molecular size and slow diffusion.[113] This restricts the thickness of the active layer in solid-state devices to less than 2 μm and with this restriction, light harvesting and J_{sc} are limited. In order to circumvent these issues, *in-situ* polymerized poly(3,4-ethylenedioxythiophene) (PEDOT) was used as an alternative HTM in iodine-free solid state DSSCs. [127, 128] The EDOT monomer molecules are small enough to diffuse into the pores of the TiO_2 network and as they get *in-situ* polymerized, the resultant PEDOT polymer grows from the pores outwards, giving good pore filling. PEDOT possess high conductivity (~300 S/cm), is highly transparent and remarkably stable in the oxidized state. [129] These excellent properties, coupled with optimization of sensitizer and polymerization conditions, high efficiency of up to 7.1% was reported.[130, 131]

1.4 Research objectives and thesis organization

Flexible DSSCs without a corrosive liquid electrolyte is a milestone that must be reached before considerations for commercialization. As such, the main objectives of this research are to explore the science and engineering of fabricating flexible DSSCs through: 1) investigating the effect of nanoparticle size on device efficiency; 2) exploring new facile methods for co-sensitization in order to extend light harvesting of DSSCs; and 3) exploring new fabrication techniques for flexible solid-state DSSCs which are suitable for future commercialization.

This dissertation is organized and structured into six chapters. Chapter one provides an introduction of this dissertation including the background of DSSCs and the boarder context of solar energy. In addition, a literature review on the evolution and progress of DSSCs since its first inception is done. The research objective and outline of this dissertation are also presented in this chapter.

Chapter two investigates the use of EPD for flexible DSSCs and the optimization of nanoparticle size for devices fabricated using this technique. TiO_2 nanoparticles of various sizes are synthesized and deposited using EPD as the photoanode. These photoanodes are completed into devices and their efficiencies are investigated. Using techniques such as IMPS and IMVS, it was found that the nanoparticle size has a profound effect on dye loading and charge collection efficiency. With the optimization of the TiO_2 film thickness and the TiO_2 nanoparticle size, an efficiency of 6.0% was obtained for fully plastic devices using 19 nm TiO_2 nanoparticles which is a marked improvement over the device using P25 nanoparticles.

Chapter three describes a facile technique for quick and effective co-sensitization of flexible DSSCs. Using this layered technique, the sensitizers are more likely to be found in discrete layers rather than randomly arranged, as is the case in the commonly used “cocktail” method.

The IPCE spectrum shows that co-sensitizated devices possess characteristic absorptions of both sensitizers with the layered devices showing higher J_{sc}. Using EIS technique, it was found that the recombination resistance in the layer by layer device is higher than that in the cocktail device which leads to significantly higher performance in the layered device. Layered devices also show superior performance as compared to singly sensitized devices.

Chapter Four reports the use of Ti foil as substrates for flexible solid-state DSSCs. High quality mesoporous and dense TiO_2 films can be fabricated on Ti substrates at sintering temperature. In order to fabricate pinhole free dense TiO_2 blocking layers, a smooth surface is required. The Ti substrates are first smoothened until a mirror finish. Moreover, to improve the weak adhesion of the TiO_2 films to the substrate, the Ti substrates are first sintered in air for the growth of a layer of native oxide. Using a sputtered semi-transparent Pt cathode, the devices are illuminated from the cathode side. Due to light loss from the cathode as well as intense absorption from the Poly(3-hexylthiophene) (P3HT) layer, a relatively low efficiency of 1.2% is obtained. This represents the first flexible solid-state DSSC on Ti foil substrates.

Chapter Five improves upon the efficiency of flexible solid-state DSSC reported in chapter four. Using indium tin oxide coated polyethylene naphthalate (ITO/PEN) substrates that are transparent, light loss is reduced and higher efficiencies can be achieved. Low temperature strategies such as atomic layer deposition (ALD) and EPD are deployed to fabricate dense and mesoporous TiO_2 films respectively.

Chapter Six gives an overall conclusion for works described in this thesis. A brief future outlook is also provided.

1.5 References

1. Goncalves, L.M., et al., *Dye-sensitized solar cells: A safe bet for the future.* Energy & Environmental Science, 2008. **1**(6): p. 655-667.

2. Peterson, C.H., et al., *Long-term ecosystem response to the Exxon Valdez oil spill.* Science, 2003. **302**(5653): p. 2082-2086.

3. Camilli, R., et al., *Tracking hydrocarbon plume transport and biodegradation at Deepwater Horizon.* Science, 2010. **330**(6001): p. 201-204.

4. Gratzel, M., *Photoelectrochemical cells.* Nature, 2001. **414**(6861): p. 338-344.

5. Grätzel, M., *Solar energy conversion by dye-sensitized photovoltaic cells.* Inorganic Chemistry, 2005. **44**(20): p. 6841-6851.

6. Green, M.A., *Photovoltaic principles.* Physica E-Low-Dimensional Systems & Nanostructures, 2002. **14**(1-2): p. 11-17.

7. Fritts, C.E., *On a New Form of Selenium Photocell.* American Journal of Science, 1883. **26**: p. 465.

8. Chapin, D.M., C.S. Fuller, and G.L. Pearson, *A new silicon p-n junction photocell for converting solar radiation into electrical power.* Journal of Applied Physics, 1954. **25**(5): p. 676-677.

9. Goetzberger, A., C. Hebling, and H.W. Schock, *Photovoltaic materials, history, status and outlook.* Materials Science and Engineering: R: Reports, 2003. **40**(1): p. 1-46.

10. Prince, M.B., *Silicon Solar Energy Converters.* Journal of Applied Physics, 1955. **26**(5): p. 534-540.

11. Wysocki, J.J. and P. Rappaport, *Effect of temperature on photovoltaic solar energy conversion.* Journal of Applied Physics, 1960. **31**(3): p. 571-578.

12. Shockley, W. and H.J. Queisser, *Detailed balance limit of efficiency pf p-n junction solar cells.* Journal of Applied Physics, 1961. **32**(3): p. 510-&.

13. Rose, A., *Photovoltaic Effect Derived from the Carnot Cycle.* Journal of Applied Physics, 1960. **31**(9): p. 1640-1641.

14. Loferski, J.J., *Theoretical Considerations Governing the Choice of the Optimum Semiconductor for Photovoltaic Solar Energy Conversion.* Journal of Applied Physics, 1956. **27**(7): p. 777-784.

15. Pizzini, S., M. Acciarri, and S. Binetti, *From electronic grade to solar grade silicon: chances and challenges in photovoltaics.* Physica Status Solidi a-Applications and Materials Science, 2005. **202**(15): p. 2928-2942.

16. Bisquert, J., *Dilemmas of Dye-Sensitized Solar Cells.* Chemphyschem, 2011. **12**(9): p. 1633-1636.

17. Candelise, C., J.F. Speirs, and R.J.K. Gross, *Materials availability for thin film (TF) PV technologies development: A real concern?* Renewable and Sustainable Energy Reviews, 2011. **15**(9): p. 4972-4981.

18. Tao, C.S., J.C. Jiang, and M. Tao, *Natural resource limitations to terawatt-scale solar cells.* Solar Energy Materials and Solar Cells, 2011. **95**(12): p. 3176-3180.

19. Wadia, C., A.P. Alivisatos, and D.M. Kammen, *Materials availability expands the opportunity for large-scale photovoltaics deployment.* Environmental science & technology, 2009. **43**(6): p. 2072-2077.

20. Hillhouse, H.W. and M.C. Beard, *Solar cells from colloidal nanocrystals: Fundamentals, materials, devices, and economics.* Current Opinion in Colloid & Interface Science, 2009. **14**(4): p. 245-259.

21. Kamat, P.V., *Quantum Dot Solar Cells. Semiconductor Nanocrystals as Light Harvesters.* Journal of Physical Chemistry C, 2008. **112**(48): p. 18737-18753.

22. Chandrasekaran, J., et al., *Hybrid solar cell based on blending of organic and inorganic materials-An overview.* Renewable & Sustainable Energy Reviews, 2011. **15**(2): p. 1228-1238.

23. Facchetti, A., *pi-Conjugated Polymers for Organic Electronics and Photovoltaic Cell Applications.* Chemistry of Materials, 2011. **23**(3): p. 733-758.

24. O'Regan, B. and M. Grätzel, *A low-cost, high-efficiency solar-cell on dye-sensitized colloidal TiO_2 films.* Nature, 1991. **353**(6346): p. 737-740.

25. Kazmerski, L.L., F.R. White, and G.K. Morgan, *Thin-film $CulnSe_2$/CdS heterojunction solar-cells.* Applied Physics Letters, 1976. **29**(4): p. 268-270.

26. Dimmler, B. and H.W. Schock, *Scaling-up of CIS technology for thin-film solar modules.* Progress in Photovoltaics, 1996. **4**(6): p. 425-433.

27. Hagfeldt, A. and M. Gratzel, *Molecular photovoltaics.* Accounts of Chemical Research, 2000. **33**(5): p. 269-277.

28. Gratzel, M., *Recent Advances in Sensitized Mesoscopic Solar Cells.* Accounts of Chemical Research, 2009. **42**(11): p. 1788-1798.

29. Gratzel, M., *Solar energy conversion by dye-sensitized photovoltaic cells.* Inorganic Chemistry, 2005. **44**(20): p. 6841-6851.

30. Green, M.A., et al., *Solar cell efficiency tables (version 40).* Progress in Photovoltaics, 2012. **20**(5): p. 606-614.

31. Kroon, J., et al., *Nanocrystalline dye-sensitized solar cells having maximum performance.* Progress in Photovoltaics: Research and Applications, 2006. **15**(1): p. 1-18.

32. Green, M.A., et al., *Solar cell efficiency tables (version 35).* Progress in Photovoltaics: Research and Applications, 2010. **18**(2): p. 144-150.

33. Hagfeldt, A. and M. Grätzel, *Molecular photovoltaics.* Accounts of Chemical Research, 2000. **33**(5): p. 269-277.

34. Burnside, S., et al., *Deposition and characterization of screen-printed porous multi-layer thick film structures from semiconducting and conducting nanomaterials for use in photovoltaic devices.* Journal of Materials Science: Materials in Electronics, 2000. **11**(4): p. 355-362.

35. Papageorgiou, N., et al., *The performance and stability of ambient temperature molten salts for solar cell applications.* Journal of the Electrochemical Society, 1996. **143**(10): p. 3099-3108.

36. Baxter, J.B., *Commercialization of dye sensitized solar cells: Present status and future research needs to improve efficiency, stability, and manufacturing.* Journal of Vacuum Science & Technology A: Vacuum, Surfaces, and Films, 2012. **30**(2): p. 020801-020801-19.

37. Grünwald, R. and H. Tributsch, *Mechanisms of instability in Ru-based dye sensitization solar cells.* The Journal of Physical Chemistry B, 1997. **101**(14): p. 2564-2575.

38. Nazeeruddin, M.K., et al., *Conversion of light to electricity by cis-X2bis(2,2'-bipyridyl-4,4'-dicarboxylate)ruthenium(II) charge-transfer sensitizers (X = Cl^-, Br^-, I^-, CN^-, and SCN^-) on nanocrystalline titanium dioxide electrodes.* Journal of the American Chemical Society, 1993. **115**(14): p. 6382-6390.

39. Chiba, Y., et al., *Dye-Sensitized Solar Cells with Conversion Efficiency of 11.1.* Japanese Journal of Applied Physics, 2006. **45**(25): p. L638-L640.

40. Nazeeruddin, M.K., et al., *Engineering of efficient panchromatic sensitizers for nanocrystalline TiO_2 based solar cells.* Journal of the American Chemical Society, 2001. **123**(8): p. 1613-1624.

41. Grätzel, M., *Recent advances in sensitized mesoscopic solar cells.* Accounts of Chemical Research, 2009. **42**(11): p. 1788-1798.

42. Hamann, T.W., et al., *Advancing beyond current generation dye-sensitized solar cells.* Energy & Environmental Science, 2008. **1**(1): p. 66-78.

43. Hardin, B.E., H.J. Snaith, and M.D. McGehee, *The renaissance of dye-sensitized solar cells.* Nature Photonics, 2012. **6**(3): p. 162-169.

44. Chen, C.-Y., et al., *Highly Efficient Light-Harvesting Ruthenium Sensitizer for Thin-Film Dye-Sensitized Solar Cells.* Acs Nano, 2009. **3**(10): p. 3103-3109.

45. Clifford, J.N., et al., *Sensitizer molecular structure-device efficiency relationship in dye sensitized solar cells.* Chemical Society Reviews, 2011. **40**(3): p. 1635-1646.

46. Imahori, H., T. Umeyama, and S. Ito, *Large pi-Aromatic Molecules as Potential Sensitizers for Highly Efficient Dye-Sensitized Solar Cells.* Accounts of Chemical Research, 2009. **42**(11): p. 1809-1818.

47. Mishra, A., M.K.R. Fischer, and P. Bäuerle, *Metal-Free Organic Dyes for Dye-Sensitized Solar Cells: From Structure: Property Relationships to Design Rules.* Angewandte Chemie International Edition, 2009. **48**(14): p. 2474-2499.

48. Horiuchi, T., et al., *High Efficiency of Dye-Sensitized Solar Cells Based on Metal-Free Indoline Dyes.* Journal of the American Chemical Society, 2004. **126**(39): p. 12218-12219.

49. Horiuchi, T., H. Miura, and S. Uchida, *Highly efficient metal-free organic dyes for dye-sensitized solar cells.* Journal of Photochemistry and Photobiology A: Chemistry, 2004. **164**(1–3): p. 29-32.

50. Horiuchi, T., H. Miura, and S. Uchida, *Highly-efficient metal-free organic dyes for dye-sensitized solar cells.* Chemical Communications, 2003. **0**(24): p. 3036-3037.

51. Ito, S., et al., *High-conversion-efficiency organic dye-sensitized solar cells with a novel indoline dye.* Chemical Communications, 2008. **0**(41): p. 5194-5196.

52. Crabb, R.L. and F.C. Treble, *Thin Silicon Solar Cells For Large Flexible Arrays.* Nature, 1967. **213**(5082): p. 1223-&.

53. Matsuyama, T., et al., *Preparation Of High-quality n-type Poly-Si Films By The Solid-Phase Crystallization (SPC) Method.* Japanese Journal of Applied Physics Part 1-Regular Papers Short Notes & Review Papers, 1990. **29**(11): p. 2327-2331.

54. Rudmann, D., et al., *Na incorporation into Cu(In,Ga)Se_2 for high-efficiency flexible solar cells on polymer foils.* Journal of Applied Physics, 2005. **97**(8): p. 084903-5.

55. Kessler, F. and D. Rudmann, *Technological aspects of flexible CIGS solar cells and modules.* Solar Energy, 2004. **77**(6): p. 685-695.

56. Herz, K., et al., *Dielectric barriers for flexible CIGS solar modules.* Thin Solid Films, 2002. **403–404**(0): p. 384-389.

57. Dhere, N.G., et al., *CIGS2 thin-film solar cells on flexible foils for space power.* Progress in Photovoltaics: Research and Applications, 2002. **10**(6): p. 407-416.

58. Tiwari, A.N., et al., *12.8% Efficiency Cu(In,Ga)Se_2 solar cell on a flexible polymer sheet.* Progress in Photovoltaics: Research and Applications, 1999. **7**(5): p. 393-397.

59. Birkmire, R., et al., *Cu(InGa)Se2 solar cells on a flexible polymer web.* Progress in Photovoltaics: Research and Applications, 2005. **13**(2): p. 141-148.

60. Krebs, F.C., *Fabrication and processing of polymer solar cells: A review of printing and coating techniques.* Solar Energy Materials and Solar Cells, 2009. **93**(4): p. 394-412.

61. Krebs, F.C., S.A. Gevorgyan, and J. Alstrup, *A roll-to-roll process to flexible polymer solar cells: model studies, manufacture and operational stability studies.* Journal of Materials Chemistry, 2009. **19**(30): p. 5442-5451.

62. Hagfeldt, A., et al., *A system approach to molecular solar cells.* Coordination Chemistry Reviews, 2004. **248**(13-14): p. 1501-1509.

63. Ito, S., et al., *High-efficiency (7.2%) flexible dye-sensitized solar cells with Ti-metal substrate for nanocrystalline-TiO_2 photoanode.* Chemical Communications, 2006. **0**(38): p. 4004-4006.

64. Pichot, F., J.R. Pitts, and B.A. Gregg, *Low-temperature sintering of TiO_2 colloids: Application to flexible dye-sensitized solar cells.* Langmuir, 2000. **16**(13): p. 5626-5630.

65. Uchida, S., et al., *Flexible dye-sensitized solar cells by 28 GHz microwave irradiation.* Journal of Photochemistry and Photobiology a-Chemistry, 2004. **164**(1-3): p. 93-96.

66. Park, N.G., et al., *Chemical sintering of nanoparticles: A methodology for low-temperature fabrication of dye-sensitized TiO_2 films.* Advanced Materials, 2005. **17**(19): p. 2349-+.

67. Weerasinghe, H.C., et al., *Low temperature chemically sintered nano-crystalline TiO_2 electrodes for flexible dye-sensitized solar cells.* Journal of Photochemistry and Photobiology A: Chemistry, 2010. **213**(1): p. 30-36.

68. Zhang, D.S., T. Yoshida, and H. Minoura, *Low-temperature fabrication of efficient porous titania photoelectrodes by hydrothermal crystallization at the solid/gas interface.* Advanced Materials, 2003. **15**(10): p. 814-+.

69. Oekermann, T., et al., *Electron transport and back reaction in nanocrystalline TiO_2 films prepared by hydrothermal crystallization.* Journal of Physical Chemistry B, 2004. **108**(7): p. 2227-2235.

70. Zhang, D.S., et al., *Room-temperature synthesis of porous nanoparticulate TiO_2 films for flexible dye-sensitized solar cells.* Advanced Functional Materials, 2006. **16**(9): p. 1228-1234.

71. Kijitori, Y., M. Ikegami, and T. Miyasaka, *Highly efficient plastic dye-sensitized photoelectrodes prepared by low-temperature binder-free coating of mesoscopic titania pastes.* Chemistry Letters, 2007. **36**(1): p. 190-191.

72. Fan, K., et al., *A novel preparation of small TiO_2 nanoparticle and its application to dye-sensitized solar cells with binder-free paste at low temperature.* Nanoscale, 2011. **3**(9): p. 3900-3906.

73. Liu, X.Z., et al., *Room Temperature Fabrication of Porous ZnO Photoelectrodes for Flexible Dye-sensitized Solar Cells.* Chemical Communications, 2007(27): p. 2847-2849.

74. Salant, A., et al., *Quantum Dot Sensitized Solar Cells with Improved Efficiency Prepared Using Electrophoretic Deposition.* Acs Nano, 2010. **4**(10): p. 5962-5968.

75. Karousis, N., et al., *Graphene oxide with covalently linked porphyrin antennae: Synthesis, characterization and photophysical properties.* Journal of Materials Chemistry, 2011. **21**(1): p. 109-117.

76. Shi, W.Y., et al., *Optical pH Sensor with Rapid Response Based on a Fluorescein-Intercalated Layered Double Hydroxide.* Advanced Functional Materials, 2010. **20**(22): p. 3856-3863.

77. Boccaccini, A.R., et al., *Electrophoretic deposition of biomaterials.* Journal of the Royal Society Interface, 2010. **7**: p. S581-S613.

78. Corni, I., M.P. Ryan, and A.R. Boccaccini, *Electrophoretic deposition: From traditional ceramics to nanotechnology.* Journal of the European Ceramic Society, 2008. **28**(7): p. 1353-1367.

79. Grinis, L., et al., *Electrophoretic deposition and compression of titania nanoparticle films for dye-sensitized solar cells.* Journal of Photochemistry and Photobiology a-Chemistry, 2008. **198**(1): p. 52-59.

80. Panigrahi, S., et al., *Electrophoretic deposition of doped ceria: Effect of solvents on deposition microstructure.* Journal of the European Ceramic Society, 2010. **30**(5): p. 1097-1103.

81. Miyasaka, T., et al., *Fabrication of dye-sensitized plastic film electrodes for flexible solar cells based on electrophoretic deposition techniques*, in *Organic Photovoltaics Iv*, Z.H. Kafafi and P.A. Lane, Editors. 2004, Spie-Int Soc Optical Engineering: Bellingham. p. 219-225.

82. Yum, J.-H., et al., *Electrophoretically deposited TiO_2 photo-electrodes for use in flexible dye-sensitized solar cells.* Journal of Photochemistry and Photobiology A: Chemistry, 2005. **173**(1): p. 1-6.

83. Tan, W.W., et al., *Preparation of nanocrystalline TiO_2 thin film at low temperature and its application in dye-sensitized solar cell.* Journal of Solid State Electrochemistry, 2009. **13**(5): p. 651-656.

84. Chiu, W.H., K.M. Lee, and W.F. Hsieh, *High efficiency flexible dye-sensitized solar cells by multiple electrophoretic depositions.* Journal of Power Sources, 2011. **196**(7): p. 3683-3687.

85. Yin, X., Z.S. Xue, and B. Liu, *Electrophoretic deposition of Pt nanoparticles on plastic substrates as counter electrode for flexible dye-sensitized solar cells.* Journal of Power Sources, 2011. **196**(4): p. 2422-2426.

86. Nath, N.C.D., et al., *Carbon Nanotubes on Fluorine-Doped Tin Oxide for Fabrication of Dye-Sensitized Solar Cells at Low Temperature Condition.* Journal of Nanoscience and Nanotechnology, 2012. **12**(7): p. 5373-5380.

87. Zhu, G., et al., *Electrophoretic deposition of carbon nanotubes films as counter electrodes of dye-sensitized solar cells.* Electrochimica Acta, 2011. **56**(27): p. 10288-10291.

88. Zhu, G., et al., *Electrophoretic deposition of reduced graphene-carbon nanotubes composite films as counter electrodes of dye-sensitized solar cells.* Journal of Materials Chemistry, 2011. **21**(38): p. 14869-14875.

89. Lindström, H., et al., *A New Method for Manufacturing Nanostructured Electrodes on Plastic Substrates.* Nano Letters, 2001. **1**(2): p. 97-100.

90. Zhao, X., et al., *The effect of compression on electron transport and recombination in plastic TiO_2 photoanodes.* Electrochimica Acta, 2011. **56**(18): p. 6401-6405.

91. Boschloo, G., et al., *Optimization of dye-sensitized solar cells prepared by compression method.* Journal of Photochemistry and Photobiology a-Chemistry, 2002. **148**(1-3): p. 11-15.

92. Yamaguchi, T., et al., *Highly efficient plastic-substrate dye-sensitized solar cells with validated conversion efficiency of 7.6%.* Solar Energy Materials and Solar Cells, 2010. **94**(5): p. 812-816.

93. Yamaguchi, T., et al., *Highly efficient plastic substrate dye-sensitized solar cells using a compression method for preparation of TiO_2 photoelectrodes.* Chemical Communications, 2007(45): p. 4767-4769.

94. Chen, H.W., et al., *Plastic dye-sensitized photo-supercapacitor using electrophoretic deposition and compression methods.* Journal of Power Sources, 2010. **195**(18): p. 6225-6231.

95. Chen, H.W., et al., *Electrophoretic deposition of ZnO film and its compression for a plastic based flexible dye-sensitized solar cell.* Journal of Power Sources, 2011. **196**(10): p. 4859-4864.

96. Yin, X., et al., *High-Performance Plastic Dye-sensitized Solar Cells Based on Low-Cost Commercial P25 TiO_2 and Organic Dye.* Acs Applied Materials & Interfaces, 2012. **4**(3): p. 1709-1715.

97. Chen, H.W., et al., *Electrophoretic deposition of mesoporous TiO_2 nanoparticles consisting of primary anatase nanocrystallites on a plastic substrate for flexible dye-sensitized solar cells.* Chemical Communications, 2011. **47**(29): p. 8346-8348.

98. Durr, M., et al., *Low-temperature fabrication of dye-sensitized solar cells by transfer of composite porous layers.* Nature Materials, 2005. **4**(8): p. 607-611.

99. Longo, C., et al., *Solid-state and flexible dye-sensitized TiO_2 solar cells: a study by electrochemical impedance spectroscopy.* Journal of Physical Chemistry B, 2002. **106**(23): p. 5925-5930.

100. Yanagida, S., Y.H. Yu, and K. Manseki, *Iodine/Iodide-Free Dye-Sensitized Solar Cells.* Accounts of Chemical Research, 2009. **42**(11): p. 1827-1838.

101. de Freitas, J.N., A.F. Nogueira, and M.A. De Paoli, *New insights into dye-sensitized solar cells with polymer electrolytes.* Journal of Materials Chemistry, 2009. **19**(30): p. 5279-5294.

102. Yum, J.H., et al., *Recent Developments in Solid-State Dye-Sensitized Solar Cells.* Chemsuschem, 2008. **1**(8-9): p. 699-707.

103. Zhang, W., et al., *Solid-State Dye-Sensitized Solar Cells with Conjugated Polymers as Hole-Transporting Materials.* Macromolecular Chemistry and Physics, 2011. **212**(1): p. 15-23.

104. Bach, U., et al., *Solid-state Dye-sensitized Mesoporous TiO_2 Solar Cells With High Photon-to-electron Conversion Efficiencies.* Nature, 1998. **395**(6702): p. 583-585.

105. Schmidt-Mende, L. and M. Grätzel, *TiO_2 pore-filling and its effect on the efficiency of solid-state dye-sensitized solar cells.* Thin Solid Films, 2006. **500**(1–2): p. 296-301.

106. Li, B., et al., *Review of recent progress in solid-state dye-sensitized solar cells.* Solar Energy Materials and Solar Cells, 2006. **90**(5): p. 549-573.

107. Etgar, L., et al., *Mesoscopic $CH_3NH_3PbI_3/TiO_2$ Heterojunction Solar Cells.* Journal of the American Chemical Society, 2012. **134**(42): p. 17396-17399.

108. Chung, I., et al., *All-solid-state dye-sensitized Solar Cells With High Efficiency.* Nature, 2012. **485**(7399): p. 486-489.

109. Yum, J.-H., et al., *Effect of Coadsorbent on the Photovoltaic Performance of Zinc Pthalocyanine-Sensitized Solar Cells.* Langmuir, 2008. **24**(10): p. 5636-5640.

110. Kim, H.S., et al., *Lead Iodide Perovskite Sensitized All-Solid-State Submicron Thin Film Mesoscopic Solar Cell with Efficiency Exceeding 9%.* Scientific Reports, 2012. **2**.

111. Lee, M.M., et al., *Efficient Hybrid Solar Cells Based on Meso-Superstructured Organometal Halide Perovskites.* Science, 2012. **338**(6107): p. 643-647.

112. Burschka, J., et al., *Sequential Deposition as a Route to High-performance Perovskite-sensitized Solar Cells.* Nature, 2013.

113. Zhang, W., et al., *Solid-State Dye-Sensitized Solar Cells with Conjugated Polymers as Hole-Transporting Materials.* Macromolecular Chemistry and Physics, 2011. **212**(1): p. 15-23.

114. Tan, S.X., et al., *Polyaniline as Hole Transport Material to Prepare Solid Solar Cells.* Synthetic Metals, 2003. **137**(1–3): p. 1511-1512.

115. Tan, S., et al., *Property Influence of Polyanilines on Photovoltaic Behaviors of Dye-Sensitized Solar Cells.* Langmuir, 2004. **20**(7): p. 2934-2937.

116. Tan, S., et al., *Influence of Small Molecules in Conducting Polyaniline on the Photovoltaic Properties of Solid-State Dye-Sensitized Solar Cells.* The Journal of Physical Chemistry B, 2004. **108**(48): p. 18693-18697.

117. Murakoshi, K., et al., *Fabrication of solid-state dye-sensitized TiO_2 solar cells combined with polypyrrole.* Solar Energy Materials and Solar Cells, 1998. **55**(1–2): p. 113-125.

118. Kitamura, T., et al., *Improved solid-state dye solar cells with polypyrrole using a carbon-based counter electrode.* Chemistry Letters, 2001(10): p. 1054-1055.

119. Murakoshi, K., et al., *Solid state dye-sensitized TiO_2 solar cell with polypyrrole as hole transport layer.* Chemistry Letters, 1997(5): p. 471-472.

120. Poplavskyy, D. and J. Nelson, *Nondispersive Hole Transport in Amorphous Films of Methoxy-spirofluorene-arylamine Organic Compound.* Journal of Applied Physics, 2003. **93**(1): p. 341-346.

121. Takahashi, K., et al., *Performance enhancement by blending merocyanine photosensitizer in TiO_2/polythiophen solid-state solar cells.* Chemistry Letters, 2005. **34**(5): p. 714-715.

122. Zhu, R., et al., *Highly Efficient Nanoporous TiO2-Polythiophene Hybrid Solar Cells Based on Interfacial Modification Using a Metal-Free Organic Dye.* Advanced Materials, 2009. **21**(9): p. 994-1000.

123. Zhang, W., et al., *High-Performance Solid-State Organic Dye Sensitized Solar Cells with P3HT as Hole Transporter.* Journal of Physical Chemistry C, 2011. **115**(14): p. 7038-7043.

124. Chang, J.A., et al., *High-Performance Nanostructured Inorganic−Organic Heterojunction Solar Cells.* Nano Letters, 2010. **10**(7): p. 2609-2612.

125. Bi, D.Q., et al., *Effect of Different Hole Transport Materials on Recombination in $CH_3NH_3PbI_3$ Perovskite-Sensitized Mesoscopic Solar Cells.* Journal of Physical Chemistry Letters, 2013. **4**(9): p. 1532-1536.

126. Heo, J.H., et al., *Efficient inorganic-organic hybrid heterojunction solar cells containing perovskite compound and polymeric hole conductors.* Nature Photonics, 2013. **7**(6): p. 487-492.

127. Xia, J., et al., *Influence of Doped Anions on Poly(3,4-ethylenedioxythiophene) as Hole Conductors for Iodine-Free Solid-State Dye-Sensitized Solar Cells.* Journal of the American Chemical Society, 2008. **130**(4): p. 1258-1263.

128. Saito, Y., et al., *Solid state dye sensitized solar cells using in situ polymerized PEDOTs as hole conductor.* Electrochemistry Communications, 2004. **6**(1): p. 71-74.

129. Groenendaal, L., et al., *Poly(3,4-ethylenedioxythiophene) and Its Derivatives: Past, Present, and Future.* Advanced Materials, 2000. **12**(7): p. 481-494.

130. Liu, X., et al., *An Efficient Organic-Dye-Sensitized Solar Cell with in situ Polymerized Poly(3,4-ethylenedioxythiophene) as a Hole-Transporting Material.* Advanced Materials, 2010. **22**(20): p. E150-E155.

131. Liu, X., et al., *Light controlled assembling of iodine-free dye-sensitized solar cells with poly(3,4-ethylenedioxythiophene) as a hole conductor reaching 7.1% efficiency.* Physical Chemistry Chemical Physics, 2012. **14**(19): p. 7098-7103.

Chapter 2 Enhanced Conversion Efficiency for Flexible Dye-Sensitized Solar Cells by Optimization of Nanoparticle Size with Electrophoretic Deposition Technique

2.1 Introduction

Electrophoretic deposition (EPD) is a widely used method to produce thin films for application in dye DSSCs[1-6]. In a typical EPD process, particles to be deposited are suspended in a solvent to form a stable colloid. Two electrodes are inserted into the colloidal suspension and a potential difference is applied across the electrodes. Charged particles in the suspension are attracted to the electrodes *via* electrostatic attraction thereby forming uniform thin films. EPD can be done at room temperature and hence suitable for plastic substrates which cannot be heated beyond 150^{o}C. EPD have the advantages of good uniformity of the films formed and the ease of scaling up for mass manufacturing. In addition, EPD can be done without any organic binders and additives and hence there is no need for any high temperature sintering process. Of particular importance is that the process only takes a few minutes[7] and the film thickness can be controlled easily by tuning the operating voltage, current, concentration of particles in colloids and the deposition time.

Though EPD is a common technique used in low temperature DSSC fabrication, the influence of nanoparticle size on device performance is not well studied. Though similar nanoparticle size-efficiency studies have been done for conventional high temperature DSSCs[8-11], the high temperature sintering process would have introduced physical changes such as pore size distribution, porosity and grain size of the particles to the films which may render the studies irrelevant to low temperature DSSCs. In particular, electron transport and recombination will be greatly affected by the absence of sintering of TiO_2 in DSSCs fabricated *via* EPD. As EPD is an

important technique that could be used for large scale photoanode fabrication for DSSCs, it is of importance to optimize the efficiency of DSSCs fabricated using EPD through studying the effect of nanoparticle size on device performance.

In this chapter, D149 dye is selected as the sensitizer because it has a large light absorption coefficient, high power conversion efficiencies in traditional DSSCs [12, 13] and can be easily synthesized in a large quantity without resource limitations unlike Ru based dyes. The chemical structure and UV absorption of D149 dye on TiO_2 are shown in Figure 2.1. In this chapter, TiO_2 nanoparticles with varied size are synthesized and used in the low temperature fabrication of DSSC *via* EPD. The effect of nanoparticle size on device performance is systematically studied. This study will help in the optimization of DSSC efficiency made from non-sintered TiO_2 films.

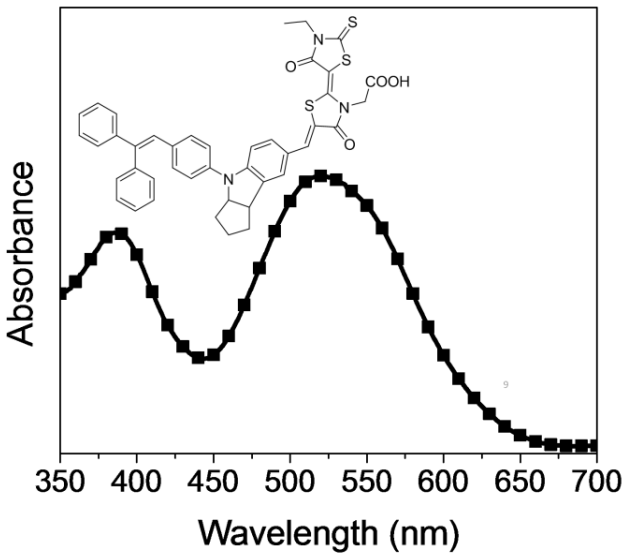

Figure 2.1 Chemical structure and UV absorption spectrum of D149 when adsorbed on a thin film of TiO_2 from a solution of acetonitrile/*tert*-butylalcohol (V/V = 1:1).[14]

2.2 Experimental Section

2.2.1 Materials

All chemicals were used as received with no further purification. Acetic acid and concentrated nitric acid were purchased from Merck. Titanium tetraisopropoxide, tetraethyl ammonium hydroxide, chenodeoxycholic acid, hexachloroplatinic acid, *tert*-butylalcohol, tetrabutylammonium iodide, lithium perchlorate, 4-*tert*-butylpyridine and iodine were purchased from Sigma Aldrich. All solvents used were of AR grade and were obtained from either Aldrich or Tedia. FTO glass substrates were available from Hartford Glass. Plastic PEN-ITO substrates were purchased from Peccell Technologies. P25 TiO_2 nanoparticles were kindly gifted by Degussa. The D149 dye was from Mitsubishi Paper Mills. 25 μm thick spacer was obtained from Solaronix.

2.2.2 Synthesis of nanoparticles

The synthesis of the various TiO_2 nanoparticles was performed using modified literature procedures.[15, 16] The general procedure is described as follows and the exact amount of each reagent used is shown in Table 2.1.

3.6 g (0.06 mol) of CH_3COOH was added to 17.6 g of titanium tetraisopropoxide and the mixture was stirred at room temperature for 15 min. The mixture was then poured into 90 mL of deionized water while stirring rapidly to prevent aggregation. The resultant milky white suspension was stirred for 1 h at room temperature. Varying amount of concentrated HNO_3 or tetraethyl ammonium hydroxide (TEAH) was added to prepare TiO_2 nanoparticles with different sizes. After that, the suspension was heated to 80 ^oC and allowed to react for another 75 min. Upon cooling to room temperature, the total volume was made up to 110 mL by adding

deionized water. The suspension was transferred to a stainless steel autoclave and heated at varying temperatures and times to yield nanoparticles of different sizes. Upon cooling, varying amount of concentrated HNO_3 was added as a post treatment step. The mixture was sonicated for 30 min before centrifugation. Deionized water was added to the sediment and the sonication/centrifuge process was repeated. The washing process was repeated until the pH of the resultant supernatant reached 7.0. The washing process was then repeated with ethanol for 3 times before drying the nanoparticles at 70 ^{o}C. The TiO_2 flakes were subsequently made into powders by grinding with a set of mortar and pestle.

2.2.3 Nanoparticle characterization

The morphology of TiO_2 nanoparticles was studied using a Transmission Electron Microscope (JEOL JEM-2100F). 2-3 mg of TiO_2 powder was suspended in 10 mL of ethanol and sonicated for 10 min. A drop of this suspension was casted onto a standard TEM copper grid. Morphology of the TiO_2 films was viewed using Field Emission Scanning Electron Microscope (FESEM, JEOL) after sputtering with platinum. Crystal structure and crystallite size was determined by X-Ray Diffraction (Shiamadzu XRD-6000). The working voltage and current were 40 kV and 20 mA, respectively. The powdered sample was placed on an aluminum substrate. Scan rate was set at 2 degrees per minute and the scanning range was set at 10 to 80 degrees. Zeta potential studies on different suspensions were performed in a DTS1060 capillary cell (Malvern) using a Zetasizer, (Nanoseries, Malvern Instruments, Malvern, U.K.). 1-2 mg of TiO_2 nanoparticle was suspended in 10 mL of a mixture of ethanol, isopropanol and butanol (V/V/V = 1:2:4) and sonicated for 30 min. The suspension was acidified with HNO_3 until pH of about 3.0 – 4.0 before injected into the sample cell using a syringe.

2.2.4 Preparation of photoanodes by EPD

The TiO_2 suspension for EPD was prepared by mixing 0.5 g of TiO_2 powder with 15 mL of a mixture of ethanol, isopropanol and butanol (V/V/V = 1:2:4), which was followed by ultrasonication for 30 min. Before the EPD process, the colloidal suspension was acidified to a pH of about 3.0 – 4.0 with HNO_3. A pair of FTO glass substrates (2 cm × 2.5 cm, 15 Ω sq^{-1}) or plastic PEN-ITO substrates (2 cm × 2.5 cm, 15 Ω sq^{-1}) were vertically immersed in the suspension. The distance between each pair of substrates was kept at 7 mm and the DC power supply was set at 30 V for a constant voltage EPD process. The thickness of the resultant film was controlled by the deposition time. The freshly coated films were left to dry in air before heated at 100 ^{o}C for 30 min for low temperature annealing and to ensure all solvent from the EPD process was removed.

2.2.5 DSSC assembly

The prepared photoanodes were subsequently subjected to a pressure of 1 ton/cm^2 (Atlas Manual 15T Hydraulic Press) for 2 min to improve the interparticle adhesion and electrical connectivity[11]. As a result of the pressing process, the thickness of the films was reduced. The photoanodes were heated at 70 °C for 30 min before immersing into a 0.5 mM D149 dye solution in acetonitrile/*tert*-butylalcohol (V/V = 1:1) with 0.5 mM chenodeoxy cholic acid as co-adsorbant for 2 h. The photoanodes were subsequently rinsed with acetonitrile and left to dry in the dark.

The rigid Pt counter electrode was prepared by spin-coating a 30 mM H_2PtCl_6 solution in isopropanol on a FTO glass substrate, followed by thermal decomposition at 400 °C for 15 min. The flexible Pt counter electrode was fabricated by sputtering Pt (20 mA for 120 s) on the PEN-ITO substrate by JEOL JFC-1600 Auto Fine Coater. DSSCs were fabricated by sandwiching a TiO_2 photoanode and a Pt counter electrode with electrolyte in a 25 μm thick spacer. The

electrolyte used has a composition of 0.5 M tetrabutylammonium iodide, 0.001 M $LiClO_4$, 0.5 M 4-*tert*-butylpyridine and 0.1 M I_2 in 3-methyoxypropionitrile. The active area of the cell was 0.16 cm^2, controlled by a metal mask.

2.2.6 Determination of dye loading

A TiO_2 film was prepared on a glass substrate by EPD as described above. An area of 30 mm^2 (5 mm × 6 mm) was immersed into a D149 dye solution of 0.5 mM in acetonitrile/*tert*-butylalcohol (V/V = 1:1) with 1 mM chenodeoxycholic acid as co-adsorbant for 2 h. The sensitized photoanode was soaked in a solution of ammonia in DMSO (0.1 M) for 30 min for dye desorption. After complete desorption, the UV-Vis absorption spectrum (Shimadzu) of the resultant solution was measured at 526 nm, the absorption maximum of the dye. The dye loading was calculated from the molar extinction of D149 (6.8×10^4 $M^{-1}cm^{-1}$ at 526 nm) using Beer-Lambert's law. The dye loading data reported were an average of 3 samples.

2.2.7 Photovoltaic measurements

The photovoltaic parameters of DSSCs were studied an AutoLAB PGSTAT 320 N Potentiostat with a solar simulator (XES-151S, San-EI Electric). The incident light was filtered with an AM1.5 filter (Asahi Spectra) and calibrated with a silicon reference cell (OptoPolymer, ISE CalLab) before each experiment

The intensity modulated photocurrent spectroscopy (IMPS) and intensity modulated photovoltage spectroscopy (IMVS) measurements were carried out using an AutoLAB PGSTAT 320 N Potentiostat with a green light emitting diode (λ = 530 nm).

2.3 Results and Discussion

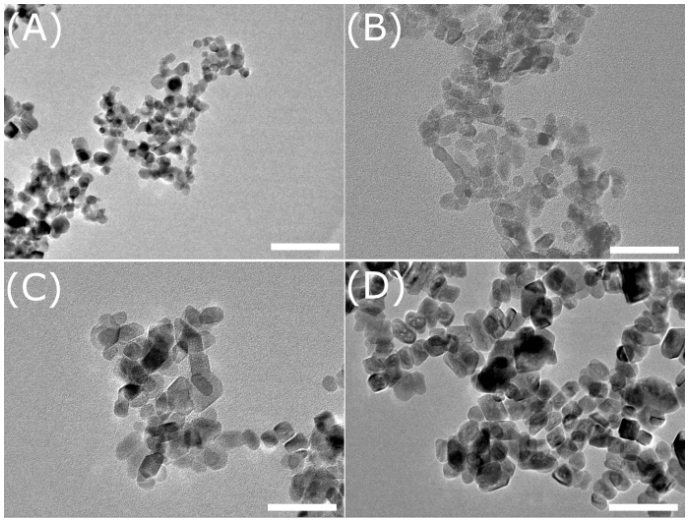

Figure 2.2 TEM images of the synthesized TiO_2 nanoparticles. (A) ~ 10 nm, (B) ~ 14 nm, (C) ~ 19 nm, (D) ~ 27 nm. Scale bar represents 50 nm.[14]

Four different batches of TiO_2 nanoparticles were synthesized by varying the reaction temperature, reaction time and peptization agent. The transmission electron microscopy (TEM) images of the synthesized nanoparticles are shown in Figure 2.2. The nanoparticles have a slightly elongated shape. The average particle size under TEM is determined by measuring and averaging both long and short end to end distances of dozens of particles. The sizes of the nanoparticles estimated from the TEM images are 11 ± 2, 15 ± 2, 20 ± 3 and 29 ± 4 nm, respectively, which indicate that longer peptization time and higher peptization temperature lead to larger nanoparticles.

X-ray Diffraction (XRD) was performed to determine the crystal phase of the synthesized TiO_2 nanoparticles. Figure 2.3 shows that all the synthesized nanoparticles are in pure anatase crystal phase. From the XRD results, the crystallite sizes of the synthesized nanoparticles are 10, 14, 19 and 27 nm, respectively, determined based on (101) peaks ($2\theta = 25.3^{o}$) using Scherrer equation:

$$\tau = \frac{0.9\lambda}{\beta cos\theta}$$

Where τ is the crystallite size (in Å), λ is the wavelength of radiation used (1.54056 Å for Cu $K_{\alpha 1}$), β is the width of the peak at half maximum intensity (in radians) and θ is the diffracted angle at maximum intensity (in radians). The crystallite sizes calculated from Scherrer equation generally agree with that observed under the TEM. The crystallite size of the nanoparticles determined *via* the Scherrer equation and the nanoparticle size determined using the TEM are summarized in Table 2.1.

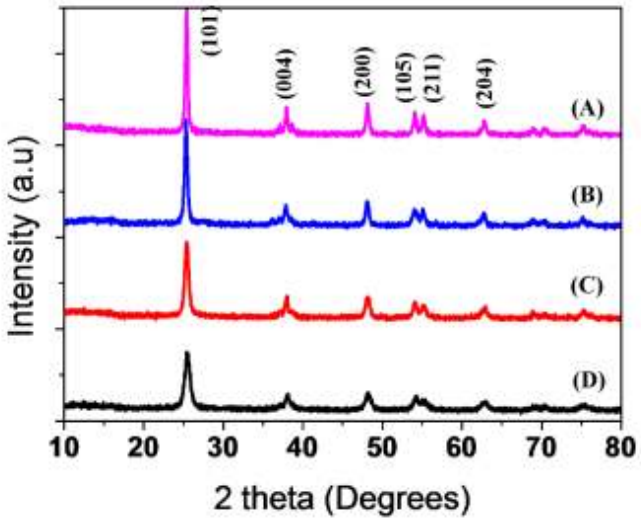

Figure 2.3 XRD spectra of TiO_2 nanoparticles. (A) ~ 27 nm, (B) ~ 19 nm, (C) ~ 14 nm, (D) ~ 10 nm. Peaks of anatase are labeled. No change was observed after compression at 1 ton/cm^2. [14]

The synthesized nanoparticles, after treatment with acid, have zeta potentials of ~+25 mV in the alcohol mixture (n-butanol:isopropanol:ethanol v/v/v = 4:2:1) used in the EPD process. The sign of charge present on the TiO_2 nanoparticle is pH dependent and under acidic conditions, positive charges are induced. [17] Due to the positive charges present on the nanoparticle surface, the colloidal suspensions were relatively stable during the EPD process. As EPD utilizes electrostatic attraction for particle deposition, the positive charges favor their direct utilization in

the EPD process without any further additives or surface modifications which are common for particles lacking surface charges.[18]

Table 2.1 Synthesis conditions for various sized TiO_2 nanoparticles using hydrothermal method [14]

Samples	Crystallite Size [a]	Particle Size [b]	Peptizing Agent	Peptization Temperature	Peptization Time	Post Treatment
A	10 nm	11±2 nm	1.2 mL Conc. HNO_3	200 ^oC	12 h	1.2 mL
B	14 nm	15±2 nm	1.2 mL Conc. HNO_3	250 ^oC	15 h	1.2 mL
C	19 nm	20±3 nm	3.6 mL Conc. HNO_3	250 ^oC	12 h	3.6 mL
D	27 nm	29±4 nm	22 mL 20 wt% TEAH solution	200 ^oC	5 h	5.0 mL

[a] According to the Scherr Equation;

[b] According to TEM.

The films made from EPD followed by compression process were mechanically stable and robust. The film, when formed on a flexible plastic substrate, can be bent easily without mechanically destroying the film. This is unlike unprocessed EPD films that need to be handled delicately in order to preserve the mechanical integrity of the film. To study the difference in film morphology brought about by compression, the films before and after compression were viewed under the FESEM. Figure 2.4(A) shows clearly that the unpressed EPD film fabricated from 19 nm TiO_2 nanoparticles had visible micropores and the interparticle connectivity is poor. After compression, however, it is clearly seen in Figure 2.4(B) that the interparticle connection

has been improved and less interparticle pores can be observed. The FESEM images indicate that compression treatment can reduce local interparticle pores and improve interparticle connectivity. In addition, the film thickness was reduced by the compression process, indicating that void spaces within the uncompressed film have been significantly reduced and the nanoparticles within the film were in closer contact after compression. The films fabricated using the other nanoparticles showed the same observations as well. In addition to the FESEM studies, the effect of compression on the crystal phase of the particles was also studied. Moreover, XRD did not show any change in crystal phase and crystallite size in the pressed samples.

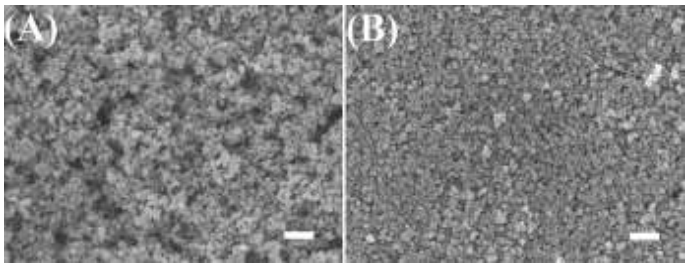

Figure 2.4 FESEM images of (A) – as prepared EPD film from 19 nm TiO_2 nanoparticles. (B) - after compression on PEN substrates. Scale bar represents 100 nm. [14]

The devices had a sandwiched structure in which the D149 sensitized photoanode and the Pt counter electrode were clipped together. A 25 μm spacer (Solaronix) was used to prevent short circuiting of the cell. A few drops of the electrolyte containing 0.5 M tetrabutylammonium iodide, 0.001 M $LiClO_4$, 0.5 M 4-*tert*-butylpyridine and 0.1 M I_2 in 3-methyoxypropionitrile was introduced to complete cell assembly.

The effect of TiO_2 film thickness on device performance was first investigated for each of the nanoparticles. The post compression thickness was controlled to be ~4, ~8, ~11 and ~15 μm. The changes in open circuit voltage (V_{oc}), short-circuit current density (J_{sc}), fill factor (FF) and overall efficiency (η) with TiO_2 film thickness are shown in Table 2.2-Table 2.5.

Table 2.2 Photovoltaic parameters of D149-sensitized solar cells fabricated from 10 nm nanoparticles on rigid glass substrate[14]

Particle Size	**Film Thickness (μm)**	**Photovoltaic Properties** [a]			
		V_{oc} (V)	**J_{sc} (mA cm^{-2})**	**FF**	**η (%)**
10 nm	4	0.79	9.3	0.64	4.8
	8	0.77	10.6	0.64	5.3
	11	0.75	10.2	0.64	5.1
	15	0.75	10.1	0.64	4.9

[a] measured under AM 1.5G (100 $mWcm^{-2}$)

Table 2.3 Photovoltaic parameters of D149-sensitized solar cells fabricated from 14 nm nanoparticles on rigid glass substrate[14]

Particle Size	**Film Thickness (μm)**	**Photovoltaic Properties** [a]			
		V_{oc} (V)	**J_{sc} (mA cm^{-2})**	**FF**	**η (%)**
14 nm	4	0.80	6.2	0.65	3.2
	8	0.79	10.7	0.63	5.4
	11	0.78	10.9	0.63	5.3
	15	0.77	10.5	0.63	5.3

[a] measured under AM 1.5G (100 $mWcm^{-2}$)

Table 2.4 Photovoltaic parameters of D149-sensitized solar cells fabricated from 19 nm nanoparticles on rigid glass substrate.[14]

Particle Size	**Film Thickness (μm)**	**Photovoltaic Properties** [a]			
		V_{oc} (V)	**J_{sc} (mA cm^{-2})**	**FF**	**η (%)**
19 nm	4	0.81	10.6	0.65	5.3
	8	0.79	12.4	0.65	6.2
	11	0.79	14.3	0.65	7.0
	15	0.78	10.7	0.65	5.6

[a] measured under AM 1.5G (100 mWcm^{-2})

Table 2.5 Photovoltaic parameters of D149-sensitized solar cells fabricated from 27 nm nanoparticles on rigid glass substrate[14]

Particle Size	**Film Thickness (μm)**	**Photovoltaic Properties** [a]			
		V_{oc} (V)	**J_{sc} (mA cm^{-2})**	**FF**	**η (%)**
27 nm	4	0.85	8.6	0.68	4.5
	8	0.85	9.0	0.68	4.7
	11	0.84	9.2	0.68	5.3
	15	0.83	8.0	0.63	4.1

[a] measured under AM 1.5G (100 mWcm^{-2})

The best performing devices fabricated using different TiO_2 nanoparticles have different TiO_2 thicknesses. For 10 nm and 14 nm nanoparticles, their corresponding devices performed optimally at a post compression film thickness of ~ 8 μm. For the larger 19 nm and 27 nm nanoparticles, the optimal film thickness was ~ 11 μm. The J-V curves of the best performing devices for each individual nanoparticle are shown in Figure 2.5 and the corresponding photovoltaic parameters are shown in Table 2.6. For the optimized devices, the V_{oc} of the devices increased from 0.77 to 0.85 V when nanoparticle size was increased from 10 nm to 27 nm. The J_{sc} of the devices increased from 10.6 to 14.3 mA/cm^2 when the nanoparticle size was increased from 10 nm to 19 nm. When the size of the nanoparticle was further increased to 27 nm, the J_{sc} decreased to 9.2 mA/cm^2. The FF of the devices was between 0.63 to 0.68. The best performing device fabricated using 10, 14, 19 and 27 nm nanoparticle yielded efficiencies of 5.3%, 5.4%, 7.0% and 5.3% respectively.

The V_{oc} of a device is determined by a number of factors,[19] namely Quasi Fermi level of the semiconductor, HOMO level of redox couple (E_{redox}), light harvesting and electron injection of sensitizer and the frequency of recombination events within the cell. Since the semiconductor, sensitizer and electrolyte used in this study are the same for all devices, the V_{oc} trend cannot be attributed to E_{redox} and the identity of the dye. Recombination is thus expected to play a key role in the observed trend in V_{oc}.

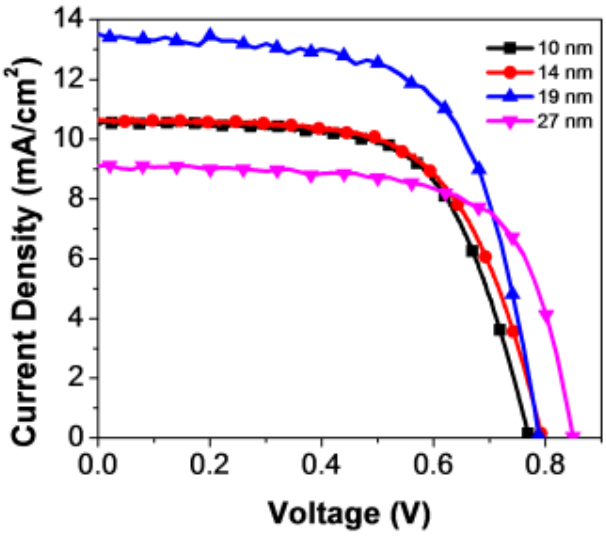

Figure 2.5 J-V curves for the best performing DSSCs fabricated on rigid glass substrates by EPD technique with compression post treatment. [14]

To understand the observed trend for V_{oc} of the devices made from different nanoparticles, intensity-modulated photovoltage (IMVS) was performed. The electron lifetime (τ_n) was calculated from the equation $\tau_n = 1/(2\pi f_{n,min})$,where $f_{n,min}$ is the characteristic frequency at the minimum of the IMVS imaginary component.[20] As shown in Figure 2.6A, electron lifetime increased from 5.7 ms to 10 ms when nanoparticle size was increased from 10 nm to 27 nm. As the electron lifetime calculated from the IMVS results is an indication of the number of recombination events, the longer electron lifetime for DSSCs with 27 nm nanoparticles as compared to that with 10 nm nanoparticles indicated that devices fabricated with larger particles undergo less recombination events. The IMVS results indicate that electron recombination has been reduced when larger nanoparticles are used and this contributes to a higher V_{oc} for the corresponding devices.

Table 2.6 Zeta potential of particles in the EPD process, photovoltaic properties and dye loading of D149-sensitized solar cells made from various sized nanoparticles on rigid glass substrate. [14]

Particle Size (nm)	Film Thickness (μm)	Zeta Potential [a] (mV)	Photovoltaic Properties [b]				Dye Loading [c]/ ($\times 10^{-7}$ mol cm^{-2})
			V_{oc} (V)	J_{sc} (mA cm^{-2})	FF	η (%)	
10	8	26.1	0.77	10.6	0.64	4.8	2.5
14	8	24.7	0.79	10.7	0.63	5.4	1.4
19	11	24.0	0.79	14.3	0.65	7.0	1.3
27	11	24.9	0.85	9.2	0.68	5.3	0.9

[a] measured in a mixture of ethanol, isopropanol and butanol (V/V/V=1:2:4);

[b] measured under AM 1.5G (100 mWcm^{-2});

[c] UV absorbance is measured in 0.1 M of aqueous NH_3 in DMSO

To check the contribution of dye loading on J_{sc} for each device, the desorbed dye solutions were measured with UV-absorption spectroscopy and the results are summarized in Table 2.6. It was found that nanoparticle size influences the dye loading significantly in our devices. For the thickness optimized devices, dye loading decreases from 2.5 to 0.9 × 10^{-7} M/cm^2 when the nanoparticle size was increased from 10 nm to 27 nm. Though dye loading is related to the device's ability to absorb incident light, the J_{sc} trend of the devices differs from the dye loading trend. This indicates that dye loading of the devices is not the sole determinant of the J_{sc} and overall device conversion efficiency.

In addition to dye loading, electron transport within the TiO_2 network could also play a part in determining the J_{sc} of the devices. To understand the electron transport within the photoanode fabricated from the differently sized TiO_2 nanoparticles at their optimized thickness, intensity modulated photocurrent spectroscopy (IMPS) was performed on the devices fabricated using the synthesized nanoparticles. The electron transport time (τ_d) was calculated from the equation τ_d =

$1/(2\pi f_{d,min})$, where $f_{d,min}$ is the characteristic frequency at the minimum of the IMPS imaginary component.[20] As shown in Figure 2.6B, electron transport time decreases from 3.2 to 1.2 ms when nanoparticle size was increased from 10 nm to 27 nm. Electron transport time is a measure of the average time taken for the collection of injected electrons and a faster electron time is associated with a higher photocurrent as it indicates that electrons hop across the TiO_2 network and gets collected at the photoanode at a faster rate.[21]

From the calculated τ_d and τ_n, charge collection efficiency can be calculated using the equation: $\eta_c = 1 - \tau_d/\tau_n$.[22] The calculated values of η_c are shown in Figure 2.6C. It is worthy to point out that the τ_d and τ_n are measured under short circuit and open circuit conditions and hence the derived η_c values are underestimates of the charge collection under working condition. The charge collection efficiency of the devices increased from 0.46 to 0.88 when TiO_2 nanoparticle size was increased from 10 to 27 nm. The improvement of charge collection efficiency with nanoparticle size can be explained using the electron trapping/detrapping model.[23-25] Larger nanoparticles have both lower surface area and smaller number of grain boundaries, which leads to less electron trapping and is beneficial to high J_{sc} and V_{oc}. Although the charge collection efficiency data would have predicted that the 27 nm TiO_2 based devices would have the highest photocurrent, however, this is not the case for J_{sc} in these devices and this indicates that charge collection efficiency alone is not indicative of the overall device performance.

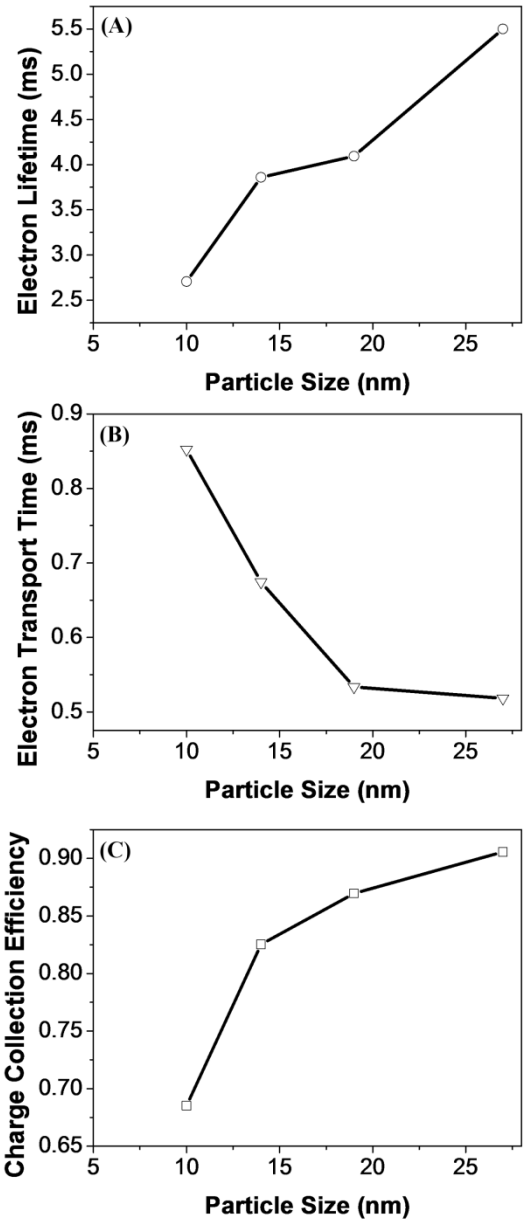

Figure 2.6 (A) electron lifetime (B) electron transport time and (C) charge collection efficiency for thickness optimized DSSCs fabricated with different sizes of TiO_2 nanoparticles. [14]

From the above studies, it is clear that the device performance is dependent on the optimization of the charge collection efficiency and dye loading. Small nanoparticles have higher dye loading for a fixed film thickness and hence thinner films can be used for devices fabricated with 10 and 14 nm TiO_2. However, devices fabricated with small nanoparticles exhibit poor charge transport

properties and this results in a poor J_{sc}. Increasing particle size decreases dye loading and increases the film thickness required for optimal performance but devices fabricated with larger particles show improved charge collection efficiency. Since the films used in this study are not sintered, the thickness for which a crack-free film can be fabricated is limited and the requirement for thick crack-free films cannot be fulfilled when the large 27 nm nanoparticles were used. From these results, a moderate nanoparticle size of 19 nm shows the best efficiency. This is ascribed to the 19 nm based devices' relatively high dye loading as well as good charge collection efficiency.

For comparison purposes, a device was fabricated with commercially available Degussa P25 TiO_2 nanoparticles. Using the same fabrication method, P25 was deposited *via* EPD and used as a photoanode in DSSCs. The change in photovolatic parameters with film thickness is shown in Table 2.7. The optimal post compression thickness is found to be ~ 11 μm. FESEM images of the film before and after compression are shown in Figure 2.7

Flexible DSSCs were fabricated with 19 nm and P25 nanoparticles respectively. The post compression thickness of the TiO_2 films was controlled to be ~11 μm which is the optimal thickness for both 19 nm and P25 devices. DSSCs with 19 nm nanoparticle as photoanode have a V_{oc} of 0.80 V, a J_{sc} of 10.3 $mAcm^{-2}$, a FF of 0.62 and an overall efficiency (η) of 5.2%. P25 based devices have a V_{oc} of 0.79 V, a J_{sc} of 9.32 $mAcm^{-2}$, a FF of 0.60 and an overall efficiency (η) of 4.5%. When compared to the devices on rigid glass substrates, the efficiency is lower. This is mainly due to the drop in photocurrent and FF which is caused by the lower light transmittance and higher electrical resistance in plastic substrate when compared to glass substrates.[26, 27]

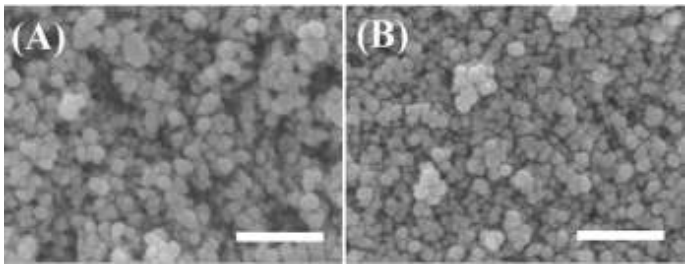

Figure 2.7 FESEM images of the P25 film prepared by EPD (A) ~ as prepared. (B) ~ after compression. Scale bar represents 100 nm [14]

Table 2.7 Photovoltaic parameters of D149-sensitized solar cells fabricated from P25 nanoparticles on rigid glass substrate [14]

Particle Size	**Film Thickness (μm)**	**Photovoltaic Properties** [a]			
		V_{oc} (V)	**J_{sc} (mA cm^{-2})**	**FF**	**η (%)**
Degussa P25	4	0.80	7.0	0.65	3.7
	8	0.79	9.4	0.65	4.9
	11	0.77	12.7	0.64	6.3
	15	0.75	10.0	0.64	4.9

[a] measured under AM 1.5G (100 mWcm^{-2})

To compensate for the loss of light transmission, large submicron TiO_2 particles (200 nm ~ 300 nm) was subsequently synthesized[27] and utilized as a scattering layer to offset the light loss caused by the plastic substrate. Based on the identical deposition method, a 2 μm scattering layer was deposited on top of the nano sized TiO_2 particles. The J-V curves of these devices are shown in Figure 2.8. As such, the efficiency of the devices is significantly improved. The 19 nm nanoparticle based devices with the scattering layer have a V_{oc} of 0.80 V, a J_{sc} of 13.8 mAcm^{-2}, a FF of 0.54 and an overall efficiency (η) of 6.0%. The P25 based device with scattering layer has a V_{oc} of 0.78 V, a J_{sc} of 11.5 mAcm^{-2}, a FF of 0.56 and an overall efficiency (η) of 5.2%. The

light scattering effect of the large submicron sized nanoparticle is well known to increase the light harvesting and hence J_{sc} of the devices. [27, 28] This leads to an overall increase in the device efficiency as compared to the devices without the scattering layer. As with the devices on the rigid substrates, the performance of the 19 nm nanoparticle based devices is superior to that of P25. Upon optimizing particle size for DSSCs fabricated *via* EPD, the use of a blocking layer to limit recombination,[29, 30] UV-O_3 treatment to reduce organic contaminants and anti-reflection film[31] for higher light utilization is expected to further improve device efficiency.

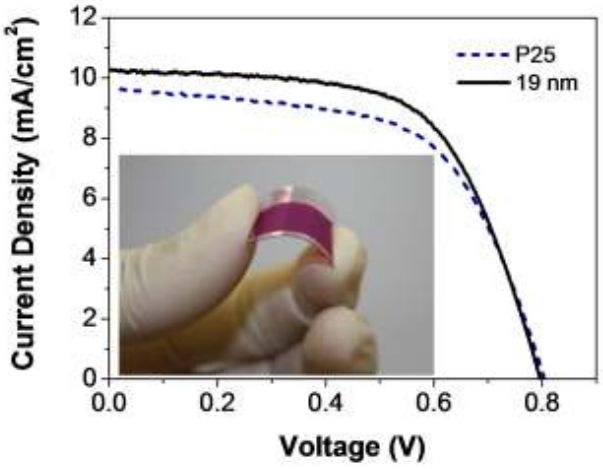

Figure 2.8 J-V curves for flexible DSSC fabricated on plastic substrates. 19 nm particles or P25 were used as the mesoporous layer and large particles (200 ~ 300 nm) were used as light scattering layers. The inset shows a typical TiO_2 film, formed by EPD and compression on ITO/PEN, sensitized with D149 dye. [14]

2.4 Conclusion

In this study, TiO_2 nanoparticles of sizes 10 nm to 27 nm have been synthesized and used to fabricate DSSCs *via* the EPD technique. This study has shown that for low temperature DSSCs fabricated by EPD, nanoparticle size plays a significant role in determining device performance. In our devices, nanoparticle size mainly influenced the J_{sc} of the devices while the V_{oc} and FF are only mildly affected. IMPS and IMVS studies indicate that the charge collection efficiency

increases with nanoparticle size. At the same time, dye loading of the devices decreases with nanoparticle size. Due to a combination of good charge transport properties and relatively high dye loading, 19 nm TiO_2 nanoparticle based devices gave the best device efficiency. Under optimized conditions, an efficiency of 6.0% was achieved on plastic substrates using 19 nm TiO_2 nanoparticles with a scattering layer. This is an improvement over the benchmark device made with P25 which only manages 5.2% efficiency. These results demonstrate that optimization of TiO_2 nanoparticle size for devices fabricated using the EPD technique is an alternative method to achieve highly efficient plastic dye-sensitized solar cells.

2.5 References

1. Chen, H.W., et al., *Plastic dye-sensitized photo-supercapacitor using electrophoretic deposition and compression methods.* Journal of Power Sources, 2010. **195**(18): p. 6225-6231.

2. Chen, H.W., et al., *Electrophoretic deposition of ZnO film and its compression for a plastic based flexible dye-sensitized solar cell.* Journal of Power Sources, 2011. **196**(10): p. 4859-4864.

3. Chiu, W.H., K.M. Lee, and W.F. Hsieh, *High efficiency flexible dye-sensitized solar cells by multiple electrophoretic depositions.* Journal of Power Sources, 2011. **196**(7): p. 3683-3687.

4. Tan, W.W., et al., *Electrophoretic deposition of nanocrystalline TiO2 films on Ti substrates for use in flexible dye-sensitized solar cells.* Electrochimica Acta, 2009. **54**(19): p. 4467-4472.

5. Yin, X., et al., *Electrophoretic Deposition of ZnO Photoanode for Plastic Dye-sensitized Solar Cells.* Electrochemistry Communications, 2010. **12**(9): p. 1241-1244.

6. Grinis, L., et al., *Electrophoretic deposition and compression of titania nanoparticle films for dye-sensitized solar cells.* Journal of Photochemistry and Photobiology a-Chemistry, 2008. **198**(1): p. 52-59.

7. Corni, I., M.P. Ryan, and A.R. Boccaccini, *Electrophoretic deposition: From traditional ceramics to nanotechnology.* Journal of the European Ceramic Society, 2008. **28**(7): p. 1353-1367.

8. Chou, T.P., et al., *Titania particle size effect on the overall performance of dye-sensitized solar cells.* Journal of Physical Chemistry C, 2007. **111**(17): p. 6296-6302.

9. Du, L.C., et al., *Mechanism of Particle Size Effect on Electron Injection Efficiency in Ruthenium Dye-Sensitized TiO_2 Nanoparticle Films.* Journal of Physical Chemistry C, 2010. **114**(18): p. 8135-8143.

10. Katoh, R., et al., *Effect of the particle size on the electron injection efficiency in dye-sensitized nanocrystalline TiO_2 films studied by time-resolved microwave conductivity (TRMC) measurements.* Journal of Physical Chemistry C, 2007. **111**(28): p. 10741-10746.

11. Nakade, S., et al., *Influence of TiO2 nanoparticle size on electron diffusion and recombination in dye-sensitized TiO_2 solar cells.* Journal of Physical Chemistry B, 2003. **107**(33): p. 8607-8611.

12. Ito, S., et al., *High-efficiency Organic-dye-sensitized Solar Cells Controlled by Nanocrystalline-TiO_2 Electrode Thickness.* Advanced Materials, 2006. **18**(9): p. 1202-1205.

13. Horiuchi, T., et al., *High efficiency of dye-sensitized solar cells based on metal-free indoline dyes.* Journal of the American Chemical Society, 2004. **126**(39): p. 12218-12219.

14. Xue, Z., et al., *Enhanced conversion efficiency of flexible dye-sensitized solar cells by optimization of the nanoparticle size with an electrophoretic deposition technique.* Rsc Advances, 2012. **2**(18): p. 7074-7080.

15. Barbe, C.J., et al., *Nanocrystalline titanium oxide electrodes for photovoltaic applications.* Journal of the American Ceramic Society, 1997. **80**(12): p. 3157-3171.

16. Kim, J.H., et al., *Hydrothermal synthesis of titanium dioxides using basic peptizing agents and their photocatalytic activity.* Chemical Engineering Science, 2007. **62**(18-20): p. 5154-5159.

17. Kosmulski, M., *The significance of the difference in the point of zero charge between rutile and anatase.* Advances in Colloid and Interface Science, 2002. **99**(3): p. 255-264.

18. Koura, N., et al., *Preparation of various oxide-films by an electrophoretic deposition method - A study of mechanism.* Japanese Journal of Applied Physics Part 1-Regular Papers Short Notes & Review Papers, 1995. **34**(3): p. 1643-1647.

19. Ning, Z.J., Y. Fu, and H. Tian, *Improvement of dye-sensitized solar cells: what we know and what we need to know.* Energy & Environmental Science, 2010. **3**(9): p. 1170-1181.

20. Kruger, J., et al., *Charge transport and back reaction in solid-state dye-sensitized solar cells: A study using intensity-modulated photovoltage and photocurrent spectroscopy.* Journal of Physical Chemistry B, 2003. **107**(31): p. 7536-7539.

21. van de Lagemaat, J. and A.J. Frank, *Effect of the surface-state distribution on electron transport in dye-sensitized TiO_2 solar cells: Nonlinear electron-transport kinetics.* Journal of Physical Chemistry B, 2000. **104**(18): p. 4292-4294.

22. Schlichthorl, G., N.G. Park, and A.J. Frank, *Evaluation of the charge-collection efficiency of dye-sensitized nanocrystalline TiO2 solar cells.* Journal of Physical Chemistry B, 1999. **103**(5): p. 782-791.

23. Nelson, J., *Continuous-time random-walk model of electron transport in nanocrystalline TiO2 electrodes.* Physical Review B, 1999. **59**(23): p. 15374-15380.

24. Gracia, F., J.P. Holgado, and A.R. Gonzalez-Elipe, *Photoefficiency and optical, microstructural, and structural properties of TiO2 thin films used as photoanodes.* Langmuir, 2004. **20**(5): p. 1688-1697.

25. Gregg, B.A., *Interfacial processes in the dye-sensitized solar cell.* Coordination Chemistry Reviews, 2004. **248**(13-14): p. 1215-1224.

26. Liu, X.Z., et al., *Room Temperature Fabrication of Porous ZnO Photoelectrodes for Flexible Dye-sensitized Solar Cells.* Chemical Communications, 2007(27): p. 2847-2849.

27. Lan, Z.A., et al., *Preparation of Sub-micron Size Anatase TiO_2 Particles for Use as Light-scattering Centers in Dye-sensitized Solar Cell.* Journal of Materials Science-Materials in Electronics, 2010. **21**(8): p. 833-837.

28. Nazeeruddin, M.K., et al., *Conversion of light to electricity by cis-X2bis(2,2'-bipyridyl-4,4'-dicarboxylate)ruthenium(II) charge-transfer sensitizers (X = Cl^-, Br^-, I^-, CN^-, and SCN^-) on nanocrystalline titanium dioxide electrodes.* Journal of the American Chemical Society, 1993. **115**(14): p. 6382-6390.

29. Palomares, E., et al., *Control of charge recombination dynamics in dye sensitized solar cells by the use of conformally deposited metal oxide blocking layers.* Journal of the American Chemical Society, 2003. **125**(2): p. 475-482.

30. Ito, S., et al., *Control of dark current in photoelectrochemical (TiO_2/I^-–I_3^-) and dye-sensitized solar cells.* Chemical Communications, 2005(34): p. 4351-4353.

31. Yamaguchi, T., et al., *Highly efficient plastic-substrate dye-sensitized solar cells with validated conversion efficiency of 7.6%.* Solar Energy Materials and Solar Cells, 2010. **94**(5): p. 812-816.

Chapter 3 Facile fabrication of co-sensitized plastic dye-sensitized solar cells using multiple electrophoretic depositions

3.1 Introduction

Dye sensitized solar cells (DSSCs) are a potential low cost alternative to conventional silicon based solar cells. [1] Though efficiency has exceeded 12%,[2] light utilization in the near infrared region of sunlight has been low. In this regard, novel dyes that have broad absorption can be developed. While this challenging task is still ongoing, alternative strategies have been used to expand the solar utilization of the cells. Other than the use of tandem cells which have complicated fabrication steps,[3-6] multiple dyes can be co-sensitized within a single device in order to expand the absorption range of the device. This will improve light utilization and increase cell efficiency. For future commercialization, in addition to efficiency considerations, fabricating the device on plastic substrates aids in mass industrial production of DSSCs due to the use of highly efficient roll to roll manufacturing processes. Moreover, flexible DSSCs have niche applications where flexibility is essential. However, conventional DSSC fabrication involves high temperature sintering which is not suitable for lightweight plastic substrates as they can only be heated up to 150 ^{o}C. In this regard, flexible DSSCs co-sensitized with multiple dyes is an important area of interest.

Co-sensitization adds an additional degree of complexity to the DSSC system. Several attempts at co-sensitization resulted in performances that are worse than the single dye devices,[7-9] a clear sign that added complexity in co-sensitized devices can be detrimental to performance. The simplest way of co-sensitization is to sensitize the photoanode with a solution containing multiple dyes, ie a dye cocktail. [8, 10-12] The cocktail method, though shown to be effective at times, is known to be highly dependent on the nature of the dyes used. Different dye pairs

present complications such as the different speed of dye uptake, different molecular size of dyes, different affinity of dyes to the TiO_2 surface and unfavourable interactions such as electron transfer and electron/hole recombination between the adsorbed dyes in close proximity on the photoanode. [8, 13, 14] The ratio of each dye in the cocktail is also known to have great influences on the resultant device's performance and the ideal ratio differs across different dye pairs.[8, 11, 12] The need for careful selection of dyes that work in synergy in a cocktail approach and the tedious work needed to optimize the cocktail limits the application of this method.

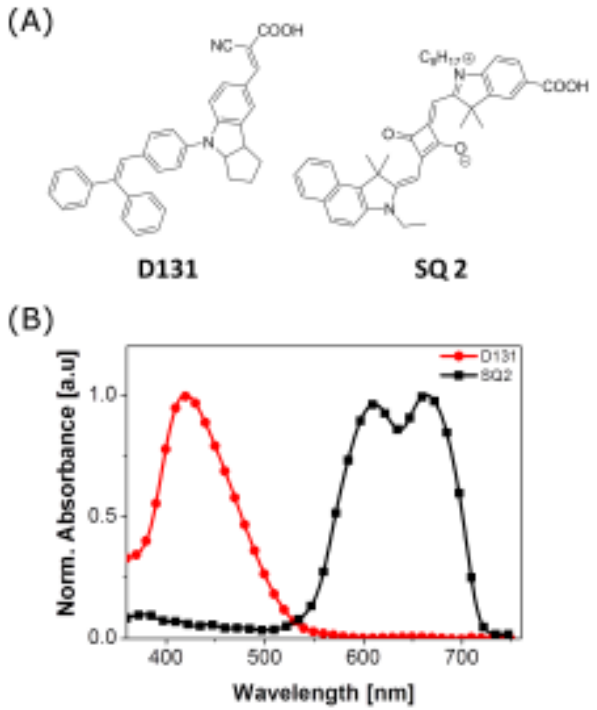

Figure 3.1 (A) Chemical structures of D131 and SQ 2 dyes. (B) Normalized absorption spectra of D131 and SQ2 when adsorbed on a thin film of TiO_2.[15]

With the careful selection of dye pairs, sequential adsorption of dyes is often used successfully as an alternative method of co-sensitization.[16-19] Effective improvements for the sequential adsorption method involving the use of pressurized CO_2[20] or Al_2O_3 blocking layer[21] were reported but they lengthened the fabrication process. Other reported methods often involve

selective desorption[22, 23] of adsorbed dyes before introducing other dyes on the desorbed sites. One such procedure involves the insertion of polystyrene into the pores of a TiO_2 film and using a solution containing sodium hydroxide and polypropylene glycol to selectively desorb dyes. [23] Another involves the use of a viscous desorption solution to desorb dye selectively and the desorption depth was controlled by desorption solution viscosity.[22] These procedures allow the selective placement of dyes in discrete layers but they involve multiple tedious adsorption/desorption cycles and waste dyes. Recently, transfer techniques have been used successfully to develop co-sensitized DSSCs. [24, 25] A TiO_2 film is first deposited and sintered conventionally to form the proper necking for high performance DSSCs. The sintered TiO_2 film is then sensitized by soaking. A second film with a different sensitizer is formed the same way. The two films are combined into a single multilayered film by transferring one of the films onto the other. This strategy avoids the problems which arise from the difference in adsorption speed of different dyes as well as the random arrangement of dyes on the TiO_2 photoanode.

In this chapter, I report an alternative method for fabricating layered co-sensitized TiO_2 films by using multiple electrophoretic depositions (EPD) of low cost P25 TiO_2 nanoparticles.[26, 27] This procedure combines the use of low cost commercially available starting materials (P25 TiO_2) with EPD that are suitable to be used on a large scale in future commercialization. This fabrication process does not involve complicated adsorption/desorption cycles or special sensitization techniques. Using this method, the working TiO_2 electrodes are fabricated within several minutes, an advantage that is favorable for rapid mass production.

In this study, D131 and SQ2 dyes are selected because they differ greatly in their absorption spectra. The chemical structures of both sensitizers and their respective absorption spectra on TiO_2 are shown in Figure 3.1. When adsorbed on TiO_2 films, D131 exhibits an absorption

maximum at ~430 nm while SQ2 has absorption maxima at ~610 nm and ~670 nm. Using this dye pair, the effect of co-sensitization on device performance can be emphasized and analysis will be made easier as there is minimal overlap between their absorption spectra.

3.2 Experimental Section

3.2.1 Materials

All chemicals were used as received with no further purification. Chenodeoxycholic acid, *tert*-butylalcohol, tetrabutylammonium iodide, lithium perchlorate, 4-*tert*-butylpyridine, lithium iodide, 1-butyl-3-methylimidazolium iodide, 3-methoxypropionitrile and iodine were purchased from Sigma Aldrich. All solvents used were of AR grade and were obtained from either Aldrich or Tedia. FTO glass substrates were available from Hartford Glass. Plastic PEN-ITO substrates were purchased from Peccell Technologies. P25 TiO_2 nanoparticles were kindly gifted by Degussa. The D131 and SQ2 dyes were from Mitsubishi Paper Mills and Eversolar Chemicals respectively. 25 μm thick spacer was obtained from Solaronix.

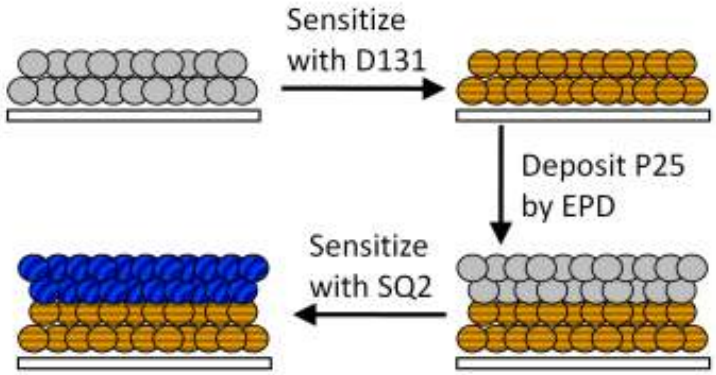

Figure 3.2 Schematic representation of the layered dye-sensitized photoanode formed *via* multiple electrophoretic depositions. [15]

3.2.2 Preparation of photoanodes by EPD

Figure 3.2 shows a schematic representation of the method used in the fabrication of the co-sensitized photoanode. 0.5 g of P25 TiO_2 nanoparticles was first suspended in a mixture of n-butanol/isopropanol/ethanol (4:2:1 by volume) and sonicated to disperse the nanoparticles. A pair of FTO glass substrates or ITO/PEN conductive substrates was immersed face to face in the prepared colloids and then a constant DC field of 2.0 Vcm^{-1} was applied. Due to the net positive charge on the surface of P25 nanoparticles, a film of TiO_2 was deposited on the cathode upon applying a potential difference. The thickness of the deposited film is controlled by the length of deposition. The freshly coated films were left to dry in air before heated at 100 ^{o}C for 30 min for low temperature annealing and to ensure all solvent from the EPD process was removed.

3.2.3 DSSC assembly

The prepared photoanodes were subsequently subjected to a pressure of 1 ton/cm^2 (Atlas Manual 15T Hydraulic Press) for 2 min to improve the interparticle adhesion and electrical connectivity. As a result of the pressing process, the thickness of the films was reduced. The photoanodes were heated at 70 °C for 30 min before being soaked in a 0.3 mM of D131 dye solution (acetonitrile:*tert*-butanol 1:1 by volume) or a 0.3 mM of SQ2 dye solution in acetonitrile:*tert*-butanol (1:1 by volume) for 2 hours. The photoanodes were subsequently rinsed with acetonitrile and left to dry in the dark.

The rigid Pt counter electrode was prepared by spin-coating a 30 mM H_2PtCl_6 solution in isopropanol on a FTO glass substrate, followed by thermal decomposition at 400 °C for 15 min. The flexible Pt counter electrode was fabricated by sputtering Pt (20 mA for 120 s) on the PEN-ITO substrate by JEOL JFC-1600 Auto Fine Coater. DSSCs were fabricated by sandwiching a

TiO_2 photoanode and a Pt counter electrode with electrolyte in a 25 μm thick spacer. The active area of the cell was 0.16 cm^2, controlled by a metal mask.

3.2.4 Determination of dye loading

A TiO_2 film was prepared on a glass substrate by EPD as described above. An area of 30 mm^2 (5 mm × 6 mm) was immersed into the dye solution for 2 h. The sensitized photoanode was soaked in a solution of KOH in MeOH (0.1 M) for 30 min for dye desorption. After complete desorption, the UV-Vis absorption spectrum (Shimadzu) of the resultant solution was measured at the absorption maximum of the dye. The dye loading was calculated from the molar extinction of the dyes (ε = 40400 $M^{-1}cm^{-1}$ at 390 nm for D131 and ε = 319000 $M^{-1}cm^{-1}$ at 652 nm for SQ2) using Beer-Lambert's law. The dye loading data reported were an average of 3 samples.

3.2.5 Photovoltaic measurements

All the measurements were performed in air at ambient conditions. UV-Vis absorption spectra were measured using Shimadzu UV-3150. To eliminate the absorbance or light scattering arising from TiO_2 film, a blank TiO_2 film was used as the reference before measuring the UV absorbance of D131 and SQ2. The photovoltaic parameters of DSSCs were studied an AutoLAB PGSTAT 320 N Potentiostat with a solar simulator (XES-151S, San-EI Electric). The incident light was filtered with an AM1.5 filter (Asahi Spectra) and calibrated with a silicon reference cell (OptoPolymer, ISE CalLab) before each experiment. Electrochemical impedance spectroscopy (EIS) was measured in the dark using the same Autolab workstation. The frequency range used is from 1 mHz to 1 MHz. The applied bias voltage and AC amplitude were set at -1.00 V and 10 mV, respectively The results were fitted with an equivalent circuit using Zview software

3.3. Results and Discussion

The thicknesses of the singly sensitized devices were first optimized. Different thicknesses of TiO_2 were first deposited by EPD on FTO glass substrates and compressed as described in the experimental section. These films were subsequently soaked in dye solutions and used as photoanodes in rigid DSSCs. The performances of these devices are shown in Table 3.1 and Table 3.2. The best performances for the D131 and SQ2 sensitized devices have a post compression thickness of ~10 μm and ~8 μm respectively. These devices are labeled as "D131" and "SQ2" respectively.

Table 3.1 Photovoltaic parameters of D131 sensitized solar cells fabricated from different thickness of TiO_2 films. Electrolyte composition is 0.1 M lithium iodide, 0.05 M iodine, 0.5 M 1-butyl-3-methylimidazolium iodide in 3-methoxypropionitrile. [15]

Device thickness (μm)	**V_{oc} (V)**	**J_{sc} (mA/cm^2)**	**FF (%)**	**η^a (%)**
5	0.66	8.9	0.61	3.6
8	0.66	9.2	0.61	3.7
10	0.65	9.9	0.60	3.9
12	0.63	10.1	0.59	3.8

[a] measured under AM 1.5G (100 mWcm^{-2}) for devices sensitized with dye D131 on rigid glass substrate/

The layered devices were fabricated as follow: a ~16 μm film of TiO_2 was deposited on the cathode after a deposition time of 2 min. After complete drying of solvents at 70 ^oC, the film was soaked in a 0.3 mM of D131 dye solution (acetonitrile:*tert*-butanol 1:1 by volume) for 2 hours. After sensitization, the D131-sensitized films were washed with acetonitrile and left to dry. Using the same EPD method, another TiO_2 film of thickness ~5 μm was formed after 1 min of deposition. After solvent removal at 70 ^oC, the bilayer film was soaked in a 0.3 mM of SQ2 dye

solution in acetonitrile:*tert*-butanol (1:1 by volume), for 2 hours. In order to enhance the interparticle and substrate adhesion of the films formed by the two EPD processes, the co-sensitized film was subjected to a similar compression process at 1 toncm^{-2} for 1 min as described before. As a result, the film thickness is reduced to ~13 μm. For comparison, photoanodes were fabricated using the same method but were sensitized with a cocktail of D131/SQ2 (0.3 mM D131 and 0.3 mM SQ2 in acetonitrile:*tert*-butanol 1:1 by volume). These samples were labeled as "layered" and "cocktail", respectively.

Table 3.2 Photovoltaic parameters of SQ2 sensitized solar cells fabricated from different thickness of TiO_2 films. Electrolyte composition is 0.1 M iodine, 0.5 M tetra-n-butylammonium iodide, 0.5 M 4-tert-butylpyridine, 0.001 M lithium perchlorate in 3-methoxypropionitrile.[15]

Device thickness (μm)	**V_{oc} (V)**	**J_{sc} (mA/cm^2)**	**FF (%)**	**η[a] (%)**
5	0.63	5.1	0.74	2.4
8	0.61	6.7	0.69	2.8
10	0.61	6.6	0.69	2.8
12	0.60	6.3	0.68	2.5

[a] measured under AM 1.5G (100 mWcm^{-2}) for devices sensitized with dye SQ2 on rigid glass substrate.

To understand whether D131 has been desorbed during the 2nd EPD step, desorption studies were performed. The dye loadings were estimated using the procedure described in the experimental section. The dye loading of the TiO_2 film just before 2nd EPD and after co-sensitization is estimated to be 2.2×10^{-7} molcm^{-2} and 2.1×10^{-7} molcm^{-2}, respectively. The difference between the dye loadings is indicative of the amount of D131 dye that gets desorbed during the 2nd EPD process. This indicates the co-sensitization process did not cause significant D131 loss and the dyes are more likely to be in discrete layers compared to the cocktail method.

The dye sensitized TiO_2 films (labeled as D131, SQ2, cocktail and layered, respectively) were subsequently examined as photoanodes in DSSCs. Figure 3.3 shows the current density- voltage (J-V) curves of these devices on glass substrates under the illumination of simulated AM1.5G solar light (100 $mWcm^{-2}$). The corresponding photovoltaic characteristics and testing parameters are presented in Table 3.3.

Table 3.3 Photovoltaic properties of DSSCs fabricated on FTO glass (ITO/PEN) substrates sensitized with different dyes. [15]

Device	**V_{oc} / V**	**J_{sc} / $mAcm^{-2}$**	**FF / %**	**η[a] / %**
D131[b,c]	0.65	9.9	0.60	3.9
	(0.63)	(9.1)	(0.60)	(3.4)
SQ2[d]	0.62	6.7	0.68	2.8
	(0.62)	(6.6)	(0.68)	(2.7)
Cocktail[c,e]	0.59	10.0	0.64	3.8
	(0.60)	(8.78)	(0.62)	(3.3)
Layered[c,e]	0.64	11.8	0.65	4.9
	(0.65)	(9.73)	(0.65)	(4.1)

[a] measured under AM 1.5G (100 mW cm^{-2}) on rigid devices. Data on flexible devices are in parentheses. [b] Device thickness is ~10 μm [c] Electrolyte composition is 0.1M lithium iodide, 0.05 M iodine, 0.5 M 1-butyl-3-methylimidazolium iodide in 3-methoxypropionitrile. [d] Electrolyte composition is 0.1 M iodine, 0.5 M tetra-n-butylammonium iodide, 0.5 M 4-*tert*-butylpyridine, 0.001 M lithium perchlorate in 3-methoxypropionitrile. Device thickness is ~8 μm [e]Device thickness is ~13 μm

The devices sensitized using the layered method show the best performance with an overall efficiency (η) of 4.9% on rigid glass substrates. This is superior to the D131 and SQ2 based devices under optimized conditions, which yielded ηs of 3.9% and 2.8%, respectively. This superior performance was brought about mainly by an increase of the device short-circuit current density (J_{sc}). A J_{sc} of 11.8 $mAcm^{-2}$ was obtained for the layered device which was significantly

higher than the D131 (9.1 $mAcm^{-2}$) and SQ2 (6.7 $mAcm^{-2}$) sensitized devices. The cocktail devices showed an efficiency of 3.8%, which is a result of lower open circuit voltage (V_{oc}), J_{sc} and fill factor (FF) when compared to the layered devices.

To elucidate the difference in V_{oc} shown in the two co-sensitized devices, the changes in dark current under applied potential were examined and shown in Figure 3.3. The onset of dark current took place at a lower applied voltage for the cocktail sensitized devices compared to the layered ones. As the dark current is correlated to the recombination of electrons with the redox mediator in the electrolyte, it implies that the layered co-sensitization method is able to reduce recombination rate and hence increase device V_{oc}. To have a further understanding of the difference in V_{oc} and recombination events, electrochemical impedance spectroscopy (EIS) was performed on the devices in the dark with an applied bias of -0.70 V.

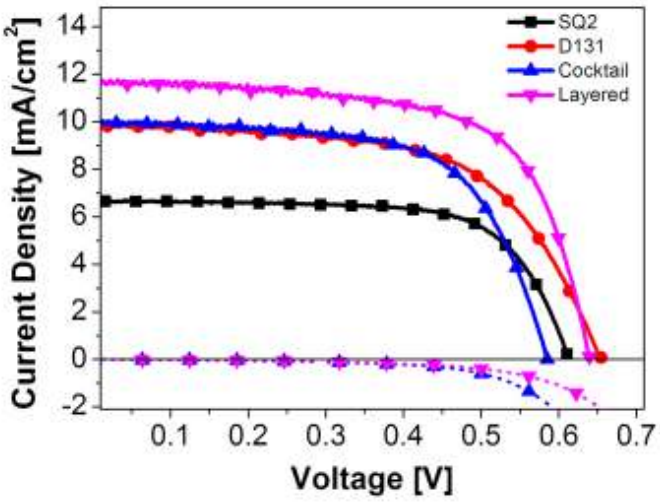

Figure 3.3 Current density – voltage characteristics curves of rigid devices (solid lines) measured under illumination of 100$mWcm^{-2}$ and in the dark (dashed lines for layered and cocktail).

The impedance spectra are shown in Figure 3.4. The Nyquist plots in Figure 3.4 represent electrochemical interfaces in the device. Generally, up to four characteristic arcs can be obtained

from EIS spectra according to the EIS model reported in the literature. [28-30] The size of the large middle arc in the Nyquist plots is indicative of the resistance of electron recombination.

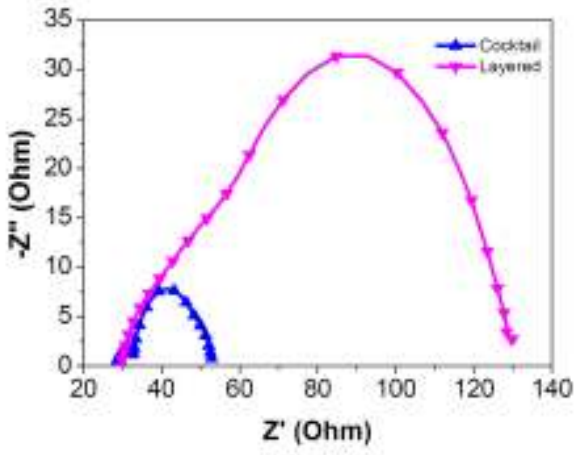

Figure 3.4 Impedance spectra (Nyquist plots) for the rigid devices sensitized with cocktail and layered method in the dark under forward bias of -0.7 V.

It can be seen obviously from Figure 3.4 that the resistance of electron recombination is significantly larger in the layered device as compared to the cocktail device. The larger resistance for electron recombination in layered devices agrees with the higher V_{oc} of layered devices and also the higher onset of dark current. As it is known that bare TiO_2 surfaces act as recombination sites, the dye loading of both the cocktail and layered films were measured to determine if there is a significant difference in TiO_2 surface coverage. For the cocktail device, the D131 dye loading was 1.81×10^{-7} molcm^{-2} whereas the SQ2 dye loading was 1.45×10^{-8} molcm^{-2}. For the layered device, the D131 and SQ2 dye loadings were 2.1×10^{-7} molcm^{-2} and 1.85×10^{-8} molcm^{-2}, respectively. The lower dye loadings for both D131 and SQ2 for the cocktail device imply that less TiO_2 sites are adsorbed with sensitizer molecules in the cocktail devices, leading to increased “bare sites”. It is thus proposed that the increased recombination in cocktail devices is due to less extensive/incomplete sensitizer coverage on TiO_2 surface. This could be due to different molecular size and uptake speed of D131 and SQ2. Subsequently their

random arrangement and aggregation on TiO_2 surface leads to inefficient coverage of binding sites and hence more frequent recombination in the devices.

To study the light response of the devices, incident photon to current efficiency (IPCE) was used to characterize the DSSCs. The IPCE spectra of the various devices on glass substrates are shown in Figure 3.5. The D131 sensitized device has a high IPCE from ~400 nm to ~550 nm, but it rapidly drops to 0 beyond 600 nm. The SQ2 sensitized device exhibits a narrower light response between 550 nm and 700 nm with a maximum IPCE attained at about 670 nm. Both the cocktail and layered devices exhibit characteristics of the singly sensitized devices, showing that both D131 and SQ2 dyes are adsorbed on the photoanodes. The layered devices show higher IPCE than the cocktail devices over the entire measured wavelength range due to higher dye loading and lower recombination rates. This is also consistent with the layered device showing a higher J_{sc}.

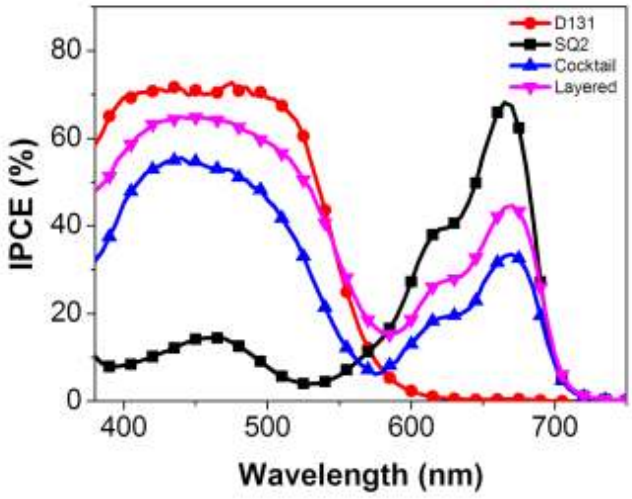

Figure 3.5 IPCE spectra of the rigid devices sensitized with D131, SQ2, cocktail and layered methods.

After optimization of device fabrication on glass substrates, devices were subsequently fabricated on ITO/PEN substrates based on the same procedures. Flexible Pt electrodes were

fabricated by sputtering on ITO/PEN substrates. The J-V curves of these devices are shown in Figure 3.6. The plastic devices showed lower J_{sc} due to the lower transparency of ITO/PEN substrate compared to FTO. Similar to the trend observed in the rigid devices, the layered device shows the highest overall efficiency of 4.1%.

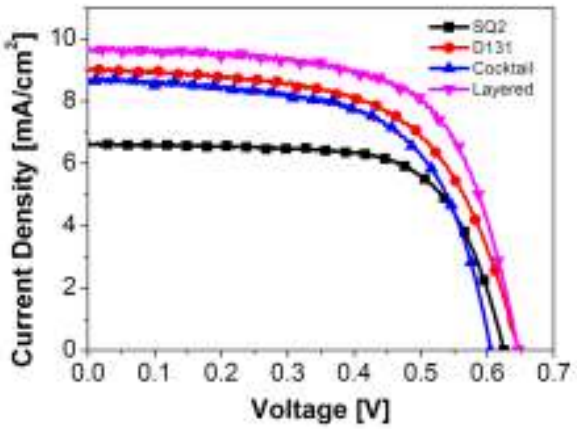

Figure 3.6 Current density – voltage characteristics curves of flexible plastic devices measured .under illumination of 100 mWcm^{-2}

3.4 Conclusions

In conclusion, a new method for rapid fabrication of co-sensitized DSSCs on a plastic substrate is reported. When compared to a cocktail approach, the resultant devices exhibited efficiencies of 4.9% and 4.1% on rigid and plastic substrates which are higher than the singly and cocktail sensitized devices. Dye loading studies showed that little dye was desorbed during EPD, which suggested that the dyes were essentially in discrete layers in the final device. Dark current and EIS revealed that the layered method reduced electron recombination and as a result, gave a higher V_{oc} when compared to the cocktail device. IPCE revealed that the light response of the layered device had characteristics of both D131 and SQ2 sensitizers, confirming successful co-sensitization. Last but not least, the layered method also combines the use of low cost commercially available P25 TiO_2 nanoparticles and EPD, a low temperature, rapid and mature

industrial process that can be used on a large scale on flexible substrates readily. With this proof of concept, it is hoped that with the tinkering of the dye pairs used, high efficiency co-sensitized plastic DSSCs can be realized.

3.5 References

1. O'Regan, B. and M. Grätzel, *A low-cost, high-efficiency solar-cell on dye-sensitized colloidal TiO_2 films.* Nature, 1991. **353**(6346): p. 737-740.

2. Yella, A., et al., *Porphyrin-Sensitized Solar Cells with Cobalt (II/III)-Based Redox Electrolyte Exceed 12 Percent Efficiency.* Science, 2011. **334**(6056): p. 629-634.

3. Durr, M., et al., *Tandem dye-sensitized solar cell for improved power conversion efficiencies.* Applied Physics Letters, 2004. **84**(17): p. 3397-3399.

4. He, J.J., et al., *Dye-sensitized nanostructured tandem cell-first demonstrated cell with a dye-sensitized photocathode.* Solar Energy Materials and Solar Cells, 2000. **62**(3): p. 265-273.

5. Kubo, W., et al., *Dye-sensitized solar cells: improvement of spectral response by tandem structure.* Journal of Photochemistry and Photobiology a-Chemistry, 2004. **164**(1-3): p. 33-39.

6. Liska, P., et al., *Nanocrystalline dye-sensitized solar cell/copper indium gallium selenide thin-film tandem showing greater than 15% conversion efficiency.* Applied Physics Letters, 2006. **88**(20): p. 203103-203103-3.

7. Ehret, A., L. Stuhl, and M.T. Spitler, *Spectral sensitization of TiO_2 nanocrystalline electrodes with aggregated cyanine dyes.* Journal of Physical Chemistry B, 2001. **105**(41): p. 9960-9965.

8. Sayama, K., et al., *Efficient sensitization of nanocrystalline TiO_2 films with cyanine and merocyanine organic dyes.* Solar Energy Materials and Solar Cells, 2003. **80**(1): p. 47-71.

9. Perera, V.P.S., et al., *A solar cell sensitized with three different dyes.* Solar Energy Materials and Solar Cells, 2005. **85**(1): p. 91-98.

10. Ogura, R.Y., et al., *High-performance dye-sensitized solar cell with a multiple dye system.* Applied Physics Letters, 2009. **94**(7): p. 073308-073308-3.

11. Wu, W.J., et al., *Co-sensitization with near-IR absorbing cyanine dye to improve photoelectric conversion of dye-sensitized solar cells.* Synthetic Metals, 2009. **159**(11): p. 1028-1033.

12. Yum, J.H., et al., *Efficient co-sensitization of nanocrystalline TiO2 films by organic sensitizers.* Chemical Communications, 2007(44): p. 4680-4682.

13. Zhao, W., et al., *Study on squarylium cyanine dyes for photoelectric conversion.* Solar Energy Materials and Solar Cells, 1999. **58**(2): p. 173-183.

14. Zhang, D.S., et al., *Photosensitization of nanocrystalline TiO2 electrodes by squarylium cyanine incorporated with a ruthenium bipyridyl complex.* Journal of Photochemistry and Photobiology a-Chemistry, 2000. **135**(2-3): p. 235-240.

15. Xue, Z., L. Wang, and B. Liu, *Facile fabrication of co-sensitized plastic dye-sensitized solar cells using multiple electrophoretic deposition.* Nanoscale, 2013. **5**(6): p. 2269-2273.

16. Kuang, D., et al., *Co-sensitization of organic dyes for efficient ionic liquid electrolyte-based dye-sensitized solar cells.* Langmuir, 2007. **23**(22): p. 10906-10909.

17. Park, B., et al., *Electron Injection from Linearly Linked Two Dye Molecules to Metal Oxide Nanoparticles for Dye-Sensitized Solar Cells Covering Wavelength Range from 400 to 950 nm.* Applied Physics Express, 2011. **4**(1): p. 012301-012301-3.

18. Bandara, J. and H. Weerasinghe, *Design of high-efficiency solid-state dye-sensitized solar cells using coupled dye mixtures.* Solar Energy Materials and Solar Cells, 2006. **90**(7-8): p. 864-871.

19. Fan, S.Q., et al., *Improved Efficiency of over 10% in Dye-Sensitized Solar Cells with a Ruthenium Complex and an Organic Dye Heterogeneously Positioning on a Single TiO(2) Electrode.* Journal of Physical Chemistry C, 2011. **115**(15): p. 7747-7754.

20. Inakazu, F., et al., *Dye-sensitized solar cells consisting of dye-bilayer structure stained with two dyes for harvesting light of wide range of wavelength.* Applied Physics Letters, 2008. **93**(9): p. 093304-093304-3.

21. Choi, H., et al., *Stepwise Cosensitization of Nanocrystalline TiO2 Films Utilizing Al2O3 Layers in Dye-Sensitized Solar Cells.* Angewandte Chemie-International Edition, 2008. **47**(43): p. 8259-8263.

22. Park, S., et al., *Expanding the spectral response of a dye-sensitized solar cell by applying a selective positioning method.* Nanotechnology, 2011. **22**(4): p. 045201.

23. Lee, K., et al., *Selective positioning of organic dyes in a mesoporous inorganic oxide film.* Nature Materials, 2009. **8**(8): p. 665-671.

24. Miao, Q.Q., et al., *A New Type of Dye-Sensitized Solar Cell with a Multilayered Photoanode Prepared by a Film-Transfer Technique.* Advanced Materials, 2011. **23**(24): p. 2764-2768.

25. Huang, F.Z., et al., *Flexible dye-sensitized solar cells containing multiple dyes in discrete layers.* Energy & Environmental Science, 2011. **4**(8): p. 2803-2806.

26. Chen, H.W., et al., *Plastic dye-sensitized photo-supercapacitor using electrophoretic deposition and compression methods.* Journal of Power Sources, 2010. **195**(18): p. 6225-6231.

27. Yin, X., et al., *High-Performance Plastic Dye-sensitized Solar Cells Based on Low-Cost Commercial P25 TiO_2 and Organic Dye.* Acs Applied Materials & Interfaces, 2012. **4**(3): p. 1709-1715.

28. Han, L.Y., et al., *Modeling of an equivalent circuit for dye-sensitized solar cells: improvement of efficiency of dye-sensitized solar cells by reducing internal resistance.* Comptes Rendus Chimie, 2006. **9**(5-6): p. 645-651.

29. Han, L.Y., et al., *Modeling of an equivalent circuit for dye-sensitized solar cells.* Applied Physics Letters, 2004. **84**(13): p. 2433-2435.

30. Hoshikawa, T., et al., *Impedance analysis of internal resistance affecting the photoelectrochemical performance of dye-sensitized solar cells.* Journal of the Electrochemical Society, 2005. **152**(2): p. E68-E73.

Chapter 4 Solid-state dye sensitized/polythiophene hybrid solar cells on flexible Ti substrate

4.1 Introduction

Since their inception, dye sensitized solar cell (DSSC) is widely regarded as a strong candidate for low cost solar to electricity conversion.[1] Efficiency of such cells has thus far exceeded 12% [2] but long term stability issues still persist. In particular, the presence of a corrosive and volatile liquid electrolyte[3] requires complicated sealing technology to prevent leakage and careful consideration of corrosion resistant electrode materials in order to avoid oxidation by iodine. To solve these issues, solid-state p-type conductors are used in place of the liquid electrolyte.[4, 5] Cu(I) salts like CuI, CuBr and CuSCN are common inorganic hole transporting materials (HTM) used in the first generation of solid-state DSSCs but they are found to be either unstable or have low hole mobility. [4, 5] Recently, solid-state DSSCs using N719 sensitizer and perovskite based inorganic $CsSnI_3$ HTMs have been reported with impressive efficiencies exceeding 8.5%.[6] In addition, novel solid-state DSSCs, where methylammonium lead iodide nanocrystals assume both the role of sensitizer and HTM simultaneously, were reported to give efficiencies of up to 7.3%. [7]

Compared to inorganic HTMs, organic HTMs have the advantage of easy structural modification, good solubility and easy film formation. 2,20,7,70-tetrakis (N,N-di-p-methoxyphenyl-amine)9,90-spirobifluorene (spiro-OMeTAD) is by far the most commonly used organic HTM because of its amorphous structure, small molecular size and good solubility. [8-10] Recently, great improvements in efficiency of solid state spiro-OMeTAD based devices have been reported. Using lead iodide perovskite as sensitizer and spiro-OMeTAD as HTM, impressive efficiencies up to 10.9% have been reported.[11-13] Other than spiro-OMeTAD, conjugated polymers have

also been used as HTMs in solid-state DSSCs. Conjugated polymeric HTMs have the advantage of low fabrication costs, high conductivity and tunable optoelectronic properties.[14] Poly(3-hexylthiophene) (P3HT) is an outstanding member of this family and possesses a hole mobility of up to 0.1 $cm^2V^{-1}s^{-1}$ which is several orders of magnitude higher than spiro-OMeTAD. [14, 15] A comparison study was previously done to investigate the differences between the performance of devices using spiro-OMeTAD and P3HT as HTMs. It was understood that the poor pore filling of the polymer contributed to lower performances of devices. [16] Nonetheless, P3HT has been reported by several groups to be a possible alternative candidate to spiro-OMeTAD. [16-21] Previously, our group has reported that organic indoline dye-sensitized P3HT based hybrid devices give a reasonable efficiency of up to 3.8%,[22, 23] which shows that P3HT is a promising low cost alternative to spiro-OMeTAD.

While long term stability of DSSCs is enhanced when liquid electrolyte is replaced, high throughput production methods are essential for future commercialization. In this respect, industrial roll to roll process, which requires DSSCs to be fabricated on flexible substrates, is preferred. In addition, light-weight and flexible dye sensitized solar cells are desirable for portable applications and in areas where complex geometries are required. Common flexible substrates used in DSSCs include polymers such as indium tin oxide coated poly(ethylene) terephthalate (ITO/PET) and ITO coated polyethylene naphthalate (ITO/PEN) as well as metal foils like stainless steel,[24-27], Ti[28-30], W, Zn, Al, Co and Ni.[3, 31].

Plastic substrates have the advantage of being light-weight and transparent but they cannot withstand typical sintering temperatures needed for high efficiency DSSCs. This requires the use of low temperature fabrication methods like electrophoretic deposition [32-34] and binder-free coatings [35, 36]. However, these low temperature alternatives do not generally produce devices

with efficiencies comparable to those of high temperature sintering. Moreover, for solid-state DSSCs, a high quality dense blocking layer, usually fabricated using spray pyrolysis at high temperature, is essential for a working device.[5, 37] Low temperature fabrication of such a high-quality dense blocking layer remains a key challenge to be overcome before plastic solid-state DSSCs can be fabricated on a large scale.

Alternative to plastic substrates, metal substrates have the advantages of having low resistance, being flexible and sintering resistant such that high quality dense and mesoporous TiO_2 films can be produced on them. In addition, the transparent electrode contributes a big bulk of the cost of DSSC and replacing costly fluorine doped tin oxide (FTO) with low cost metal substrates lower fabrication costs. [38] On the flipside, owing to their non-transparency, light needs to be shone from the cathode side for such devices, which requires a semi-transparent cathode. As long term stability and flexibility are important issues for DSSCs, fabrication of low cost flexible iodine-free solid-state DSSCs is a key milestone that needs to be reached. In this chapter, we report, for the first time, the fabrication of iodine-free solid-state DSSCs on low cost flexible Ti substrates.

4.2 Experimental Section

4.2.1 Materials

All chemicals were used as received with no further purification. Titanium diisopropoxide bis(acetylacetonate), titanium tetrachloride, bis(trifluoromethylsulfonyl)amine lithium salt and 4-tert-butylpyridine were purchased from Sigma Aldrich. All solvents used were of AR grade and were obtained from either Aldrich or Tedia. FTO glass substrates were available from Hartford Glass. Titanium substrates were purchased from Sigma Aldrich. TiO_2 paste was ordered from

Solaronix. The D102 organic sensitizer and P3HT polymer were from Mitsubishi Paper Mills and Rieke Metals respectively.

4.2.2 Preparation of Ti substrates for DSSC fabrication

Ti substrates were first polished with ultrafine sandpaper of designated grit size P2500 until a smooth mirror finish was achieved. The polished Ti substrates were then cut into desired sizes and cleaned ultrasonically with deionized water and ethanol. They were then heated at 400^{o}C in air for 30 min for the growth of an even layer of native TiO_2 layer. This increases the adhesion of the subsequent dense and mesoporous TiO_2 layers to the Ti substrate.

4.2.3 Preparation of solid-state DSSC with P3HT as HTM

Procedures for fabrication of solid-state DSSCs with P3HT as HTM were modified from previous reports.[22, 23] FTO glass or Ti substrates were ultrasonically cleaned with deionized water, acetone and ethanol. A dense TiO_2 film of thickness ~100 nm was deposited on the substrates by spray pyrolysis of 0.2 M titanium diisopropoxide bis(acetylacetonate) ($Ti(OPr)_2(acac)_2$) solution in ethanol at 450 ^{o}C. After this, TiO_2 paste was diluted with 2-methoxyethanol and spin-coated on the substrates. The films were then sintered at 450^{o}C for 30 min to form the mesoporous TiO_2 film. The film thickness was controlled to be ~1.0 μm by adjusting the spin-coating speed and/or paste concentration. The mesoporous TiO_2 film was subsequently treated with 40 mM $TiCl_4$ aqueous solution for 30 min at 70 ^{o}C. After rinsing with deionized water and ethanol, the films were then sintered again at 500 ^{o}C for 30 min and upon subsequent cooling to 80 ^{o}C, placed in commercial D102 dye solution (0.3 mM in acetonitrile/tertbutanol (1:1 V/V) overnight. After dye loading, the films were rinsed with acetonitrile and dried under N_2 flow. The D102-sensitized TiO_2 samples were then immersed into an acetonitrile solution containing $Li(CF_3SO_2)_2N$ (6 mg mL^{-1}) and 4-tert-butylpyridine (TBP,

30 mg mL^{-1}) for 3 min and dried under nitrogen flow. After Li salt and TBP treatment, P3HT (15 mg mL^{-1}) in chlorobenzene was spin-coated onto the D102-sensitized TiO_2 films (600 rpm for 12 s, followed by 3000 rpm for 30 s). The films were transferred into a high vacuum chamber and Pt was sputtered (JOEL JFC-1600; 10 mA) with a mask onto the P3HT layer as the cathode. The active device area of 0.20 cm^2 was controlled by a metal mask.

4.2.4 UV absorbance measurements

All the measurements were performed in air at ambient conditions. UV-Vis absorption spectra were measured using Shimadzu UV-3150. To eliminate the absorbance or light scattering arising from TiO_2 film, a blank TiO_2 film was used as the reference before measuring the UV absorbance of D102 or P3HT adsorbed on TiO_2 films. For Pt electrode transmittance measurements, bare FTO glass was used as reference. The thickness of mesoporous TiO_2 films was examined by a profilometer (Tencor Alpha-step 500). Cross section of the devices was viewed using Field Emission Scanning Electron Microscope (FESEM, JEOL) after sputtering with Pt.

4.2.5 Photovoltaic measurements

Photovoltaic measurements were recorded by using PGSTAT30, Autolab electrochemical workstation or Keithley 2400 sourcemeter. A solar simulator (XES-151S, San-EI Electric) was used as the light source for measuring the solar cells. The intensity of incident light was calibrated using a reference cell (OptoPolymer, ISE CalLab) before each experiment. Electrochemical impedance spectroscopy (EIS) was measured in the dark using the same Autolab workstation. The frequency range used is from 1 mHz to 1 MHz. The applied bias voltage and AC amplitude were set at -1.00 V and 10 mV, respectively The results were fitted with an equivalent circuit using Zview software. The Incident Photon to Charge Carrier

Efficiency (IPCE) was measured using a 300 W Xe light source (MAX-310, Asahi Spectra) and a monochromator (TMS300, Bentham). X-ray photoelectron spectroscopy (XPS) was performed with Kratos Axis Ultra instrument (Shimadzu) and the results are fitted with the accompanying software.

4.3 Results and Discussion

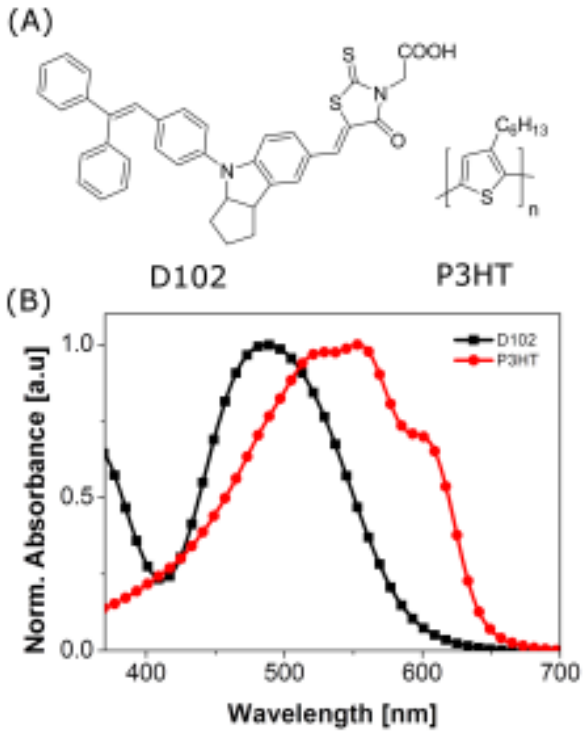

Figure 4.1UV-vis absorbance of D102 and P3HT adsorbed on a thin film of TiO_2.

Figure 4.1 shows the chemical structures of dye D102 and P3HT polymer and their UV-vis absorbance on TiO_2 films. D102 dye was chosen in this work as it was formerly shown to be highly efficient in solid-state DSSCs.[22, 39, 40] D102 has a rather narrow absorbance range with a maximum at ~485 nm when adsorbed on a thin film of TiO_2. P3HT has a significantly broader absorbance in the UV-vis region and possesses an absorbance maximum at ~550 nm.

The energy level diagram for each of the components of the cell is shown in Figure 4.2. We previously reported that lithium bis(trifluoromethylsulfonyl)imide salt (Li salt) and 4-*tert*-butyl pyridine (TBP) treatments can alter the energy levels of adsorbed dye molecules and consequently improve photocurrent of the devices. [22, 23] Addition Li salt changes the effective polarity of the medium surrounding the dye which subsequently results in significant increases in charge transfer rate and efficiency from dye to TiO_2. [41] For D102 dye after Li salt and TBP treatment, it has a LUMO level of ~-3.38 eV which is higher than that of TiO_2 conduction band edge. (~-4.00 eV), allowing efficient electron injection upon excitation. Meanwhile, the HOMO level of D102 after Li salt and TBP treatment (-5.32 eV) is lower than the HOMO of P3HT (-5.10 eV) which allows easy electron injection from the HOMO of P3HT into the hole left behind in the HOMO of D102 after electron excitation. Finally, a Pt cathode completes the circuit by collecting electrons *via* the external circuit.

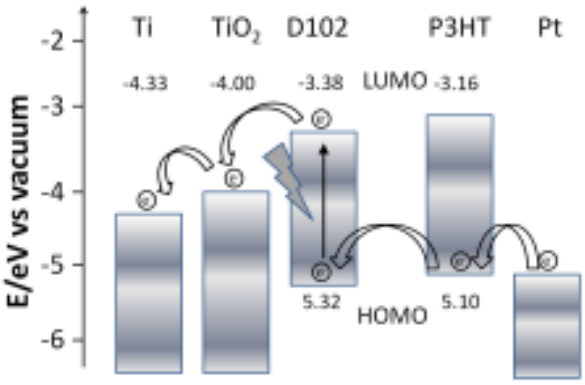

Figure 4.2 Energy level diagram for various components of the solid-state DSSC.

For backside illuminated devices, it is important to optimize the thickness of the semi-transparent Pt cathode. Thicker Pt layers decrease charge transfer resistances of the devices which improves fill factor (FF) but that is offset by decreased transmittance which will decrease short-circuit current density (J_{sc}). Pt was first sputtered under different conditions and the transmittance of the

resultant films was measured. In particular, transmittance between 300 – 700 nm is important as the absorbance range of D102 and P3HT lies mainly within this region. The transmittance was measured on FTO glass substrates using a blank FTO glass as reference. As such, only the effect of the Pt film on transparency was captured without the impact of the FTO glass substrate. The transparency measurements of the Pt films are shown in Figure 4.3. It can be seen that the transmittance is almost independent of the wavelength of incident light. This suggests that decreased transmittance of Pt film is caused by scattering and/or reflection rather than by absorbance. When the sputtering time is increased from 30s to 120s, transmittance decreased from ~88% to ~60% over the entire 300 – 700 nm range.

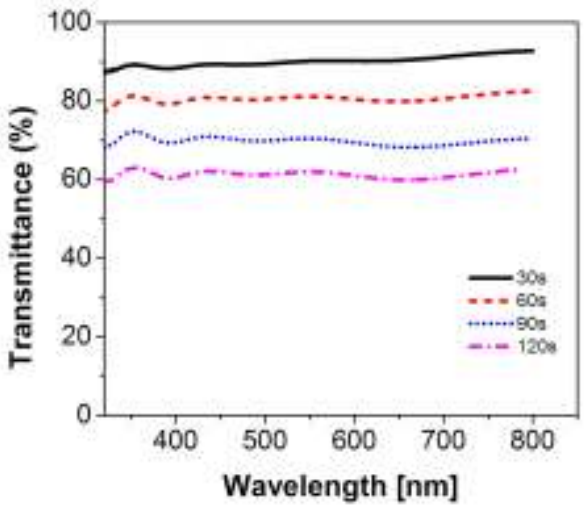

Figure 4.3 Transmittance of Pt films prepared with different sputtering times at a constant current of 10 mA.

Devices were first fabricated on FTO glass substrates using previously optimized conditions [22, 23] (~100 nm dense TiO_2/~1.0 μm mesoporous TiO_2) but with a semi-transparent Pt cathode. It is worthy to point out that there is a minimum amount of Pt needed for the device to be functional. From these experiments, 60 s of sputtering is the minimum required for a device to function properly. The photovoltaic properties of these devices are presented in Table 4.1. For

front side illuminated devices, the overall device efficiency (η) increases from 1.73 % to 2.57% when the Pt sputtering time is increased from 60 s to 120 s. This is mainly due to the increase in J_{sc} and FF which is ascribed to the higher reflectivity and lower series resistance of the Pt electrode when sputtering time is increased.

Sputtering Time	Pt transmittance (400 – 800 nm)	P3HT solution concentration (mg mL^{-1})	Percentage of light absorbed between ~ 400 nm to 700 nm by P3HT	Photovoltaic Properties [a,b]			
				V_{oc} (V)	J_{sc} ($mAcm^{-2}$)	FF	η (%)
120 s	~60%	15.0	~39%	0.94 (1.01)	1.69 (4.62)	0.59 (0.55)	0.94 (2.57)
90 s	~70%	15.0	~39%	0.94 (1.00)	2.04 (4.56)	0.51 (0.52)	0.97 (2.38)
60 s	~ 80%	15.0	~39%	0.96 (1.00)	2.67 (4.03)	0.43 (0.43)	1.10 (1.73)
60 s	~ 80%	12.0	~32%	0.96 (1.00)	1.97 (3.53)	0.43 (0.44)	0.81 (1.55)
60 s	~ 80%	13.5	~50%	0.94 (1.00)	2.85 (3.65)	0.47 (0.48)	1.27 (1.75)
60 s	~ 80%	16.5	~55%	0.91 (0.99)	1.45 (4.15)	0.47 (0.46)	0.62 (1.89)

[a] measured under AM 1.5G (100 $mWcm^{-2}$). [b] Data on frontside illuminated devices are in parentheses

Table 4.1 Photovoltaic parameters of devices fabricated on rigid glass substrates

These devices are less efficient than those in our previous reports due to higher resistance and lower reflectivity of Pt electrode as compared to Ag. [22, 23] The trend for the backside illuminated devices, however, is very different. The V_{oc} decreases from 0.96 V to 0.94 V as the sputtering time increases from 60s to 120s. The decreasing V_{oc} trend can be explained by the decreased light intensity that eventually reaches the anode as the transmittance of the Pt cathode

decreases. [42-45] There are two competing factors to consider. Firstly, lower light intensity causes decreased charge generation rate and a decreased chemical potential within the device and correspondingly a lower V_{oc}. However, lower light intensity also increases charge lifetime and this increases the chemical potential within the device which serves to increase the V_{oc}. The observed decreasing V_{oc} with lower light intensity implies that in D102 sensitized TiO_2/P3HT hybrid systems, the decrease in charge generation is more significant than the increase in charge lifetime, leading to the overall effect of decreasing V_{oc} with decreasing light intensity.[42-45] J_{sc}, decreases from 2.67 to 1.69 $mAcm^{-2}$ when transmittance of the Pt cathode decreases from 80% to 60%. The increase of FF of the devices when sputtering time is attributed to the decreased resistance of the cathode when the thickness of Pt increases.

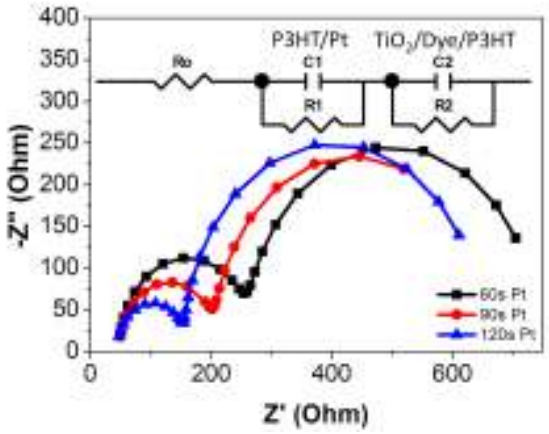

Figure 4.4 Impedance spectra (Nyquist plots) for devices with different Pt sputtering times measured in the dark under forward bias of -1.00 V. Inset shows the equivalent circuit used for fitting.

To investigate how the charge transfer resistance at the Pt/P3HT interface is affected by the length of Pt sputtering, Electrochemical Impedance Spectroscopy (EIS) was performed in the dark with an applied forward bias of −1.00 V. The measured (points) and fitted (lines) Nyquist plots are shown in Figure 4.4. Generally, up to four characteristic arcs can be obtained from EIS

spectra according to the EIS model reported in the literature. [46-48] Of particular interest is the P3HT/Pt interface which occurs in the high frequency region, the first arc from the left. It can be seen that the size of this arc decreases when the Pt sputtering time is increased from 60 s to 120 s, indicating that the charge transfer resistance at the P3HT/Pt interface decreases with increased Pt sputtering. The impedance spectra were fitted with an equivalent circuit shown in the inset of Figure 4.4 and the fitted parameters are shown in Table 4.2. It was found that the series resistance (R_o) and charge transfer resistance at the TiO_2/dye/P3HT interface (R_2) are relatively invariant (within limits of experimental error) while the charge transfer resistance at the Pt cathode (R_1) of the devices decreases from 212 Ω (60 s), 157 Ω (90 s) to 110 Ω (120 s). This shows that the time used for sputtering has a large impact on the charge transfer resistance at the cathode. High J_{sc} of the devices requires both high transmittance and low charge transfer resistance at the cathode but these parameters are inversely correlated. Despite the relatively large charge transfer resistance in the devices with 60 s of Pt sputtering, it is the best compromise between a reasonable charge transfer and a good transmittance level.

Table 4.2 Device parameters obtained after fitting impedance spectra with an equivalent circuit.

Sputtering Time	**Ro (Ω)**	**R_1 (Ω)**	**R_2 (Ω)**
60 s	47.4	212	486
90 s	47.6	157	465
120 s	44.6	110	498

The FESEM image of the cross section of a typical device is shown in Figure 4.5. The different layers of the device are clearly labeled and distinguished. Due to the backside illumination for

the devices from the cathode, light first passes through the P3HT overlayer, where a significant portion of radiation is absorbed. The P3HT overlayer is essential in preventing the direct ohmic contact of the Pt cathode with the TiO_2/dye/P3HT hetrojunction which will short device. The optimal thickness of the P3HT overlayer should thus prevent short-circuiting yet absorb minimal amount of light. The thickness of the P3HT overlayer is optimized by changing the concentration of the P3HT solution from 12 to 16.5 mg mL^{-1}. The photovoltaic parameters of these devices are presented in Table 4.1.

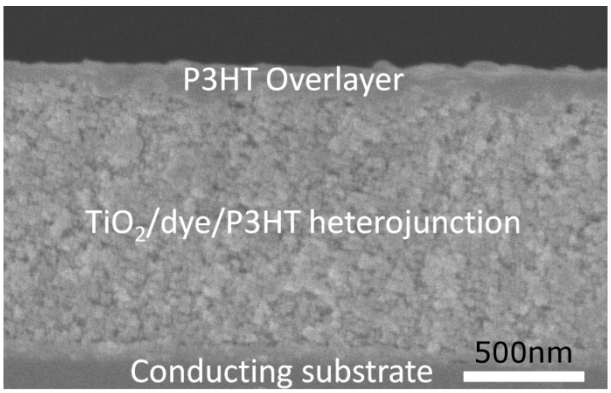

Figure 4.5 FESEM image for the cross section of a typical device.

When concentration of P3HT is decreased from 16.5 to 12 mg mL^{-1}, V_{oc} of the devices increases from 0.91 to 0.96 V due to higher illumination intensity reaching the anode. For the same reason, J_{sc} of the devices increases from 1.45 to 2.85 $mAcm^{-2}$ when concentration of P3HT is decreased from 16.5 to 13.5 mg mL^{-1}. When concentration of P3HT is further decreased to 12 mg mL^{-1}, the J_{sc} of the device decreases to 1.97 $mAcm^{-2}$ despite a higher transmittance. This is ascribed to an insufficiently thick P3HT overlayer and/or pinholes which lead to partial shorting of the device and photocurrent leakage. This is supported by the fact that decreasing P3HT concentration further resulted in devices with negligible efficiency presumably due to the direct contact of the Pt cathode with the active dye/TiO_2/P3HT layer.

From these results, 60 s of Pt sputtering, which gives a transmittance of ~80%, coupled with a P3HT concentration of 13.5 mg mL^{-1}, gave the best performing device with V_{oc} of 0.94 V, J_{sc} of 2.85 $mAcm^{-2}$, FF of 0.47 with an overall conversion efficiency (η) of 1.27%. These conditions represent the compromise among transmittance, charge transfer resistance and shorting prevention.

To investigate the contribution of photocurrent from D102 and P3HT, incident photon to charge carrier efficiency (IPCE) of the best performing device was performed. The spectrum is shown in Figure 4.6. The highest IPCE occurs in between the 450 nm to 550 nm region, which is near the absorbance maximum of ~485 nm for D102 as seen in Figure 4.1. The low IPCE beyond 650 nm, where P3HT is expected to have a reasonably strong absorbance, indicates that P3HT does not contribute significantly to the photocurrent, a conclusion that is consistent with previous reports.[23] In addition, devices were also fabricated with the same procedures but without dye sensitization. Typically, these devices show a V_{oc} of ~0.30 V, a J_{sc} of ~45 μAcm^{-2}, a FF of ~38.6% with a negligible efficiency. This further supports the notion that P3HT does not contribute significantly to the photocurrent.

In order to estimate the percentage of light absorbed by P3HT when illuminated, the transmittance of the P3HT film in the devices was measured. TiO_2 films were first fabricated as per normal and P3HT was spin-coated onto the non dye-sensitized TiO_2 films. Using blank TiO_2 films as reference, the transmittance of the P3HT films as measured and shown in Figure 4.7. By integration of the transmission curves, the intensity of radiation absorbed by the P3HT film over the wavelengths between 400 nm and 700 nm can be estimated. The calculated values are shown in Table 4.1. Note, however, that it is expected to be an overestimation as the D102 sensitizer in the actual device will absorb light competitively in the TiO_2/dye/P3HT layer. From the

integration of the curves, it was estimated that up to ~55% of radiation between 400 nm to 700 nm is absorbed by P3HT, a non trivial percentage. As such, for the devices reported here using backside illumination, the lower efficiency compared to our previous reports [22, 23] is due to light loss from the semi-transparent Pt cathode and the strong absorbance from P3HT.

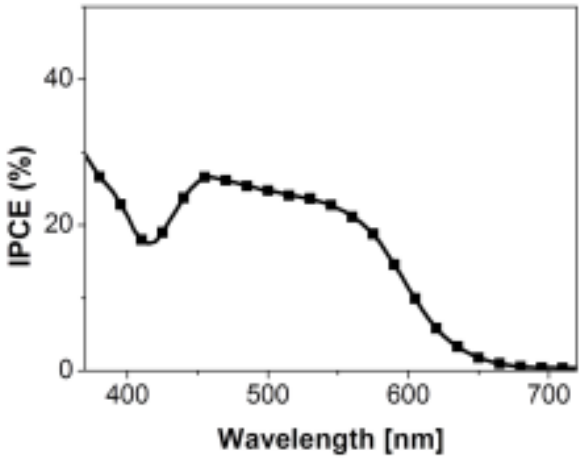

Figure 4.6 IPCE spectrum of the optimized device fabricated on rigid glass substrate.

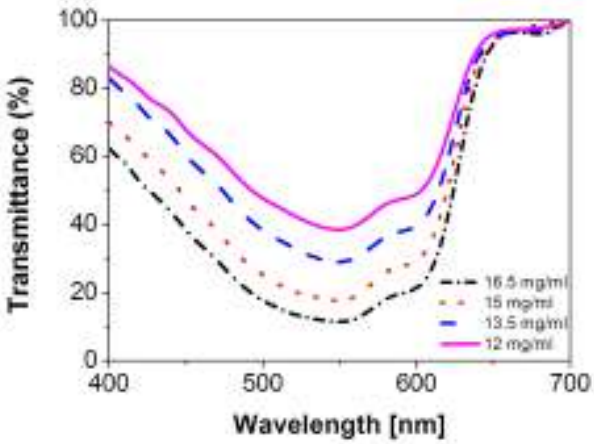

Figure 4.7 Transmittance of P3HT films on 1.0 μm mesoporous TiO_2.

With the optimization of fabrication conditions on glass substrates, flexible devices were fabricated under the same conditions with Ti foil as substrate. When the Ti foils were used as received, it was found that the adhesion of the TiO_2 layers to the Ti substrate was poor and this

resulted in poor efficiency. Moreover, the high surface roughness of the as received substrate imposes challenges to the fabrication of the dense compact blocking layer as the uneven surface resulted in pinholes and consequently photocurrent leakage. To overcome these issues, the Ti substrates' surface was first polished until a smooth mirror finish was achieved. They were subsequently sintered in air at 400 ^{o}C for the growth of an even layer of native TiO_2.

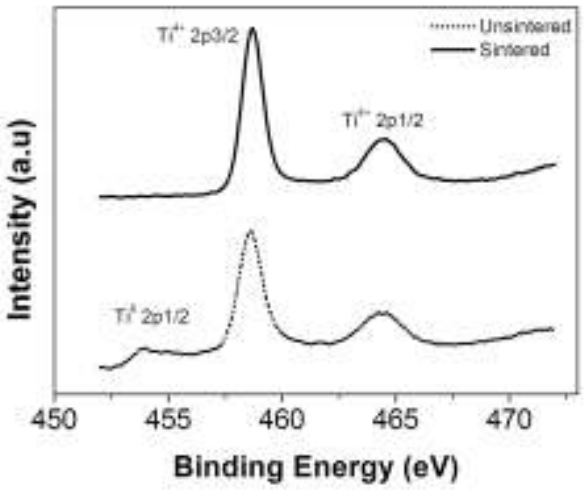

Figure 4.8 XPS spectra for Ti foil substrates before and after sintering.

To investigate the surface changes caused by sintering, X-ray photoelectron spectroscopy (XPS) was performed on the Ti substrates before and after sintering and the spectra are shown in Figure 4.8. Spectra of Ti 2p energy region consisted dominantly of a doublet peak at ~459 eV and ~465 eV. These two major peaks in each sample were attributed to the tetravalent titanium form i.e., Ti^{4+} 2p3/2 and Ti^{4+} 2p1/2, respectively.[49, 50] In the unsintered Ti foil, there is a small peak at ~454 eV which is attributed to metallic Ti. [49, 50] It is well known that the surface of Ti is oxidized into a thin layer of native oxide under ambient conditions and the XPS measurements are indicative of such an oxide layer on the unsintered Ti substrate. As the penetration depth of XPS is only ~10 nm, the fact that the Ti^0 peak can still be seen indicates that the native TiO_2 layer was only a few nanometers thick. After sintering, the disappearance of the Ti^0 peak is

attributed to the growth of TiO_2 on the surface of the Ti substrate during the sintering process and this confirms that the sintering process in air is able to increase the thickness of the native TiO_2 layer. With the polishing and sintering pretreatments, the adhesion of the subsequent dense and mesoporous TiO_2 layers on the Ti substrate was improved. The J-V curve and photovoltaic parameters of the device on Ti foil are shown in Figure 4.9. The flexible device fabricated on the treated Ti foil gave V_{oc} of 0.94 V, J_{sc} of 2.78 $mAcm^{-2}$, FF of 0.46 and an η of 1.20%. This is comparable to the rigid device on glass substrate.

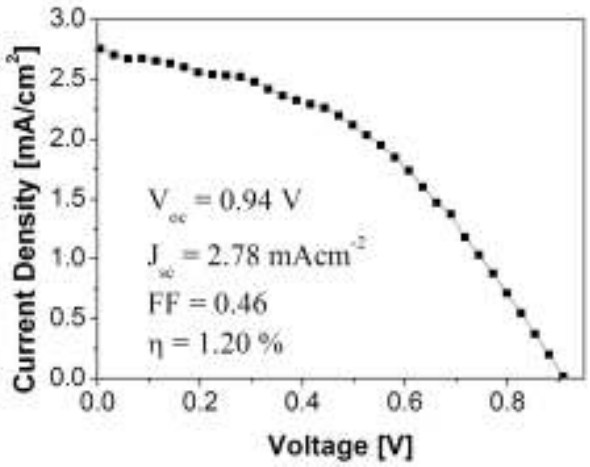

Figure 4.9 J-V curve for flexible solid-state DSSC fabricated on Ti substrate.

4.4 Conclusion

We report, for the first time, the fabrication of flexible solid-state DSSCs on low cost Ti foil. This low-cost fabrication method eliminates the use of costly transparent conducting substrates. The Ti substrate can withstand spray pyrolysis and sintering temperatures, which allow the fabrication of high quality TiO_2 dense and mesoporous layers. The high surface roughness and weak adhesion of the Ti substrate to the TiO_2 films were overcome by polishing and the growth of a thin native TiO_2 layer. After optimization of each cell component, flexible solid-state DSSCs were successfully fabricated on Ti foil with an overall efficiency of 1.20%. The lower efficiency

as compared to conventional devices is due to light loss from the Pt cathode and strong absorbance from the P3HT layer when the devices are illuminated from the cathode.

4.5 References

1. O'Regan, B. and M. Grätzel, *A low-cost, high-efficiency solar-cell on dye-sensitized colloidal TiO_2 films.* Nature, 1991. **353**(6346): p. 737-740.

2. Yella, A., et al., *Porphyrin-Sensitized Solar Cells with Cobalt (II/III)-Based Redox Electrolyte Exceed 12 Percent Efficiency.* Science, 2011. **334**(6056): p. 629-634.

3. Jun, Y. and M.G. Kang, *The characterization of nanocrystalline dye-sensitized solar cells with flexible metal substrates by electrochemical impedance spectroscopy.* Journal of the Electrochemical Society, 2007. **154**(1): p. B68-B71.

4. Li, B., et al., *Review of recent progress in solid-state dye-sensitized solar cells.* Solar Energy Materials and Solar Cells, 2006. **90**(5): p. 549-573.

5. Yum, J.H., et al., *Recent Developments in Solid-State Dye-Sensitized Solar Cells.* Chemsuschem, 2008. **1**(8-9): p. 699-707.

6. Chung, I., et al., *All-solid-state dye-sensitized Solar Cells With High Efficiency.* Nature, 2012. **485**(7399): p. 486-489.

7. Etgar, L., et al., *Mesoscopic $CH_3NH_3PbI_3/TiO_2$ Heterojunction Solar Cells.* Journal of the American Chemical Society, 2012. **134**(42): p. 17396-17399.

8. Yum, J.-H., et al., *Effect of Coadsorbent on the Photovoltaic Performance of Zinc Pthalocyanine-Sensitized Solar Cells.* Langmuir, 2008. **24**(10): p. 5636-5640.

9. Burschka, J., et al., *Tris(2-(1H-pyrazol-1-yl)pyridine)cobalt(III) as p-Type Dopant for Organic Semiconductors and Its Application in Highly Efficient Solid-State Dye-Sensitized Solar Cells.* Journal of the American Chemical Society, 2011. **133**(45): p. 18042-18045.

10. Bach, U., et al., *Solid-state Dye-sensitized Mesoporous TiO_2 Solar Cells With High Photon-to-electron Conversion Efficiencies.* Nature, 1998. **395**(6702): p. 583-585.

11. Kim, H.S., et al., *Lead Iodide Perovskite Sensitized All-Solid-State Submicron Thin Film Mesoscopic Solar Cell with Efficiency Exceeding 9%.* Scientific Reports, 2012. **2**.

12. Crossland, E.J., et al., *Mesoporous TiO2 single crystals delivering enhanced mobility and optoelectronic device performance.* Nature, 2013. **495**(7440): p. 215-219.

13. Lee, M.M., et al., *Efficient hybrid solar cells based on meso-superstructured organometal halide perovskites.* Science, 2012. **338**(6107): p. 643-647.

14. Zhang, W., et al., *Solid-State Dye-Sensitized Solar Cells with Conjugated Polymers as Hole-Transporting Materials.* Macromolecular Chemistry and Physics, 2011. **212**(1): p. 15-23.

15. Poplavskyy, D. and J. Nelson, *Nondispersive Hole Transport in Amorphous Films of Methoxy-spirofluorene-arylamine Organic Compound.* Journal of Applied Physics, 2003. **93**(1): p. 341-346.

16. Yang, L., et al., *Comparing spiro-OMeTAD and P3HT hole conductors in efficient solid state dye-sensitized solar cells.* Physical Chemistry Chemical Physics, 2012. **14**(2): p. 779-789.

17. Jiang, K.-J., et al., *Photovoltaics Based on Hybridization of Effective Dye-Sensitized Titanium Oxide and Hole-Conductive Polymer P3HT.* Advanced Functional Materials, 2009. **19**(15): p. 2481-2485.

18. Sadoughi, G., et al., *Enhanced electronic contacts in SnO2-dye-P3HT based solid state dye sensitized solar cells.* Physical Chemistry Chemical Physics, 2013. **15**(6): p. 2075-2080.

19. Mor, G.K., et al., *Visible to Near-Infrared Light Harvesting in TiO2 Nanotube Array−P3HT Based Heterojunction Solar Cells.* Nano Letters, 2009. **9**(12): p. 4250-4257.

20. Humphry-Baker, N., et al., *Time-Evolution of Poly(3-Hexylthiophene) as an Energy Relay Dye in Dye-Sensitized Solar Cells.* Nano Letters, 2011. **12**(2): p. 634-639.

21. Chang, J.A., et al., *High-Performance Nanostructured Inorganic−Organic Heterojunction Solar Cells.* Nano Letters, 2010. **10**(7): p. 2609-2612.

22. Zhu, R., et al., *Highly Efficient Nanoporous TiO2-Polythiophene Hybrid Solar Cells Based on Interfacial Modification Using a Metal-Free Organic Dye.* Advanced Materials, 2009. **21**(9): p. 994-1000.

23. Zhang, W., et al., *High-Performance Solid-State Organic Dye Sensitized Solar Cells with P3HT as Hole Transporter.* Journal of Physical Chemistry C, 2011. **115**(14): p. 7038-7043.

24. Park, J.H., et al., *Fabrication of an efficient dye-sensitized solar cell with stainless steel substrate.* Journal of the Electrochemical Society, 2008. **155**(7): p. F145-F149.

25. Toivola, M., F. Ahlskog, and P. Lund, *Industrial sheet metals for nanocrystalline dye-sensitized solar cell structures.* Solar Energy Materials and Solar Cells, 2006. **90**(17): p. 2881-2893.

26. Jun, Y., J. Kim, and M.G. Kang, *A study of stainless steel-based dye-sensitized solar cells and modules.* Solar Energy Materials and Solar Cells, 2007. **91**(9): p. 779-784.

27. Kang, M.G., et al., *A 4.2% efficient flexible dye-sensitized TiO2 solar cells using stainless steel substrate.* Solar Energy Materials and Solar Cells, 2006. **90**(5): p. 574-581.

28. Ito, S., et al., *High-efficiency (7.2%) flexible dye-sensitized solar cells with Ti-metal substrate for nanocrystalline-TiO2 photoanode.* Chemical Communications, 2006(38): p. 4004-4006.

29. Onoda, K., et al., *The superiority of Ti plate as the substrate of dye-sensitized solar cells.* Solar Energy Materials and Solar Cells, 2007. **91**(13): p. 1176-1181.

30. Tan, W.W., et al., *Electrophoretic deposition of nanocrystalline TiO2 films on Ti substrates for use in flexible dye-sensitized solar cells.* Electrochimica Acta, 2009. **54**(19): p. 4467-4472.

31. Kang, M.G., et al., *Flexible metallic substrates for TiO2 film of dye-sensitized solar cells.* Chemistry Letters, 2005. **34**(6): p. 804-805.

32. Yin, X., et al., *High-Performance Plastic Dye-sensitized Solar Cells Based on Low-Cost Commercial P25 TiO_2 and Organic Dye.* Acs Applied Materials & Interfaces, 2012. **4**(3): p. 1709-1715.

33. Yin, X., et al., *Electrophoretic Deposition of ZnO Photoanode for Plastic Dye-sensitized Solar Cells.* Electrochemistry Communications, 2010. **12**(9): p. 1241-1244.

34. Xue, Z., et al., *Enhanced Conversion Efficiency of Flexible Dye-sensitized Solar Cells by Optimization of the Nanoparticle Size With an Electrophoretic Deposition Technique.* Rsc Advances, 2012. **2**(18): p. 7074-7080.

35. Miyasaka, T., M. Ikegami, and Y. Kijitori, *Photovoltaic performance of plastic dye-sensitized electrodes prepared by low-temperature binder-free coating of mesoscopic titania.* Journal of the Electrochemical Society, 2007. **154**(5): p. A455-A461.

36. Zhang, D.S., T. Yoshida, and H. Minoura, *Low temperature synthesis of porous nanocrystalline TiO2 thick film for dye-sensitized solar cells by hydrothermal crystallization.* Chemistry Letters, 2002(9): p. 874-875.

37. Meng, Q.B., et al., *Fabrication of an efficient solid-state dye-sensitized solar cell.* Langmuir, 2003. **19**(9): p. 3572-3574.

38. Smestad, G., C. Bignozzi, and R. Argazzi, *Testing of dye sensitized TiO_2 solar cells I: Experimental photocurrent output and conversion efficiencies.* Solar Energy Materials and Solar Cells, 1994. **32**(3): p. 259-272.

39. Kruger, J., et al., *High Efficiency Solid-state Photovoltaic Device Due to Inhibition of Interface Charge Recombination.* Applied Physics Letters, 2001. **79**(13): p. 2085-2087.

40. Schmidt-Mende, L., et al., *Organic dye for highly efficient solid-state dye-sensitized solar cells.* Advanced Materials, 2005. **17**(7): p. 813-+.

41. Abrusci, A., et al., *Influence of Ion Induced Local Coulomb Field and Polarity on Charge Generation and Efficiency in Poly(3-Hexylthiophene)-Based Solid-State Dye-Sensitized Solar Cells.* Advanced Functional Materials, 2011. **21**(13): p. 2571-2579.

42. Koster, L.J.A., et al., *Light intensity dependence of open-circuit voltage of polymer : fullerene solar cells.* Applied Physics Letters, 2005. **86**(12).

43. Ramsdale, C.M., et al., *The origin of the open-circuit voltage in polyfluorene-based photovoltaic devices.* Journal of Applied Physics, 2002. **92**(8): p. 4266-4270.

44. Barker, J.A., C.M. Ramsdale, and N.C. Greenham, *Modeling the current-voltage characteristics of bilayer polymer photovoltaic devices.* Physical Review B, 2003. **67**(7).

45. Snaith, H.J., et al., *Light intensity, temperature, and thickness dependence of the open-circuit voltage in solid-state dye-sensitized solar cells.* Physical Review B, 2006. **74**(4).

46. Han, L.Y., et al., *Modeling of an equivalent circuit for dye-sensitized solar cells: improvement of efficiency of dye-sensitized solar cells by reducing internal resistance.* Comptes Rendus Chimie, 2006. **9**(5-6): p. 645-651.

47. Han, L.Y., et al., *Modeling of an equivalent circuit for dye-sensitized solar cells.* Applied Physics Letters, 2004. **84**(13): p. 2433-2435.

48. Hoshikawa, T., et al., *Impedance analysis of internal resistance affecting the photoelectrochemical performance of dye-sensitized solar cells.* Journal of the Electrochemical Society, 2005. **152**(2): p. E68-E73.

49. Carley, A.F., J.C. Roberts, and M.W. Roberts, *Dissociative chemisorption and localized oxidation states at titanium surfaces.* Surface Science, 1990. **225**(3): p. L39-L41.

50. Lu, G., S.L. Bernasek, and J. Schwartz, *Oxidation of a polycrystalline titanium surface by oxygen and water.* Surface Science, 2000. **458**(1–3): p. 80-90.

Chapter 5 Fabrication of flexible plastic solid-state dye sensitized solar cells using low temperature techniques

5.1 Introduction

Solid-state dye sensitized solar cells (DSSCs) were first developed as an alternative to corrosive liquid electrolyte which presents long term stability and sealing issues. Over the years, solid-state DSSCs have seen tremendous improvements. Early reported devices utilized the red dyes N3 [cis-bis(isothiocyanato)-bis(2,2'-bipyridyl-4,4'-dicarboxylato)ruthenium(II)] and its partially deprotonated form N719 as sensitizers and 2,20,7,70-tetrakis (N,N-di-p-methoxyphenyl-amine)9,90-spirobifluorene (spiro-OMeTAD) as hole transport material (HTM).[1] An efficiency of 2.56% was achieved in 2001 when *tert*-butylpyridine and $Li(CF_3SO_2)_2N$ were added to the HTM, a result of inhibited interfacial recombination. [2] Several strategies, such as using a silver complex of the sensitizer[3], the application of hydrophobic sensitizers[4] and p-type doping[5] were reported and efficiencies up to 7.2% was achieved. Recently, significant improvements in solid-state DSSCs have been reported in quick succession. Solid-state devices using perovskite based inorganic HTMs have been reported with efficiencies exceeding 8%.[6, 7] In addition, solid state DSSCs with lead iodide perovskite as sensitizer and spiro-OMeTAD as HTM was reported to give efficiencies up to approximately 15%.[8-10]

Although spiro-OMeTAD based devices have shown high efficiency, its low hole mobility (~ 10^{-4} $cm^2V^{-1}s^{-1}$)[11] and high fabrication cost[12] provide motivation for the search of alternative HTMs. Conjugated polymers have the advantages of low fabrication cost, high conductivity and tunable optoelectronic properties.[13] Poly(3-hexylthiophene) (P3HT) is an outstanding member of this family and possesses a hole mobility of up to 0.1 $cm^2V^{-1}s^{-1}$ which is several orders of

magnitude higher than spiro-OMeTAD. [11, 13] Previously, our group has reported that P3HT based hybrid devices give a reasonably high efficiency of up to 3.8%.[14, 15] Using lead iodide perovskite as sensitizer and P3HT as HTM, reasonable efficiencies of up to 6.7% were reported recently.[16, 17] These reports show that there is wide interest in the use of P3HT as a low cost alternative HTM.

Notwithstanding the impressive improvements with solid-state DSSCs, these were all reported on rigid glass substrates. Flexible and lightweight solid-state DSSCs are preferred for efficient large scale roll-to-roll manufacturing and flexible applications such as portable power generators. Indium tin oxide coated poly(ethylene) terephthalate (ITO/PET) and ITO coated polyethylene naphthalate (ITO/PEN) are typical flexible transparent conducting substrates.

Since recombination rates are much faster in solid-state DSSCs when compared to conventional DSSCs with a liquid electrolyte[18, 19], it is important to fabricate thin films with good interparticle connectivity and with minimal surface traps to minimize these undesirable recombination reactions. Conventionally, good quality mesoporous films are fabricated using nanometer size TiO_2 nanoparticles which are prepared by the hydrolysis of a precursor such as titanium isopropoxide, followed by peptization and hydrothermal growth. These nanoparticles are then dispersed in ethanol before terpineol and ethyl cellulose are added. The mixture is concentrated into a viscous paste by rotary evaporation that can be applied by doctor-blading or screen printing.[20] These films will be sintered at ~500^{o}C to enhance interparticle connectivity as well as to remove polymeric binders.

Other than the mesoporous TiO_2 layers, high quality pinhole-free dense TiO_2 blocking layers are essential for solid-state DSSCs. The dense blocking layer prevents the ohmic contact of the HTM

with the fluorine-doped tin oxide (FTO) conducting substrate which will short the device. Dense blocking layers can be formed by sol-gel deposition, magnetron sputtering or chemical vapor deposition. But the best quality dense blocking layers are formed by aerosol spray pyrolysis at sintering temperatures[21] which are not suitable for plastic substrates.

As such, the key challenges for plastic solid-state DSSCs are to fabricate high quality dense and mesoporous TiO_2 films at low temperature which are suitable for plastic substrates. Previously, we have reported that electrophoretic deposition (EPD) is a simple technique which produces high quality mesoporous photoanodes on polymeric conducting substrates at room temperature.[22-25] Atomic layer deposition (ALD) is a well known method of the deposition for uniform, high quality and pinhole free thin films for a wide range of materials.[26] ALD can be done at temperatures low enough for plastic substrates and it opens new opportunities for deposition of dense TiO_2 layers on plastic substrates.[27]

In this chapter, we report the fabrication of flexible solid-state hybrid DSSCs using P3HT as HTM on light weight ITO/PEN substrates. ALD was used for the fabrication of the dense blocking layer and EPD was used to deposit the mesoporous films. The entire fabrication process is done at temperatures lower than 150^{o}C, which is suitable for low temperature fabrication of flexible DSSCs on plastic substrates.

5.2 Experimental Section

5.2.1 Materials

All chemicals were used as received with no further purification. Titanium diisopropoxide bis(acetylacetonate), titanium tetrachloride, bis(trifluoromethylsulfonyl)amine lithium salt and 4-tert-butylpyridine were purchased from Sigma Aldrich. All solvents used were of AR grade and

were obtained from either Aldrich or Tedia. FTO glass substrates were available from Hartford Glass. Plastic PEN-ITO substrates were purchased from Peccell Technologies. P25 TiO_2 nanoparticles were kindly gifted by Degussa. The D102 organic sensitizer and P3HT polymer were from Mitsubishi Paper Mills and Rieke Metals respectively.

5.2.2 Atomic layer deposition of TiO_2

ALD was performed using a home-built ALD system.[27] The precursors used were $TiCl_4$ and deionized water. Each deposition cycle consisted of 0.5 s of $TiCl_4$ exposure, 30 s of N_2 purging, 0.5 s of deionized water exposure, followed by 30 s of N_2 purge at a base of pressure of 1×10^{-3} torr and a N_2 flow rate of 50 sccm. The films were grown at a rate of 1 Å/cycle at a constant temperature of 150 ^{o}C. The films were then cooled to room temperature and stored in a dessicator.

5.2.3 Spray Pyrolysis of TiO_2

0.2 M titanium diisopropoxide bis(acetylacetonate) in ethanol was used as the spray pyrolysis precursor and oxygen gas as the carrier. FTO glass substrates were preheated to 450^{o}C for 30 min and the precursor solution was sprayed at a constant height of ~ 20 cm under oxygen flow. 200 μL of precursor solution was used in each spraying cycle and spraying cycles are timed 30 s apart for the temperature to equilibrate at 450^{o}C.

5.2.4 Preparation of photoanodes by EPD

The TiO_2 suspension for EPD was prepared by mixing 0.5 g of TiO_2 powder with 15 mL of a mixture of ethanol, isopropanol and butanol (V/V/V = 1:2:4), which was followed by ultrasonication for 30 min. Before the EPD process, the colloidal suspension was acidified to a pH of about 4.0 with HNO_3. A pair of FTO glass substrates (1.5 cm × 1.5 cm, 15 Ω sq^{-1}) or

plastic PEN-ITO substrates (1.5 cm × 1.5 cm, 15 Ω sq^{-1}) were vertically immersed in the suspension. The distance between each pair of substrates was kept at 5 mm and the DC power supply was set at 20 V for a constant voltage EPD process. The thickness of the resultant film was controlled by the deposition time. The freshly coated films were left to dry in air before annealing at 100 ^{o}C for 30 min to ensure all solvents from the EPD process was removed. The prepared TiO_2 films were subsequently subjected to a pressure of 1 ton/cm^2 (Atlas Manual 15T Hydraulic Press) for 2 min to improve the interparticle adhesion and electrical connectivity[11]. As a result of the pressing process, the thickness of the films was reduced. Before dye sensitization, the compressed films were exposed to UV-O_3 (Femto Science, 150 W) for 30 min. After UV-O_3 treatment, the films, while warm, were soaked in a solution of 0.3 mM D102 in acetonitrile/tertbutanol (1:1 V/V) overnight. The photoanodes were subsequently rinsed with acetonitrile and left to dry in the dark.

5.2.5 DSSC assembly

The D102-sensitized TiO_2 films were immersed into an acetonitrile solution containing $Li(CF_3SO_2)_2N$ (6 mg mL^{-1}) and 4-tert-butylpyridine (TBP, 30 mg mL^{-1}) for 5 min and dried under air flow. After Li salt and TBP treatment, P3HT in chlorobenzene (15 $mgml^{-1}$) was spin-coated onto the D102-sensitized films. The films were subsequently transferred into a high vacuum chamber where ~80 nm of Ag was deposited onto the P3HT layer by thermal evaporation as the back electrode. The active area of the cell was 0.20 cm^2, controlled by a metal mask.

5.2.6 X-ray diffraction (XRD)

Crystal structure of the TiO_2 films was determined by X-ray diffraction (Shiamadzu XRD-6000). For XRD experiments, particularly thick TiO_2 films (~500 nm) were prepared on glass substrates

because XRD signals for thin films are weak. The working voltage and current were 40 kV and 20 mA, respectively. The scan rate was set at 2 degrees per minute and the scanning range was set at 10 to 80 degrees.

5.2.7 I-V Behavior Measurements

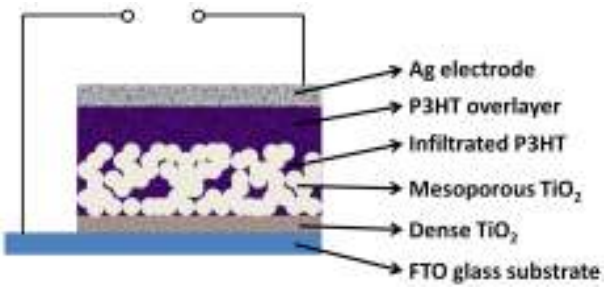

Figure 5.1 Cross section view of the simple p-n device fabricated for I-V behavior measurements. [28]

Simple p-n devices with the structure FTO/dense TiO_2/mesoporous TiO_2/P3HT/Ag were first fabricated on rigid glass substrates. Dense TiO_2 layer was first deposited by ALD as described before. ~1 μm of P25 TiO_2 nanoparticles was then deposited on top of the dense layer. The TiO_2 films were not dye-sensitized. P3HT was spin-coated on the TiO_2 layers and a layer of Ag was evaporated as the back electrode. A schematic showing the cross section of these devices is shown in Figure 5.1

I-V measurements were performed on these devices in the dark using an AutoLAB PGSTAT 320 N Potentiostat workstation. The scanning range was from -1.0 V to 1.0 V with the FTO as the negative electrode. Scan rate was 0.1 Vs^{-1}.

5.2.8 Photovoltaic measurements

The photocurrent-photovoltage (J-V) measurements of the SDSCs were recorded by a Keithley 2400 source meter. A solar simulator (XES-151S, San-EI Electric) was used as the light source for measuring the solar cells (<385 nm was cut off by XUL0385 filter, Asahi Spectra). The

incident light intensity of 100 mW cm^2 was calibrated using a reference cell (OptoPolymer, ISE CalLab) before each experiment. Incident photon-to-current conversion efficiency (IPCE) was measured using a 300 W xenon light source (MAX-310, Asahi Spectra) and a monochromator (TMS300, Bentham).

The standard silicon cell for IPCE measurement was calibrated by Bentham Instruments, Ltd. The illuminated electrochemical impedance spectra were measured using an Autolab potentiostat/galvanostat in the frequency range of 101 to 105 Hz.

The photovoltaic parameters of DSSCs were studied on an AutoLAB PGSTAT 320 N Potentiostat with a solar simulator (XES-151S, San-EI Electric). The incident light was filtered with an AM1.5 filter (Asahi Spectra) and calibrated with a silicon reference cell (OptoPolymer, ISE CalLab) before each experiment

5.3 Results and Discussion

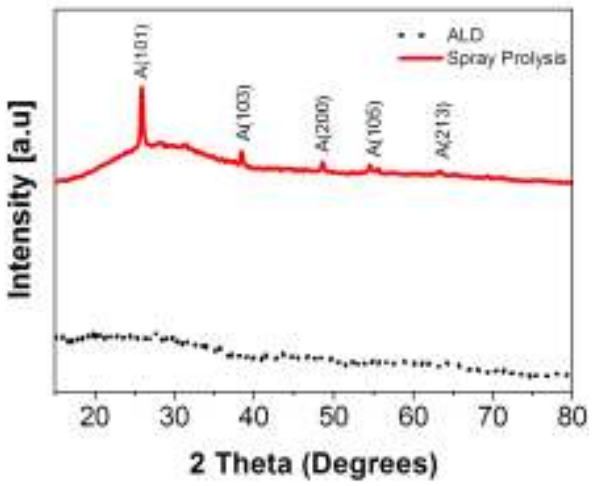

Figure 5.2 XRD spectra of the TiO_2 films prepared by spray pyrolysis and ALD respectively. Peaks of anatase are labelled. [28]

The dense TiO_2 films fabricated using ALD and conventional spray pyrolysis were first analyzed using XRD. The XRD spectra of the films are shown in Figure 5.2. It can be seen that the films

prepared using spray pyrolysis at 450^{o}C have the anatase crystal phase whereas the XRD spectrum of the films prepared using ALD do not have any clear peaks, revealing that the TiO_2 film produced with ALD is amorphous. The morphology of the films was also viewed under the scanning electron microscope (SEM). As seen in Figure 5.3, the TiO_2 film fabricated using the two methods show obvious differences in morphology. Figure 5.3A shows that the surface of TiO_2 film formed using spray pyrolysis is rough and made up of small crystallites, each estimated to be up to a few tens of nanometers in length. The crystallites are stacked compactly onto one another. Figure 5.3B shows the film formed by ALD, which has been deliberately scratched for focusing purposes, is smooth and featureless even under high magnification of 30,000×. The lack of obvious crystallites is consistent with the film's amorphous nature. The unscratched portion of the film appears to be complete and free of pinholes despite its low thickness. According to reports, optimal thickness of the dense TiO_2 blocking layer fabricated by spray pyrolysis varies but ranges from ~100 to 200 nm.[19, 29] They key reason for the need for such a relatively thick film is because films fabricated by spray pyrolysis contain unavoidable pinholes at low thicknesses. It was suggested that these films first grow from isolated spots at low thickness before combining into a continuous pinhole-free compact film as thickness increases. [29] Higher than necessary thicknesses are reported to lower fill factor (FF) and short-circuit current density (J_{sc}) of the eventual devices due to increased series resistance and reduced electron collection efficiency. [19, 29] As the resistance of amorphous TiO_2 films is higher than anatase films of similar thickness[30], the thickness of amorphous ALD dense TiO_2 films required to achieve the same blocking effect as anatase based conventional dense TiO_2 films is expected to be lower. As such, stringent requirements are placed on the fabrication technique to

produce high quality pinhole-free compact films at low film thickness and ALD is a technique known to satisfy these demands. [26]

The function of the dense TiO_2 blocking layer is to form a blocking interface between the FTO and HTM because these two materials form an ohmic contact.[19] As such, recombination occurs readily between electrons in FTO and the holes in HTM, leading to photocurrent loss. The dense blocking layer is supposed to impede these recombination processes through a rectifying behaviour. Ideally, the dense TiO_2 blocking layer should block the passage of holes from P3HT from HTM to FTO (or electrons from FTO to HTM) without impeding hole/electron transport significantly in the opposite direction.

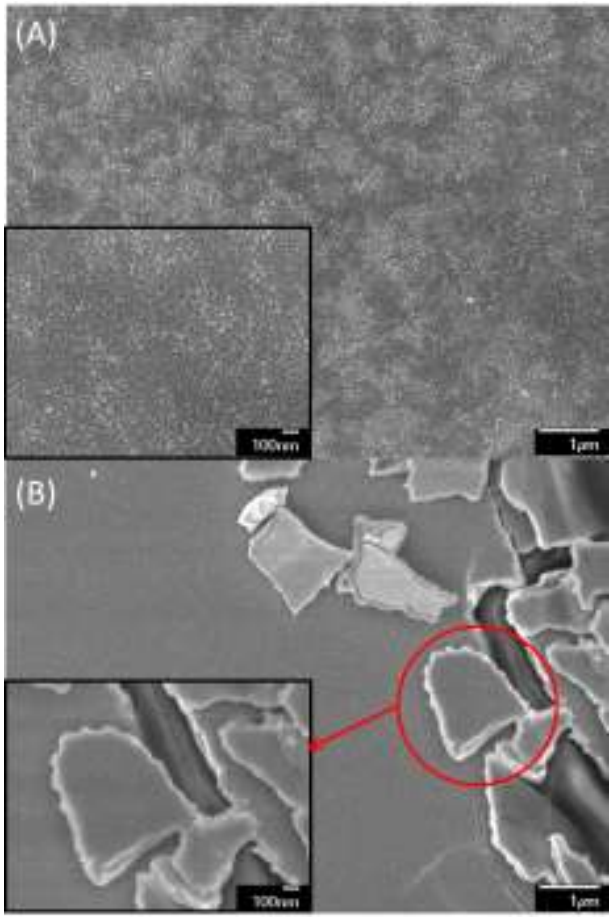

Figure 5.3 SEM images of (A) – a TiO2 dense film produced by spray pyrolysis. Inset shows a larger magnification of the same film. (B) - an ALD TiO2 film that has been deliberately scratched. Inset shows a larger magnification of the circled area. [28]

Different thicknesses of TiO_2 films were produced by ALD and the rectifying behavior of these films were investigated by fabricating simple p-n devices whose structure is shown in Figure 5.1. The FTO electrode is biased negative and the voltage was increased from -1.0 V to + 1.0 V continuously in the dark. The J-V curves of the devices fabricated with different thickness of the dense TiO_2 films are shown in Figure 5.4. In the case of the device with no dense film, there is a linear J-V relationship, which indicates that Ohm's law is obeyed: a similar resistance was obtained regardless of the applied bias and no rectification behavior was observed. When a ~10 nm dense film was used in the device, the relationship is still linear. The smaller gradient of the

line, however, indicates increased resistance of the device brought about by the addition of a layer of dense TiO_2.

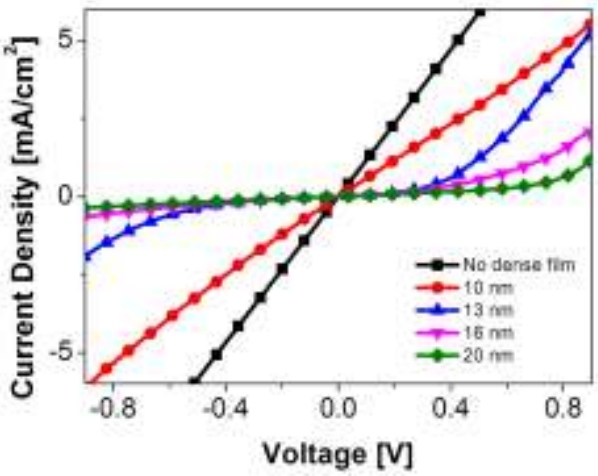

Figure 5.4 Current-voltage curves of p-n devices fabricated with different thicknesses of dense TiO_2 films

Obvious rectifying behavior was observed when at least a ~13 nm thick TiO_2 dense film was used. In the negative bias region, the magnitude of breakdown voltage increases when the thickness of dense TiO_2 is increased from ~13 nm to ~20 nm. Also, the magnitude of current density in this region decreases with the thickness of the dense TiO_2 layer. These indicate improved rectifying behavior with increased dense TiO_2 thickness, ie transfer of holes from P3HT to FTO (or transfer of electrons from FTO to P3HT) becomes increasingly difficult with increased dense TiO_2 thickness. In terms of device performance, this indirectly implies that photocurrent loss due to recombination between injected electrons and HTM will decrease with increasing dense TiO_2 thickness.

In the positive bias region, the current density decreases as the thickness of the dense TiO_2 film was increased from ~13 nm to ~20 nm. This shows that increasing thickness of dense TiO_2 decreases the amount of holes injected from FTO to P3HT (or electrons from P3HT to FTO).

This indicates that electron transport towards FTO becomes increasingly difficult with increased dense TiO_2 thickness and this is expected to decrease device charge collection efficiency.

From the I-V behavior studies, it can be seen that a minimum thickness of dense TiO_2 is required before rectifying behavior can be observed. A thicker dense TiO_2 film can better impede the transfer of holes from P3HT to FTO which prevents recombination. On the other hand, a thicker dense TiO_2 film can also impede electron collection at the FTO electrode, reducing J_{sc}. As such, there exists an optimal thickness such that there is a balance between rectifying property and electron collection.

Table 5.1 Photovoltaic parameters of solid-state devices fabricated using different thickness of TiO_2 dense films on rigid FTO substrates. The post-compression thickness of the mesoporous TiO_2 layer was ~ 1.0 μm for all these devices. [28]

Dense film	**V_{oc} (V)**	**J_{sc} (mAcm^{-2})**	**FF**	**η (%)**
ALD 10 nm	Negligible			
ALD 13 nm	0.74	3.21	0.39	0.94
ALD 16 nm	0.96	4.19	0.54	2.17
ALD 20 nm	0.83	0.48	0.40	0.16
Spray pyrolysis 100 nm	0.93	4.53	0.52	2.20

The dense TiO_2 films prepared by ALD on FTO glass substrates were subsequently used as blocking layers in solid-state DSSCs with P3HT as the HTM. The mesoporous TiO_2 layer was deposited using EPD of commercially available P25 nanoparticles at room temperature, followed by compression to increase interparticle adhesion and connectivity. For comparison purposes, devices were also fabricated using conventional dense films prepared using spray pyrolysis at

450^{o}C, all other parts of the device being the same. For these devices, the post-compression thickness of the mesoporous layer was ~1.0 μm. The photovoltaic parameters of these devices are shown in Table 5.1. The devices fabricated with ~10 nm dense TiO_2 film gave an open-circuit voltage (V_{oc}) of less than 1 mV, a short circuit current density (J_{sc}) in the μAcm^{-2} range and a linear J-V line which did not show any appreciable efficiency (η). Evidently, the device has shorted and negligible efficiency can be obtained from such a device. This indicates that a minimum thickness of dense film is needed before a properly functioning device can be fabricated, supporting the conclusions of the I-V behavior results. When the thickness of the TiO_2 dense film was increased to ~ 13 nm, an overall η of 0.94% was obtained. When a thicker ~16 nm film was used, the η increased to 2.17%. However, a further increment of the dense TiO_2 thickness to ~20 nm caused the η to decrease significantly to 0.16% mainly due to a significant decrease in J_{sc}. This can be understood as an overly thick blocking layer which impedes the electron transport from mesoporous TiO_2 to FTO despite being effective in blocking hole transfer from P3HT to FTO. In addition, the increase of the thickness of dense TiO_2 film from ~16 nm to ~20 nm also leads to a decrease in fill factor (FF). The series resistance of these devices can be estimated from the inverse of the gradient of the J-V curves near V_{oc}. The increase of series resistance from ~305 Ωcm^{-2} to ~826 Ωcm^{-2} when the thickness of dense TiO_2 is increased from ~16 to ~20 nm is significant and contributes to the decrease in FF. Interestingly, the devices fabricated using the conventional dense TiO_2 gave comparable η of 2.20%. This is interpreted as indirect evidence that the quality of the ~100 nm anatase film is similar to the ~ 16 nm amorphous films formed by ALD and both perform similarly well as dense blocking layers. These results show that thin amorphous TiO_2 films are a potential alternative to relatively thick conventional anatase blocking films in solid-state DSSCs.

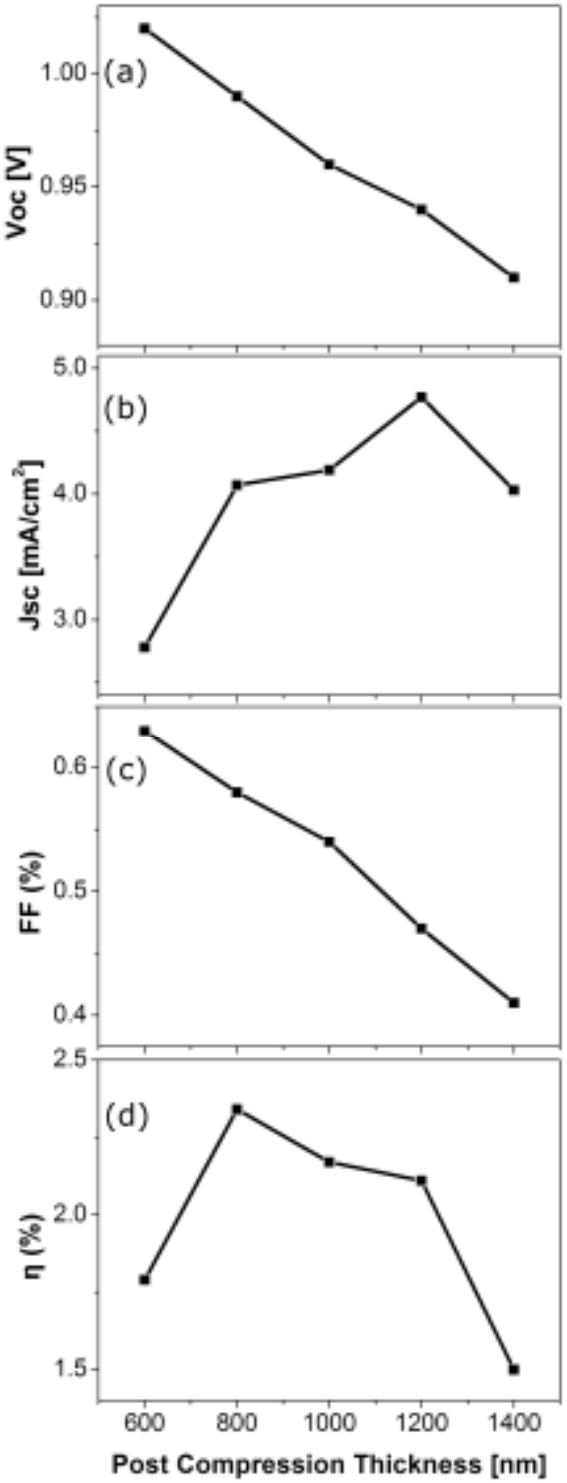

Figure 5.5 Change of (a) open-circuit voltage (b) short-circuit current density, (c) fill factor and (d) conversion efficiency with film mesoporous TiO_2 film thickness. [28]

As the thickness of the mesoporous TiO_2 layer has a big impact on the performance of solid-state DSSCs, the length of EPD time was varied to produce mesoporous films of varying thicknesses on FTO glass substrates. The post-compression thicknesses were varied from ~600 nm to ~1400 nm and the photovoltaic parameters of these devices are shown in Figure 5.5. As shown in Figure 5.5a, the V_{oc} of the devices decreases from 1.02 V to 0.91 V with increasing mesoporous TiO_2 film thickness from ~600 nm to ~ 1400 nm. This is attributed to the larger number of defects and recombination sites for thicker films.[31] The J_{sc}, shown in Figure 5.5b, increases from 2.78 $mAcm^{-2}$ to 4.77 $mAcm^{-2}$ when mesoporous TiO_2 film thickness is increased from ~600 nm to 1200 nm. This is ascribed to the increased dye loading with increased film thickness. However, further increasing the mesoporous TiO_2 thickness to 1400 nm led to a decrease of J_{sc} in spite of increased dye loading. This could be understood as incomplete pore-filling of the polymeric P3HT and increased recombination in thicker films, leading to photocurrent loss. [19] The FF, as shown in Figure 5.5c, decreases from 0.63 to 0.41 when mesoporous TiO_2 thickness is increased from ~600 nm to ~1400 nm due to a combination of decreased pore filling of P3HT and increased series resistance for thicker films. [18, 32] The overall device efficiency is shown in Figure 5.5d. The devices fabricated with a mesoporous TiO_2 film thickness of ~ 800 nm performed the best with a V_{oc} of 0.99 V, a J_{sc} of 4.07 $mAcm^{-2}$, a FF of 0.58 and an overall η of 2.34%.

With the optimization of the fabrication conditions on rigid FTO glass substrates, flexible devices were fabricated with the same steps with flexible ITO/PEN polymer substrates. The J-V curve of a typical flexible device is shown in Figure 5.6. Flexible devices show a Voc of 0.99 V, a J_{sc} of 3.83 mA, a FF of 0.51 and η of 1.93%. The lower efficiency as compared to the rigid

devices is attributed to the higher resistance and the lower transmittance of the ITO/PEN substrates. [33, 34]

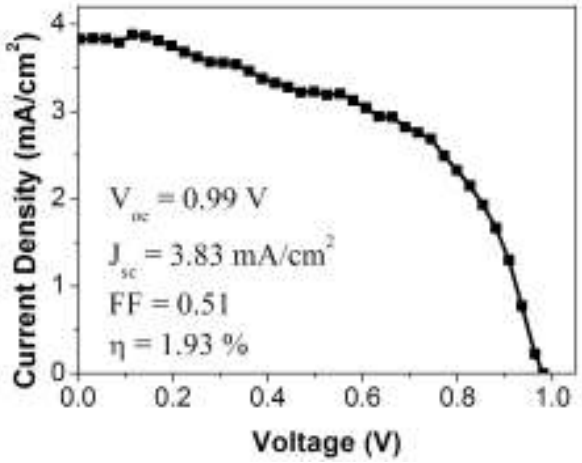

Figure 5.6 J-V curve of optimized flexible solid-state DSSC fabricated on ITO/PEN. [28]

5.4 Conclusion

For the first time, flexible solid-state DSSCs are fabricated on plastic substrates. Optimized devices on plastic substrates gave an overall η of 1.93%. The dense TiO_2 blocking layer was fabricated at 150 ^oC using ALD. These thin amorphous TiO_2 films have been shown to exhibit rectifying behaviour in simple *pn* devices. Optimized films gave similar performance as conventional dense TiO_2 layers which confirms that amorphous thin TiO_2 films formed by ALD is a low temperature alternative fabrication technique for dense blocking layers in solid-state DSSCs. The mesoporous TiO_2 layer was fabricated using EPD at room temperature, followed by compression. These low temperature processes are compatible for roll-to-roll fabrication of flexible solid-state DSSCs on plastic substrates.

5.5 References

1. Bach, U., et al., *Solid-state Dye-sensitized Mesoporous TiO_2 Solar Cells With High Photon-to-electron Conversion Efficiencies.* Nature, 1998. **395**(6702): p. 583-585.

2. Kruger, J., et al., *High Efficiency Solid-state Photovoltaic Device Due to Inhibition of Interface Charge Recombination.* Applied Physics Letters, 2001. **79**(13): p. 2085-2087.

3. Kruger, J., et al., *Improvement of the Photovoltaic Performance of Solid-state Sye-sensitized Sevice by Silver Complexation of the Sensitizer Cis-bis(4,4 '-dicarboxy-2,2 ' bipyridine)-bis(isothiocyanato) ruthenium(II).* Applied Physics Letters, 2002. **81**(2): p. 367-369.

4. Schmidt-Mende, L., S.M. Zakeeruddin, and M. Grätzel, *Efficiency Improvement in Solid-state-dye-sensitized Photovoltaics With an Amphiphilic Ruthenium-dye.* Applied Physics Letters, 2005. **86**(1).

5. Burschka, J., et al., *Tris(2-(1H-pyrazol-1-yl)pyridine)cobalt(III) as p-Type Dopant for Organic Semiconductors and Its Application in Highly Efficient Solid-State Dye-Sensitized Solar Cells.* Journal of the American Chemical Society, 2011. **133**(45): p. 18042-18045.

6. Etgar, L., et al., *Mesoscopic $CH_3NH_3PbI_3/TiO_2$ Heterojunction Solar Cells.* Journal of the American Chemical Society, 2012. **134**(42): p. 17396-17399.

7. Chung, I., et al., *All-solid-state dye-sensitized Solar Cells With High Efficiency.* Nature, 2012. **485**(7399): p. 486-489.

8. Kim, H.S., et al., *Lead Iodide Perovskite Sensitized All-Solid-State Submicron Thin Film Mesoscopic Solar Cell with Efficiency Exceeding 9%.* Scientific Reports, 2012. **2**.

9. Burschka, J., et al., *Sequential Deposition as a Route to High-performance Perovskite-sensitized Solar Cells.* Nature, 2013.

10. Lee, M.M., et al., *Efficient Hybrid Solar Cells Based on Meso-Superstructured Organometal Halide Perovskites.* Science, 2012. **338**(6107): p. 643-647.

11. Poplavskyy, D. and J. Nelson, *Nondispersive Hole Transport in Amorphous Films of Methoxy-spirofluorene-arylamine Organic Compound.* Journal of Applied Physics, 2003. **93**(1): p. 341-346.

12. Ding, I.K., et al., *Deposition of Hole-transport Materials in Solid-state Dye-sensitized Solar Cells by Doctor-blading.* Organic Electronics, 2010. **11**(7): p. 1217-1222.

13. Zhang, W., et al., *Solid-State Dye-Sensitized Solar Cells with Conjugated Polymers as Hole-Transporting Materials.* Macromolecular Chemistry and Physics, 2011. **212**(1): p. 15-23.

14. Zhu, R., et al., *Highly Efficient Nanoporous TiO2-Polythiophene Hybrid Solar Cells Based on Interfacial Modification Using a Metal-Free Organic Dye.* Advanced Materials, 2009. **21**(9): p. 994-1000.

15. Zhang, W., et al., *High-Performance Solid-State Organic Dye Sensitized Solar Cells with P3HT as Hole Transporter.* Journal of Physical Chemistry C, 2011. **115**(14): p. 7038-7043.

16. Bi, D.Q., et al., *Effect of Different Hole Transport Materials on Recombination in $CH_3NH_3PbI_3$ Perovskite-Sensitized Mesoscopic Solar Cells.* Journal of Physical Chemistry Letters, 2013. **4**(9): p. 1532-1536.

17. Heo, J.H., et al., *Efficient Inorganic-organic Hybrid Heterojunction Solar Cells Containing Perovskite Compound and Polymeric Hole Conductors.* Nature Photonics, 2013. **7**(6): p. 487-492.

18. Hardin, B.E., H.J. Snaith, and M.D. McGehee, *The Renaissance of Dye-sensitized Solar Cells.* Nature Photonics, 2012. **6**(3): p. 162-169.

19. Yum, J.H., et al., *Recent Developments in Solid-State Dye-Sensitized Solar Cells.* Chemsuschem, 2008. **1**(8-9): p. 699-707.

20. Ito, S., et al., *Fabrication of Thin Film Dye Sensitized Solar Cells With Solar to Electric Power Conversion Efficiency Over 10%.* Thin Solid Films, 2008. **516**(14): p. 4613-4619.

21. Kavan, L. and M. Grätzel, *Highly efficient semiconducting TiO2 photoelectrodes prepared by aerosol pyrolysis.* Electrochimica Acta, 1995. **40**(5): p. 643-652.

22. Yin, X., et al., *High-Performance Plastic Dye-sensitized Solar Cells Based on Low-Cost Commercial P25 TiO_2 and Organic Dye.* Acs Applied Materials & Interfaces, 2012. **4**(3): p. 1709-1715.

23. Yin, X., et al., *Electrophoretic Deposition of ZnO Photoanode for Plastic Dye-sensitized Solar Cells.* Electrochemistry Communications, 2010. **12**(9): p. 1241-1244.

24. Xue, Z., et al., *Enhanced Conversion Efficiency of Flexible Dye-sensitized Solar Cells by Optimization of the Nanoparticle Size With an Electrophoretic Deposition Technique.* Rsc Advances, 2012. **2**(18): p. 7074-7080.

25. Xue, Z., L. Wang, and B. Liu, *Facile Fabrication of Co-sensitized Plastic Dye-sensitized Solar Cells Using Multiple Electrophoretic Deposition.* Nanoscale, 2013. **5**(6): p. 2269-2273.

26. George, S.M., *Atomic Layer Deposition: An Overview.* Chemical Reviews, 2010. **110**(1): p. 111-131.

27. Jiang, C.Y., et al., *Low Temperature Processing Solid-state Dye Sensitized Solar Cells.* Applied Physics Letters, 2012. **100**(11): p. 113901-113903.

28. Xue, Z., et al., *Fabrication of Flexible Plastic Solid-State Dye-Sensitized Solar Cells Using Low Temperature Techniques.* The Journal of Physical Chemistry C, 2013.

29. Peng, B., et al., *Systematic Investigation of the Role of Compact TiO_2 Layer in Solid State Dye-sensitized TiO_2 Solar Cells.* Coordination Chemistry Reviews, 2004. **248**(13-14): p. 1479-1489.

30. Zoppi, R.A., B.C. Trasferetti, and C.U. Davanzo, *Sol-gel Titanium Dioxide Thin Films on Platinum Substrates: Preparation and Characterization.* Journal of Electroanalytical Chemistry, 2003. **544**: p. 47-57.

31. Ito, S., et al., *High-efficiency Organic-dye-sensitized Solar Cells Controlled by Nanocrystalline-TiO_2 Electrode Thickness.* Advanced Materials, 2006. **18**(9): p. 1202-1205.

32. Schmidt-Mende, L., et al., *Effect of Hydrocarbon Chain Length of Amphiphilic Ruthenium Dyes on Solid-State Dye-Sensitized Photovoltaics.* Nano Letters, 2005. **5**(7): p. 1315-1320.

33. Liu, X.Z., et al., *Room Temperature Fabrication of Porous ZnO Photoelectrodes for Flexible Dye-sensitized Solar Cells.* Chemical Communications, 2007(27): p. 2847-2849.

34. Lan, Z.A., et al., *Preparation of Sub-micron Size Anatase TiO_2 Particles for Use as Light-scattering Centers in Dye-sensitized Solar Cell.* Journal of Materials Science-Materials in Electronics, 2010. **21**(8): p. 833-837.

Chapter 6 Conclusions and outlook

6.1 Conclusions

This thesis is focused on the fabrication and optimization of flexible dye sensitized solar cells (DSSCs). The major findings are summarized as follows:

(1) TiO_2 nanoparticles of various sizes are synthesized by a hydrothermal method and deposited as the photoanode by electrophoretic deposition (EPD). The relationship between nanoparticle size and device performance is systematically studied. Charge collection efficiency is found to increase with increasing nanoparticle size. Conversely, dye loading is found to decrease with increasing nanoparticle size. Due to these opposing factors, a moderate nanoparticle size of 19 nm is found to give the highest efficiency. Under optimized conditions an efficiency of 6.0 % is achieved on plastic devices using 19 nm TiO_2 nanoparticle under standard 100 $mWcm^{-2}$ AM 1.5G illumination. This represents a 20 % enhancement over devices using commercially available P25 TiO_2 nanoparticles.

(2) Using organic dyes D131 and SQ2, a proof of concept of a facile layer-by-layer co-sensitization technique is shown. The technique is rapid and suitable for plastic substrates. Using Electrochemical Impedance Spectroscopy (EIS), it was found that devices sensitized with the traditional cocktail method has lower recombination resistance as compared to devices sensitized using the layered technique. Layered devices are also found to have higher dye loading. These lead to the layered devices showing higher photocurrent and open circuit voltage than cocktail devices. For optimized plastic devices tested under 100 $mWcm^{-2}$ AM 1.5G illumination, the layered devices give an efficiency of 4.1%, a 24 % improvement over the cocktail devices (3.3 %).

(3) For the first time, the fabrication of flexible solid-state DSSCs on low cost Ti foil is reported. This low-cost fabrication method eliminates the use of costly transparent conducting substrates. The Ti substrate can withstand spray pyrolysis and sintering temperatures, which allow the fabrication of high quality TiO_2 dense and mesoporous layers. The high surface roughness and weak adhesion of the Ti substrate to the TiO_2 films were overcome by polishing and the growth of a thin native TiO_2 layer. After optimization of each cell component, flexible solid-state DSSCs were successfully fabricated on Ti foil with an overall efficiency of 1.20%. The lower efficiency as compared to conventional devices is due to light loss from the Pt cathode and strong absorbance from the poly(3-hexylthiophene) (P3HT) layer when the devices are illuminated from the cathode.

(4) For the first time, flexible solid-state DSSCs are fabricated on plastic substrates. The dense TiO_2 blocking layer was fabricated at 150 ^oC using ALD. These thin amorphous TiO_2 films have been shown to exhibit rectifying behaviour in simple *pn* devices. Optimized films gave similar performance as conventional dense TiO_2 layers which confirms that amorphous thin TiO_2 films formed by ALD is a low temperature alternative fabrication technique for dense blocking layers in solid-state DSSCs. The mesoporous TiO_2 layer was fabricated using EPD at room temperature, followed by compression. These low temperature processes are compatible for roll-to-roll fabrication of flexible solid-state DSSCs on plastic substrates. Optimized devices on plastic substrates gave an overall efficiency of 1.9 %.

6.2 Outlook

(1) With the successful co-sensitization of plastic DSSCs (chapter 3), near infra-red (NIR) sensitizers with strong absorption beyond 700 nm should be developed. Most of the current sensitizers have weak absorption tails and the limited capture of NIR radiation is limiting device

efficiency. Co-sensitization of current sensitizers, which have strong absorption below 700 nm, with new NIR sensitizers is expected to increase DSSC efficiency significantly.

(2) The efficiency of P3HT based devices is still inferior than those based on 2,20,7,70-tetrakis (N,N-di-p-methoxyphenyl-amine)9,90-spirobifluorene (spiro-OMeTAD) due to combination of fast recombination kinetics and low electron lifetime of P3HT based devices. In order to promote P3HT as a low cost alternative, strategies such as physical/chemical doping, structural modification and chemical additives can be utilized to improve electron lifetime.

(3) With the fabrication of the plastic solid-state DSSC using low temperature techniques, the stability of the devices under long term light soaking should be investigated.

A LIST OF PUBLICATIONS

1. Yin, X.; **Xue, Z**.; Liu, B., Electrophoretic deposition of Pt nanoparticles on plastic substrates as counter electrode for flexible dye-sensitized solar cells. *J. Power Sources* **2011,** *196* (4), 2422-2426.

2. Yin, X.; **Xue, Z**.; Wang, L.; Cheng, Y.; Liu, B., High-Performance Plastic Dye-sensitized Solar Cells Based on Low-Cost Commercial P25 TiO2 and Organic Dye. *ACS Appl. Mater. Interfaces* **2012,** *4* (3), 1709-1715.

3. **Xue, Z**.; Zhang, W.; Yin, X.; Cheng, Y.; Wang, L.; Liu, B., Enhanced conversion efficiency of flexible dye-sensitized solar cells by optimization of the nanoparticle size with an electrophoretic deposition technique. *RSC Advances* **2012,** *2* (18), 7074-7080.

4. Wang, L.; **Xue, Z**.; Liu, X.; Liu, B., Transfer of asymmetric free-standing TiO_2 nanowire films for high efficiency flexible dye-sensitized solar cells. *RSC Advances* **2012,** *2* (20), 7656-7659.

5. Liu, X.; Wang, L.; **Xue, Z**.; Liu, B., Efficient flexible dye-sensitized solar cells fabricated by transferring photoanode with a buffer layer. *RSC Advances* **2012,** *2* (16), 6393-6396.

6. Etgar, L.; Gao, P.; **Xue, Z**.; Peng, Q.; Chandiran, A. K.; Liu, B.; Nazeeruddin, M. K.; Grätzel, M., Mesoscopic $CH_3NH_3PbI_3/TiO_2$ Heterojunction Solar Cells. *J. Am. Chem. Soc.* **2012,** *134* (42), 17396-17399.

7. Cai, L.; Tsao, H. N.; Zhang, W.; Wang, L.; **Xue, Z**.; Grätzel, M.; Liu, B., Organic Sensitizers with Bridged Triphenylamine Donor Units for Efficient Dye-Sensitized Solar Cells. *Advanced Energy Materials* **2013,** *3* (2), 200-205.

8. **Xue, Z.**; Wang, L.; Liu, B., Facile fabrication of co-sensitized plastic dye-sensitized solar cells using multiple electrophoretic deposition. *Nanoscale* **2013,** *5* (6), 2269-2273.

9. Etgar, L.; Yanover, D.; Čapek, R. K.; Vaxenburg, R.; **Xue, Z**.; Liu, B.; Nazeeruddin, M. K.; Lifshitz, E.; Grätzel, M., Core/Shell PbSe/PbS QDs TiO_2 Heterojunction Solar Cell. *Advanced Functional Materials* **2013,** *23* (21), 2736-2741.